Fall 2018

Tumor Suppressor MIR-489 Regulates Proliferation, Autophagy and Overcomes Drug-Resistance in Breast Cancer

Mithil Soni

TUMOR SUPPRESSOR MIR-489 REGULATES PROLIFERATION, AUTOPHAGY AND OVERCOMES DRUG-RESISTANCE IN BREAST CANCER

by

Mithil Soni

Bachelor of Pharmacy
Nirma University of Science and Technology, 2007

Master of Science
University of Houston Clear Lake, 2009

Submitted in Partial Fulfillment of the Requirements

For the Degree of Doctor of Philosophy in

Biological Sciences

College of Arts and Sciences

University of South Carolina

2018

Accepted by:

Hexin Chen, Major Professor

Marj Pena, Committee Member

Alan Waldman, Committee Member

Jason Stewart, Committee Member

Daping Fan, Committee Member

Cheryl L. Addy, Vice Provost and Dean of the Graduate School

DEDICATION

This work is dedicated to my Guruhari P.P. Hariprasad Swamiji, YDS Columbia and Charlotte and my family who have made my life so enjoyable.

ACKNOWLEDGEMENTS

First, I would like to thank Dr. Hexin Chen for providing me an opportunity to conduct research in his laboratory and for his guidance, vision and funding over the years. I would also like to thank my committee members Dr. Marj Pena, Dr. Alan Waldman, Dr. Jason Stewart and Dr. Daping Fan for their valuable guidance and suggestions. I would also like to extend my gratitude to people in the department of Biology including Yogin Patel, Liu Shou, Nirav Shah, Rachel Botbyl, Ryann Shealy, Susan Bare, Karen Barbour, Sapna Shah, Sam Burnett and Evelyn Chukwurah. I am very grateful to Yogin Patel, Nirav Shah and Shou Liu, who have taught me how to all the techniques, experiments and data analysis.

I was able start and complete my research due to blessings and inspiration from my Guruhari P.P. Hariprasad Swamiji. Without his exceptional support and inspiration, it wouldn't be possible. In fact, it was his decision that I should pursue doctoral studies. I would like to acknowledge my mentor Kishanji and Bhaktipriya Swami for their guidance and motivation. I would like to acknowledge Yogin's family including his wife Krupaben and mother Lilaben along with Kamleshbhai and Rupalben who have supported me throughout the journey. I would like to thank my parents Kamleshbhai and Mitaben along with my brother Milind, his wife Sarmistha and daughter Yashashree for their support on each step of my expedition. My special acknowledgement to all members of YDS Columbia, Charlotte and Atlanta who have supported me throughout my stay at USC.

ABSTRACT

Despite decades of extensive research, breast cancer remains an untamable disease due to complexity and heterogeneity of disease. It is for this very reason, most efforts targeting a single pathway did not yield satisfactory results. Discovery of a novel therapeutic agents targeting multiple pathways, such as miRNAs, holds promise for future cancer therapy. This study was aimed to explore therapeutic potential of one such microRNA, miR-489. In the first study, we identified autophagy as a novel pathway targeted by miR-489 and reported ULK1 and LAPTM4B to be a direct of miR-489 target. We showed that miR-489 mediated autophagy inhibition and autophagosome accumulation is necessary for its cytotoxic effect. Furthermore, we demonstrated autophagy inhibition and LAPTM4B down regulation as a novel mechanism responsible for miR-489 mediated doxorubicin sensitization. Finally, we found that miR-489 and LAPTM4B levels were inversely correlated in human tumor specimens, and more importantly, miR-489 expression levels predict overall survival in patients with 8q22 amplification (Soni et al.). We then established that miR-489 is an estrogen regulated miRNA and is highly expressed in hormone positive breast tumors and cell lines. For the first time we reported that miR-489 negatively regulates estrogen signaling. Depletion of miR-489 using Anti-miR-489 siRNA or CRISPR-Cas9 significantly increased proliferation, colony formation ability and stem like cell population. Mechanistically, we report that miR-489 modulates estrogen induced

estrogen receptor localization into nucleus. We further established that downregulation of p38 MAPK is responsible for miR-489's effect of estrogen receptor localization. We showed that estrogen activates p38 MAPK and this activated p38 MAPK is necessary for nuclear translocation of estrogen receptor. Furthermore, we also report that miR-489 prevents activation of ERα by inhibiting its phosphorylation. We demonstrated that miR-489 inhibits ERK and AKT activation which are responsible kinase for ERα phosphorylation at Ser 118 and Ser 167 site, respectively. We then demonstrated that miR-489 is lost in tamoxifen resistant breast tumors and cell lines and restoration of miR-489 significantly inhibits its proliferation and overcomes both *de novo* and acquired tamoxifen resistance. miR-489 exerts this effect through its unique ability to target HER2, MAPK and PI3K-AKT signaling pathway at the same time. These data advocates strongly for therapeutic potential of miR-489 in ERα positive and tamoxifen resistant breast cancer. In summary, our data shows that miR-489 expression is inversely correlated with aggressiveness of breast cancer and drug resistance and proposes miR-489 as a promising prognostic biomarker or therapeutic agent in breast cancer.

TABLE OF CONTENTS

LIST OF FIGURES

LIST OF ABBREVIATIONS

AL ..... Autolysosome

AO..... Acridine orange

AP ..... Autophagosome

CALCR..... Calcitonin Receptor

CRISPR ..... Clustered regularly interspaced short palindromic repeats

CSC ..... Cancer stem cell

E2 ..... 17β-estradiol

ER..... Estrogen receptor

HER2 ..... Human Epidermal Growth Receptor 2

IHC..... Immuno Histochemistry

MAPK..... Mitogen Activated Protein Kinase

miR ..... miRNA

P4 ..... Progesterone

PI3K ..... PhosphoInositide 3-Kinase

siRNA..... Short Interfering RNA

TAM ..... Tamoxifen

TNBC ..... Triple Negative Breast Cancer

CHAPTER 1

INTRODUCTION

1.1 BREAST CANCER

A highly dynamic development process exits within the epithelia of mammary gland, featuring morphogenetic variation during puberty, pregnancy, lactation, and regression. The identification of mammary stem cells (MaSCs) via lineage-tracing studies has substantiated a hierarchical organization of the mammary epithelia. Due to this massive remodeling, breast tissue is particularly sensitive to developing cancer. In fact, with an average lifetime risk of 8–10%, breast cancer is the most common malignancy in women in the western world. According to cancer statistics, approximately 1.7 million new cases arise around the globe every year and 2,66,120 new cases are expected in 2018 in the United States (Kubista, 2001).

Due to its heterogeneity, this disease is distinguished by up to 21 distinct histological subtypes and four major molecular subtypes which are biologically variable in presentation, response to treatment and outcomes. Gene expression profiling have pointed out different genetic variability even among tumors belonging to same subtype. Four subtypes are defined based on presence or absence of receptor molecules on cell surface which include the presence or absence of hormone receptors, (estrogen or progesterone) (HR+/HR-) and over-

expression of human epidermal growth receptor 2 (HER2+/HER2-). Among this luminal A (Banegas et al.) is the most abundant (74%) breast cancers express the estrogen (ER+) and/ or the progesterone receptor (PR+) but not HER2 (HER2-) (Figure 1.1). These cancers tend to be slow growing and less aggressive than other subtypes. This type of cancer is associated with favorable prognosis because of hormone receptors have better response to hormonal therapy. Triple negative (HR-/HER2-) type consists of about 12% of breast cancer. It is called triple negative because of lacking ER, PR and HER2 on their cell receptor. These cancers have a poorer short-term prognosis than other breast cancer types due to lacking targeted therapies. Luminal B breast cancers are consisting of hormone receptor positive and HER2 positive tumor cells. Moreover, this subtype also has highly positive Ki67 (indicator of a large proportion of actively dividing cells) cells. Luminal B is more aggressive than Luminal A. HER2 enriched (HR-/HER2+) breast cancers have HER2 over expressing tumor cells. They are mostly hormone receptor negative. These cancers tend to grow and spread more aggressively than other breast cancers and are associated with poorer short-term prognosis compare to ER+ breast cancers.

1.2 MIRNA

miRNAs belong to a small non-coding regulatory RNAs that are 18-24 nucleotide long single stranded highly conserved RNA molecules. They are synthesized from precursor hairpin shaped double-stranded RNAs. miRNAs regulate expression of their target protein by binding to 3'-UTR of mRNA in sequence dependent manner. This binding either promotes target mRNA

degradation and/or inhibition of their translation. Since each miRNA can target hundreds of genes, they can play pivotal role in regulation of all cellular processes. (Mukherji et al., 2011; Ramalingam et al., 2014).

miRNAs have been classified as either Intergenic miRNAs or intronic miRNA based on their location on the genome(Olena & Patton, 2010). Intergenic miRNAs possess independent promoter and are transcribed independently while intronic miRNAs are in the intron of a protein coding genes and most of the time share a promoter with its host gene. Most miRNAs are transcribed through RNA Pol II into 1000-2000bp long primary miRNA (pri-miRNA) with long stem loop structure. These pri-miRNAs are cleaved in to approximately 70-100 nucleotide long precursor microRNA (pre-miRNA) by RNAse III endonuclease Drosha. These pre-miRNAs are transported by mainly exportin-5. The pre-miRNAs are cleaved into mature 18-24 nucleotide long miRNA by RNAse III type enzyme Dicer. Dicer is highly specific enzyme which forms complex with two other proteins TRBP and PACT to form miRNA induced silencing (RISC) complex. RISC complex directly involve in RNA silencing process in which miRNA functions as a guide by base pairing with its target mRNAs, whereas AGO proteins function as effectors by recruiting factors that induce translational repression, mRNA deadenylation and mRNA decay. miRNA binding sites are usually located in 3’ untranslated region (UTR) of mRNAs. The 5’ end of miRNAs that spans from nucleotide position 2 to 7 is critical for target recognition and has been given term ‘miRNA seed’. miRNAs are very crucial molecules since each miRNA targets hundreds of genes and majority of protein coding genes are miRNA targets. Thus, their expression is

tightly regulated and their dysregulation is often associated with various human disease including cancer and neurodevelopmental disorders (Bartel, 2004; H. Y. Lee & Doudna, 2012; Y. Lee et al., 2003; Shah & Chen, 2014). miRNA biogenesis has been demonstrated in figure 1.2.

1.3 Autophagy And Cancer

Macroautophagy (referred to as autophagy now onwards) is a highly conserved process by which cells capture intracellular proteins, lipids and organelles, and deliver them to the lysosomal compartment for degradation (Fulda & Kogel, 2015). It is a complex process that involves more than 30 genes that regulates one of the three stages of the process namely Initiation, Elongation and Maturation. Core genes involved the process are known as ATG, an abbreviation of Autophagy related genes. During autophagy initiation pre-autophagosomal structures (PAS), also known as phagophore, elongate and fuse while engulfing a portion of cytoplasm within double-membraned vesicles, called autophagosomes. The autophagosomes first fuse with endosomes to form hybrid organelles called amphisomes that later fuse with acidic lysosomes where the entrapped cytosolic contents are degraded (Fig. 1.3). Final maturation stage of autophagy involves fusion of autophagosome and lysosome that give rise to “Autolysosome”.

Key functions of autophagy are to provide energy and metabolic precursors under conditions of starvation and to alleviate stress by removal of damaged proteins and organelles, which are deleterious for cell survival. Therefore, autophagy appears to serve as a pro-survival stress response in most settings. However, its role in cancer seems to be complex and context-dependent as

evidences exist for its oncogenic as well as tumor suppressive role in cancer (Figure 1.4). In tumor cells with defects in apoptosis, autophagy allows prolonged survival. Paradoxically, autophagy defects are associated with increased tumorigenesis, but the mechanism behind this has not been determined. Recent evidence suggests that autophagy provides a protective function to limit tumor necrosis and inflammation, and to mitigate genome damage in tumor cells in response to metabolic stress. So far, these data suggest that autophagy may limit tumor initiation by protecting cells from mutations while may function as oncogenic pathway by protecting cancer cell under metabolic stress frequently seen in established tumors.

1.4 Estrogen Receptor Positive Breast Cancer And Endocrine Resistance

17β-Estradiol or estrogen (referred as E2 hereafter), a steroid hormone that plays a significant role in mammary gland development, serves as one of the main risk factors for breast cancer development. In fact, approximately 75% of diagnosed breast tumors express estrogen receptor α (ERα). ERα is a ligand-dependent transcription factor that, upon binding with E2, regulates genes involved in cell proliferation, differentiation, and migration. Therefore, deregulated actions of ERα signaling are associated with breast cancer development (Manavathi et al., 2013).

The ERα is a ligand-dependent transcription factor that belongs to the nuclear receptor superfamily of proteins with defined functional domains that can both activate and repress the expression of genes. In the absence of ligand, ERα

is sequestered in complex with an inhibitory heat shock protein in target cell nuclei. Upon ligand binding, the receptor detaches from the heat shock protein complex and undergoes dimerization(Klein-Hitpass, Schorpp, Wagner, & Ryffel, 1986). The interaction of ERα with target gene promoters can occur either directly, through specific estrogen response elements (ERE), or indirectly through contacts with other DNA-bound transcription factors such as activation protein 1, specificity protein (SP) 1, or NF-κB. Once tethered to DNA, the receptor can either positively or negatively regulate target gene transcription (O'Lone, Frith, Karlsson, & Hansen, 2004). ERα regulates many genes that are involved in mammary gland development, and their altered expression is associated with breast cancer progression (Welboren, Sweep, Span, & Stunnenberg, 2009).

In addition to the classical genomic actions exerted by E2, E2 is also known to activate various growth factors through membrane-initiated steroid signaling (MISS). Figure 1.5 depicts various ER signaling pathways (Winter, Jung, Keller, Gregory, & Diederichs, 2009). Apart of genomic and non-genomic actions of estrogen on estrogen receptor, emerging studies suggest that posttranslational modifications, especially phosphorylation can also regulate function of estrogen receptor. Studies have shown that estrogen receptor can be activated in absence of ligand by MAPK, mTOR and AKT kinases. These kinases phosphorylate ERα at Ser 118 or Ser 167. Therefore, these kinases have been implicated in endocrine resistance to tamoxifen(Hayes & Lewis-Wambi, 2015). Due to several levels of complexity to the action of ERα in breast cancer cells, many patients receiving endocrine treatments develop resistance to therapy. Different molecular events

have been reported to cause resistance, such as ligand independent activation of ERα, overexpression of epidermal growth factor receptor or v-erb-b2 erythroblastic leukemia viral oncogene homolog 2 (ERBB2), over expression of co-activators such as NCOA3, FOXA1; and DNA methylation at the ERα promoter (6). Figure 1.6 describes various mechanisms responsible for tamoxifen resistance(Hayes & Lewis-Wambi, 2015).

1.5 miRNAs in Cancer Therapeutics

Approximately 2000 miRNAs have been identified in humans (www.mirbase.org). Despite their small number, they regulate 30% of all genes. Therefore, they play crucial role in almost all biological processes (Iorio et al., 2005). miRNAs have been identified to play a crucial role in various human diseases, and therefore, they are interesting for drug discovery. One major limitation of novel drug discovery is drug target selection. Less than 1% of all approved drugs do not bind to proteins, whereas more than 80% of all drugs target only two protein classes: enzymes or receptors(Hopkins & Groom, 2002). Furthermore, not every protein can be targeted or modulated by a drug molecule. By contrast, intervention at the miRNA level may allow specific manipulation of every protein population: miRNA inhibitors induce selective upregulation of one protein population; by contrast, miRNA mimics induce gene silencing, thus resulting in downregulation of the target protein. Hence, miRNAs can be potential drug candidate for ‘undruggable’ proteins, enabling the cure of diseases, which, at present, seems impossible(Schmidt, 2014). Additionally, most drug molecules only target single molecule or a signaling pathway. Hence, such agents frequently face

resistance issues. Also, diseases such as cancers are known to possess cellular and molecular heterogeneity and therefore are notoriously known for resistance and relapse following chemotherapy. miRNAs due to their ability of targeting multiple pathways at same time offers another crucial advantage over traditional drug therapy. As a result, miRNAs are regarded as high-value drug targets. Several miRNA and RNAi based therapeutic are in fact currently under clinical trials. These agents are listed in Table 1(Chakraborty et al., 2017).

1.6 Goals of the Project

The overall goal of this project is to understand the role of miR-489 in breast cancer for the development of novel prognostic biomarker or therapeutic agent. Previously, we have established miR-489 as a tumor suppressor miRNA in breast cancer by targeting HER2 signaling pathway (Patel et al., 2016). Since then, several groups have demonstrated its tumor-suppressive role in many different cancers including gastric cancer, lung cancer, ovarian cancer, hepatic cancer, osteosarcoma, and bladder cancer (X. Chen et al., 2016; Kikkawa et al., 2010; J. Li et al., 2016; Wu et al., 2014; Yuan et al., 2017; Zhang et al., 2016). Remarkably, miR-489 has been reported to induce cell-cycle arrest and apoptosis, inhibit metastasis and epithelialto-mesenchymal transition in context-dependent manner. A thorough understanding of miR-489–mediated tumor suppression in a specific cancer will be valuable in evaluating the possibility of miRNA-489–based therapy. Hence, this study was aimed to identify novel pathways and molecular targets affected by miR-489, which will lead to better understanding of miR-489–mediated tumor suppression.

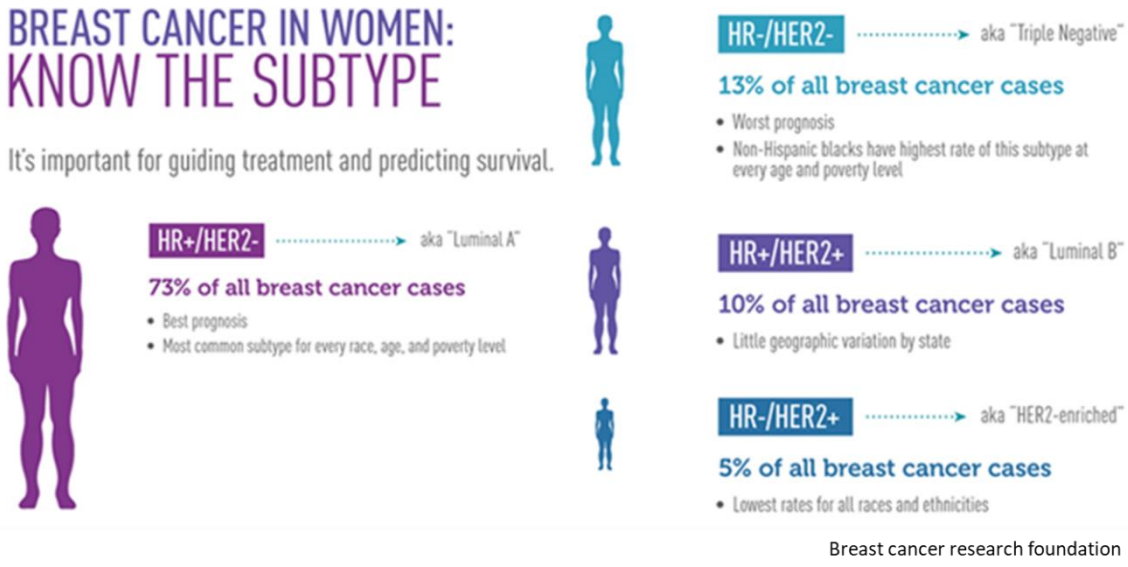

Figure 1.1: Breast cancer subtypes and their prevalence. Breast cancer is broadly classified in four subtypes based on surface receptor expression. Hormone positive breast cancer is most prevalent subtype with best prognosis and response to therapy. HER2-enriched cancer shows aggressive phenotype but respond well to HER2 targeted therapies while triple negative breast cancer tend to have the worst prognosis among all due to lack of specific target receptor or protein. This figure is adapted from breast cancer research foundation.

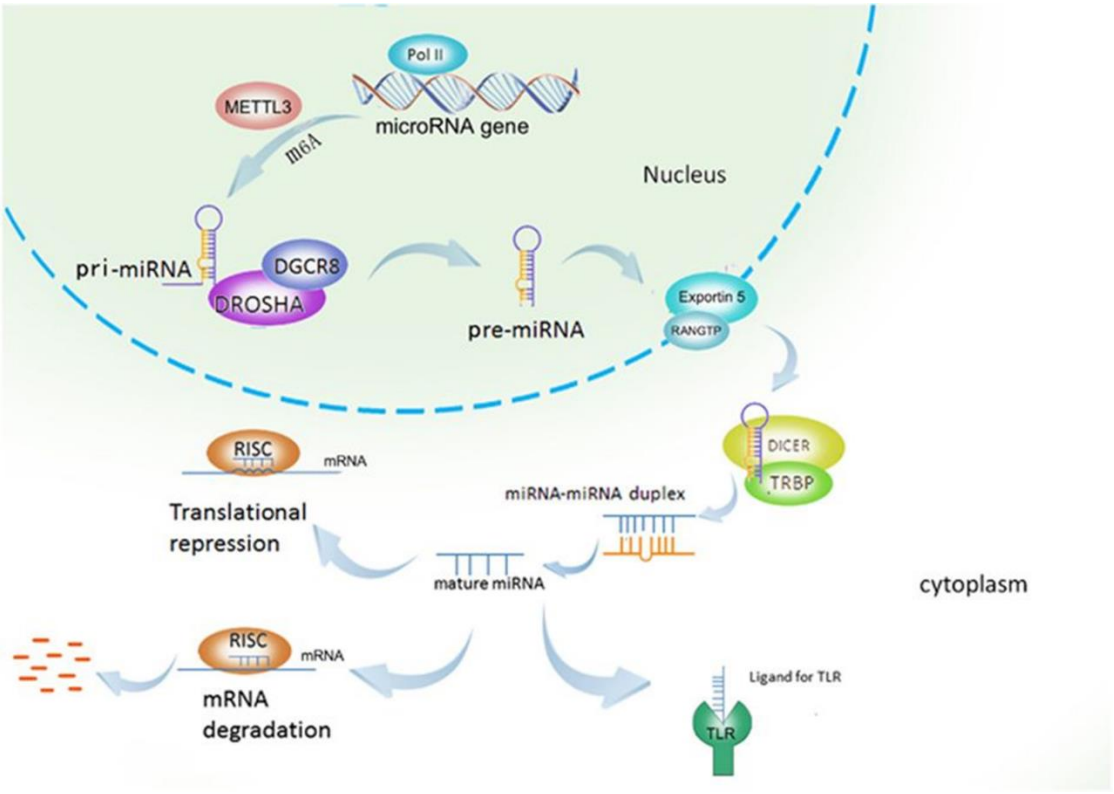

Figure 1.2: General mechanism of miRNA biogenesis. The canonical miRNA maturation includes the production of the primary miRNA transcript (pri-miRNA) by RNA polymerase II or III and cleavage of the pri-miRNA transcript (pri-miRNA) by Drosha-DGCR8 in the nucleus. The resulting pre-miRNA is exported by Exportin5-RAN-GTP. In the cytoplasm, the RNase Dicer in complex with the double-stranded RNA-binding protein TRBP cleaves the pre-miRNA hairpin to mature length. The functional strand of the mature miRNA is loaded together with Argounaute (Ago2) proteins into the RNA-induced silencing complex (RISC) where it guides RISC to silence its target mRNAs through mRAN cleavage, translational repression or deadenylation. This figure has been adapted from (Peng & Croce, 2016)

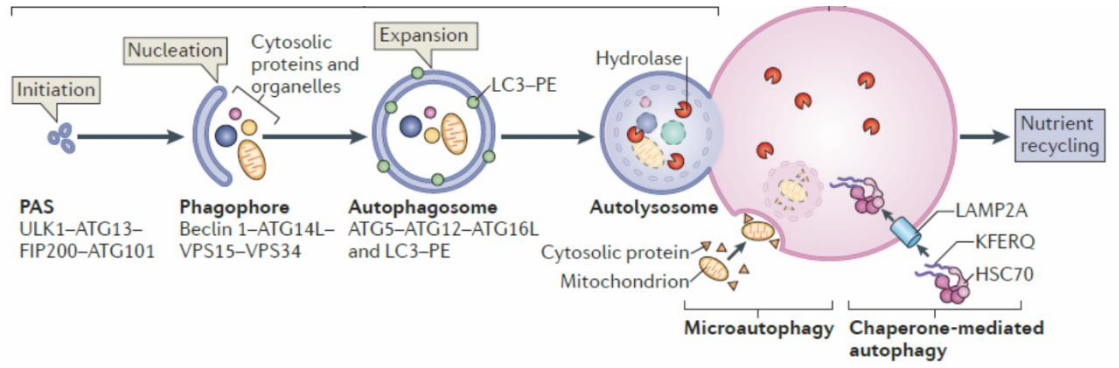

Figure 1.3: Overview of mammalian autophagy pathway. Autophagy initiation begins with the formation of the phagophore assembly site (PAS). This is mediated by the UNC51-like kinase (ULK) complex, which consists of ULK1 (or ULK2), autophagy-related protein 13 (ATG13), Further nucleation requires the class III PI3K complex, which is composed of the vacuolar protein sorting 34 (VPS34) PI3K, along with its regulatory subunits ATG14L, VPS15 and beclin 1. Phagophore membrane elongation and autophagosome completion requires two ubiquitin-like conjugation pathways. The first produces the ATG5–ATG12 conjugate, which forms a multimeric complex with ATG16L, whereas the second results in the conjugation of phosphatidylethanolamine (PE) to LC3. PE-conjugated LC3 (LC3–PE) is required for the expansion of autophagic membranes, their ability to recognize autophagic cargoes and the fusion of autophagosomes with lysosomes. The resulting autophagosome fuses with lysosomal compartments, ultimately leading to formation of the autolysosome. This figure has been adapted from (Kaur & Debnath, 2015)

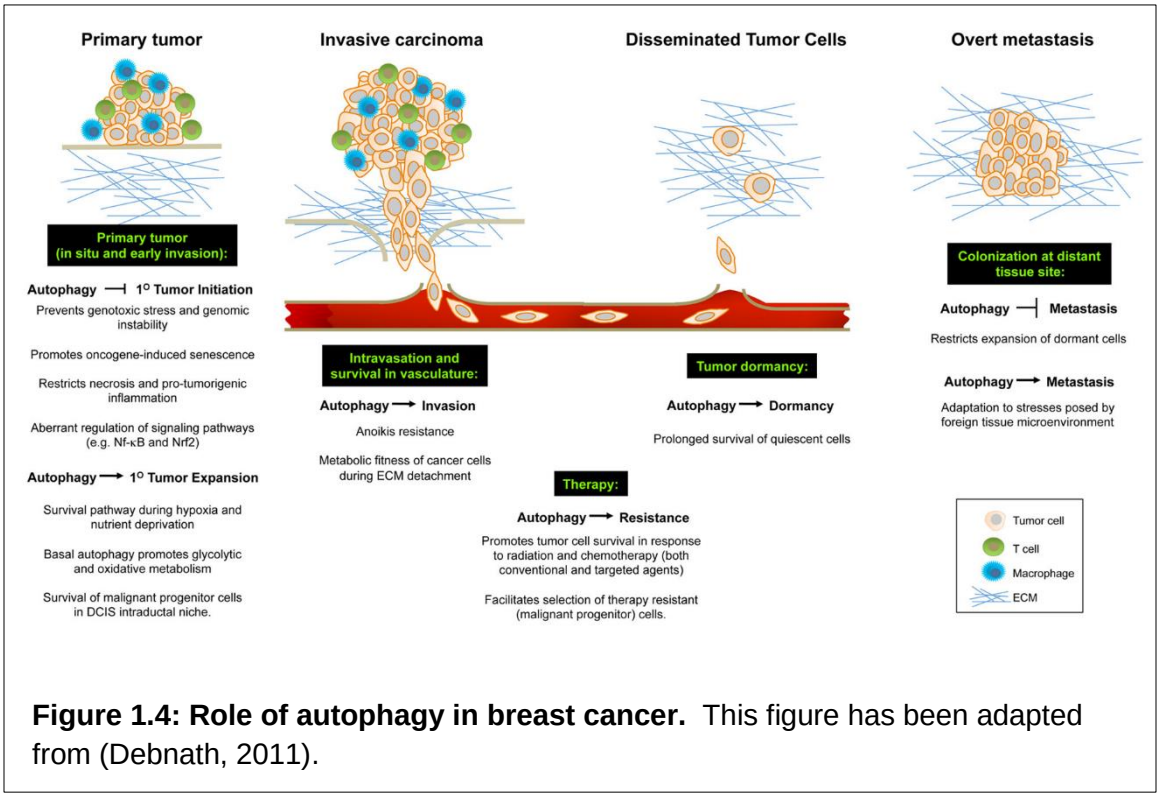

Figure 1.4: Role of autophagy in breast cancer. This figure has been adapted from (Debnath, 2011).

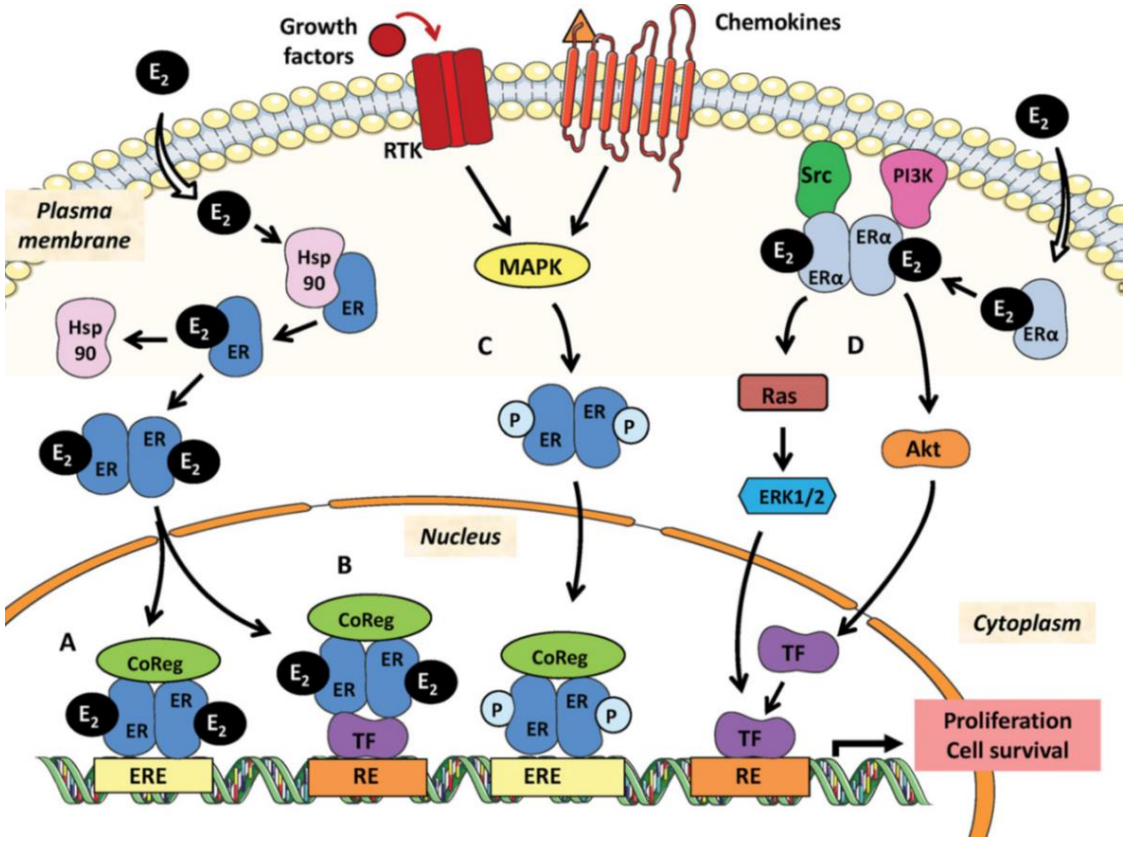

Figure 1.5: Estrogen Receptor signaling pathways. The figure depicts various ER signaling pathways. Pathway A is called the classical genomic pathway, also known as Nuclear Initiated Steroid Signaling (NISS), where estrogen-ERα activates or repress transcription of estrogen response genes. Pathway B, the nonclassical genomic pathway, involves ER interactions with other transcription factors like AP-1, SP-1 or NFκB. Pathway C is E2-independent activation of ER through phosphorylation induced by growth factors such as MAPK, AKT, EGFR. Pathway D, known as Membrane Initiated Steroid Signaling (MISS), involves a small pool of membrane associated that, through recruitment of protein kinases (Src and PI3K), activate signaling cascades (Akt, MAPK). All these pathways converge to cell proliferation and survival. This figure has been adapted from (Le Romancer et al., 2011).

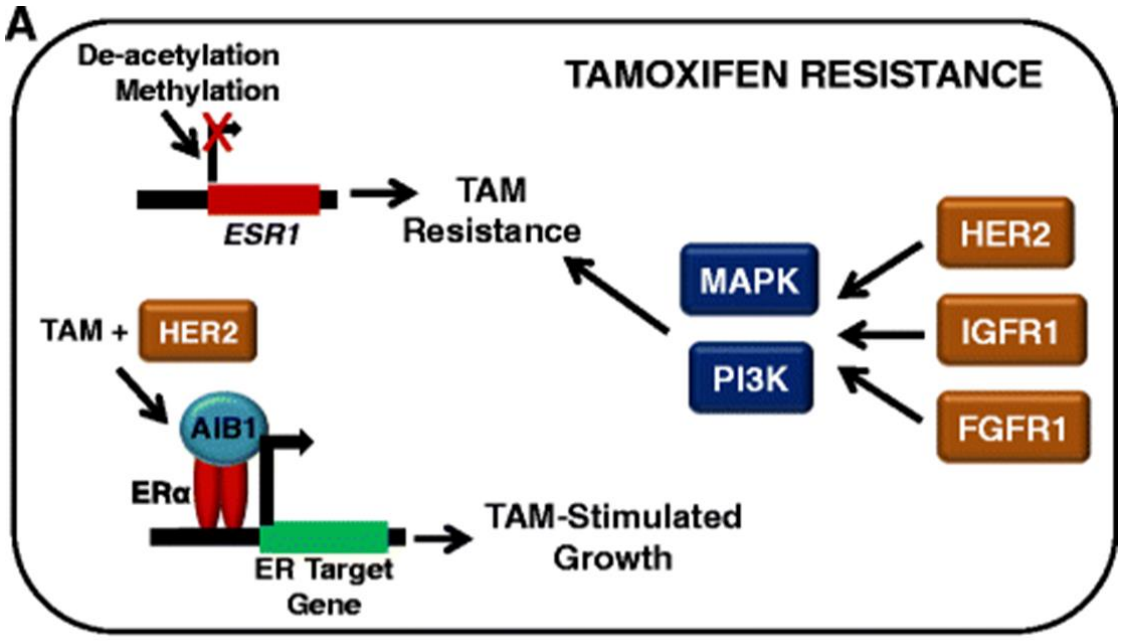

Figure 1.6: Mechanisms of Tamoxifen resistance. One of the mechanisms of tamoxifen (TAM) resistance involves loss of estrogen receptor (ER) alpha expression through epigenetic silencing of ESR1 gene. Tamoxifen-resistant growth is also stimulated by the upregulation of growth factor signaling pathways (HER2, IGFR1, and FGFR1) and subsequent activation of the mitogen-activated protein kinase (MAPK) cascade or phosphoinositide 3-kinase (PI3K) pathway. Finally, tamoxifen has even been shown to stimulate the growth of breast cancer cells when bound to certain coactivators, such as AIB1, and this is especially true in HER2-expressing cells. This figure has been adapted from (Hayes & Lewis-Wambi, 2015).

Table 1.1: List of miRNAs under clinical trials or under development phase for prognostic marker or therapeutic agent. This figure has been adapted from (Chakraborty, Sharma, Sharma, Doss, & Lee, 2017)

Therapeutic miRNAs	Indication	Biopharmaceutical Company	Remarks
Miravirsen	the indication of the hepatitis C virus (HCV) infection	Santaris Pharma	phase IIa clinical trial
MRX34	for the treatment of a variety of cancers such as colon cancer, non-small-cell lung cancer (NSCLC), hepatocellular carcinoma, cervical cancer, ovarian cancer, etc.	Mirna Therapeutics	phase 1 clinical trial halted because of immune responses
RG-101	for the treatment of HCV	Regulus Therapeutics	an owned GalNAc-conjugated anti-miR
RG-012	for the treatment of Alport syndrome	Regulus Therapeutics	in the pipeline to initiate clinical trial phase II
MGN-1374	for the treatment of post-myocardial infarction remodeling	miRagen Therapeutics	targets miR-15 and miR-195; it is in the preclinical stage
MGN-2677	for the treatment of vascular disease	miRagen Therapeutics	targets miR-143/145; it is in the pipeline
MGN-4220	for the treatment of cardiac fibrosis	miRagen Therapeutics	targets miR-29; it is in the pipeline
MGN-4893	for the treatment of disorders like abnormal red blood cell production such as polycythemia vera	miRagen Therapeutics	targets miR-451; it is in the pipeline
MGN-5804	for the treatment of cardiometabolic disease	miRagen Therapeutics	targets miR-378; it is in the pipeline
MGN-6114	for the treatment of peripheral arterial disease	miRagen Therapeutics	targets miR-92; it is in the pipeline
MGN-9103	for the treatment of chronic heart failure	miRagen Therapeutics	targets miR-208; it is in the pipeline

This table has been adapted from (Chakraborty, Sharma, Sharma, Doss, & Lee, 2017)

CHAPTER 2

MIR-489 REGULATES CELL VIABILITY AND CHEMO-RESISTANCE BY INHIBITING AUTOPHAGY

2.1 INTRODUCTION

Breast cancer is a heterogeneous disease with several subtypes identified by presence or absence of surface receptors. Traditionally, breast cancer is classified in three major subtypes namely, Hormone positive, HER2 positive (HER2+) and Triple negative breast cancer (TNBC). (Heiser et al., 2012; Higgins & Baselga, 2011; Shah & Chen, 2014). Recent gene expression studies identified novel molecular signatures within the subtype suggesting patients with same subtype of breast cancer may show transcriptional and genomic heterogeneity and therefore may not respond similarly. Due to the discrepancies in transcriptional and genomic heterogeneity alnog with complex resistance mechanisms, the development of broad-range treatments has been restricted. Therefore, identification of a single therapeutic agent targeting multiple oncogenic and prosurvival pathways would provide a promising future cancer therapy. Since a single miRNA targets multiple pathways and controls gene expression of many[1]

[1] Soni M, Patel Y, Markoutsa E, Jie C, Liu S, Xu P, et al. *Autophagy, Cell Viability and Chemo-resistance are Regulated by miR-489 in Breast Cancer*. Molecular cancer research: MCR 2018. Doi: 10.1158/1541-7786.MCR-17-0634. Reprinted here with permission from the publisher.

genes, they could offer considerable therapeutic options. miRNAs are small noncoding RNAs that posttranscriptionally regulate expression of their target genes. Because miRNAs regulate many genes, their dysregulation have been shown to cause various pathologic conditions including cancer. Identifying such dysregulated miRNAs and their targets might provide insights for the development of novel therapy.

Autophagy has recently received great attention in the field of cancer and chemo-resistance due to its pro-survival role under stressful conditions.The role of autophagy in cancer remains controversial, as it exhibits tumor suppressive and tumor promoting activity in context and molecular subtype dependent manner. Studies have reported that autophagy protects cancer cells from metabolic stress such as starvation or hypoxia (Eskelinen, 2011). Due to its cytoprotective function it enables cancer cells to cope with cytotoxic or other stress induced by treatment. Indeed, autophagy inhibition has been shown to reverse resistance to several chemotherapeutic agents. Currently, chloroquine, an anti-malarial drug, is under clinical trials for adjuvant therapy to reduce resistance via autophagy inhibition in various cancers. Many miRNAs have also been shown to sensitize cancer cells to chemotherapy by inhibiting autophagy. For example, miR-200b has been shown to reverse autophagy mediated resistance to docetaxel by targeting ATG12 (Pan et al., 2015), while miR-140-5p disrupts cancer stem cell growth in colorectal cancer via autophagy inhibition (Wei, Cao, Deng, Su, & Cai, 2016; Zhai, Fesler, Ba, Wu, & Ju, 2015). Understanding the role of miRNA in autophagy mediated

cancer cell survival and resistance may provide detailed insight on potential miRNA based therapies.

In the present study, for the first time we reported that miR-489 inhibits autophagy by affecting multiple genes involved in the process. We further found that miR-489 reduces tumor cell survival and sensitizes tumor cells under metabolic stress induced by starvation via inhibiting autophagosome degradation. Moreover, we found that miR-489 can also sensitize breast cancer cells to doxorubicin via autophagy inhibition. From the combination of our in-vitro and in-vivo studies, we report that miR-489 inhibits autophagy by targeting ULK1 and LAPTM4B and sensitizes tumor cells to doxorubicin by inhibiting doxorubicin induced cytoprotective autophagy and LAPTM4B expression.

2.2 RESULTS

2.2.1 IDENTIFICATION OF NOVEL PATHWAYS AND TARGETS REGULATED BY MIR-489 IN BREAST CANCER.

Previously, we established that miR-489 functions as tumor suppressor miRNA in HER2+ breast cancer by directly inhibiting HER2 signaling pathway. To identify novel pathways regulated by miR-489, we first examined effect of miR-489 on cell viability of 12 different breast cancer cell lines covering all three subtypes of breast cancer. Our MTT based cell viability assay showed that miR-489 significantly reduces cell viability, although to different extent, in all three subtype of breast cancers (Fig. 2.1). Interestingly, some of the TNBC cell lines were much more sensitive to miR-489 compared to HER2+ cell lines. This result suggests

miR-489 targets other pathways involved in proliferation and survival besides the HER2 signaling pathway.

To identify novel genes regulated by miR-489 in breast cancer, we conducted microarray analysis by transiently transfecting control scramble siRNA (scr) or miR-489 mimic (mimic) in T47D cell line (Fig. 2.2A). Our gene expression analysis also revealed multiple pathways affected by miR-489. We observed that several genes involved in autophagy were affected by forced expression of miR-489 (Fig. 2.2B). We utilized target prediction tools such as miRwalk and TargetScan to identify potential miR-489 targets involved in autophagy. Consistent with our microarray data, target prediction tools also suggested multiple genes involved in regulation of autophagy such as ULK1, ATG4A, LAPTM4B, ATG4C, ATG2B, ATG3, ATG5, ATG7, ATG12 and ATG14 as potential target of miR-489. (Fig. 2.2C). Interestingly, miR-489 mediated cytotoxicity was associated with distinct morphological features, including the appearance of dense intracellular vacuolar structures (Fig. 2.3). This further indicated a possible perturbation of autophagy. To investigate effect of miR-489 on autophagy, we transfected breast cancer cell lines with non-targeting scramble miRNA (scr) miR-489 mimic (mimic) and miR-489 inhibitor (inh) and monitored the effect on autophagy marker LC3B using western blot. Conversion of non-lipidated soluble LC3B (LC3B-I) to phosphatidylethanolamine-conjugated LC3B (LC3B-II) serves as a sensitive indicator of autophagy (Klionsky et al., 2016). We found significant accumulation of LC3B-II upon miR-489 overexpression, while inhibition of miR-489 completely reversed this deposition (Fig. 2.4A-B).

We observed this effect in HER2 positive, estrogen positive and triple negative breast cancer cells suggesting autophagy modulation by miR-489 is independent of breast cancer subtype. In summary, we identified autophagy as a novel pathway modulated by miR-489 expression.

2.2.2 MIR-489 INHIBITS AUTOPHAGY MAINLY BY BLOCKING MATURATION STEP

Autophagy is complex multistep process. Numerous assays have been developed to precisely decipher the effect on basal autophagy or autophagic flux. Although change in LC3B-I and II is an indicator of change in autophagy flux, it fails to provide conclusive information about autophagy activation or inhibition (Klionsky et al., 2016). Deposition of LC3B-II can be caused by induction of autophagosome (AP) formation or blockage of autophagosome degradation via fusion of autophagosome with lysosome (Autolysosome). To distinguish these two possibilities, we first used Bafilomycin A1 immunoblot. Bafilomycin A1 is a lysomotropic agent which inhibits the V-ATPase responsible for acidification of the lysosome, and prevents fusion of autophagosomes and lysosomes (Klionsky et al., 2016). Comparison of LC3-II levels in the absence and presence of Bafilomycin A1 allows the effects of formation and degradation to be uncoupled. As shown in Figure 2.5A, 2.5B and 2.5C, no significant difference was detected between double treatment and lysomotropic agent alone at 48hrs and 72hrs time points, suggesting that miR-489 might be blocking degradation of autophagosome. Moreover, our finding on the clearance of cargo protein p62, another distinctive feature of autophagy, also indicated blockage of autophagosome degradation (Fig. 2.5D.

2.5E and 2.5F) (Klionsky et al., 2016; Mizushima, Yoshimori, & Levine, 2010). These results suggest that miR-489 inhibits autophagy by blocking formation of autophagosome and lysosome fusion (Autolysosome).

We then asked whether autophagy inhibitors that block autophagosome formation such as 3-methyladenine (3-MA) or siATG5 can prevent miR-489 induced autophagosome deposition. Consistent with previous observations, 3-MA and ATG5 knockdown indeed attenuated miR-489 induced p62 and LC3B-II deposition (Fig. 2.6A, 2.6B, 2.6C). Conversely, in conditions such as starvation that induces autophagosome synthesis, miR-489 restoration further increased LC3B-II and p62 deposition suggesting blockage at maturation step (Fig. 2.6D). Interestingly, this accumulation was comparable to that of Bafilomycin A1, which also blocks the fusion step. To further confirm that miR-489 inhibits formation of autolysosome (AL) by blocking fusion of autophagosome and lysosome, we used common dual fluorescent LC3B reporter, which expresses an N-terminal fusion of mCherry and GFP to human LC3B (Klionsky et al., 2016). This reporter system enables real time monitoring of autophagic flux. Since, low pH quenches GFP fluorescence, AL is seen as distinct red aggregates, while AP appears as yellow aggregates due to overlap of red and green fluorescence. (Fig. 27A). If the autophagy pathway is in flux, then these yellow aggregates will be transient as APs fuse with acidic lysosomes to form ALs, in which the low pH quenches GFP fluorescence, resulting in rapid accumulation of dense red aggregates. However, blockage of autophagy at the fusion step results in accumulation of yellow puncta. Consistent with our earlier results, miR-489 mimic transfected cells show presence

of more yellow puncta compared to control, further suggesting miR-489 causes accumulation of AP by blocking fusion step (Fig. 2.7B, 2.7C). Together, these results indicate that miR-489 inhibits autophagy mainly by blocking the fusion of APs to lysosome.

2.2.2 miR-489 INHIBITS AUTOPHAGY BY DIRECTLY TARGETING ULK1 AND LAPTM4B

Next, we seek to identify autophagy related genes that are directly targeted by miR-489. Our gene expression analysis along with target predication algorithm analysis revealed multiple genes as potential targets of miR-489 that are directly involved in autophagy pathway such as ATG4A, ULK1, ATG4C, LAPTM4B, EIG121, VMA21, WIPI1, ATP6V1C1 and EI24 (Fig. 2.2B). To validate our microarray results, we performed qRT-PCR after transient transfection of miR-489 or control siRNA in indicated breast cancer cell lines (Fig. 2.8A). As shown in the figure, the expression of four out of six genes were greatly diminished upon miR-489 reconstitution in multiple breast cancer cell lines. To further confirm, we performed western blot analysis and found downregulation of LAPTM4B and ULK1 but not EI24 in all three cell lines (Fig. 2.8B). We were also interested in investigating whether knockdown of endogenous miR-489 would affect target genes expression. Indeed, miR-489 inhibitor efficiently increased the amounts of ULK1 and LAPTM4B (Fig. 2.8B). We then performed 3'UTR luciferase assay to identify direct targets. Our assay revealed that ULK1 (35% reduction, p-value = 0.0184) and LAPTM4B (40% reduction, p-value = 0.0038) are direct target of miR-489 while ATG4A might be an indirect target (Fig. 2.9A and 2.9B). Since, ULK1

and LAPTM4B are positive regulators of autophagy, these results further suggest that miR-489 negatively regulates autophagy.

2.2.3 MIR-489 REDUCES TUMOR CELL SURVIVAL AND SENSITIZES TUMOR CELLS UNDER METABOLIC STRESS INDUCED BY STARVATION

Since miR-489 inhibited autophagy, we seek to investigate contribution of autophagy inhibition in tumor suppressive effect of miR-489 and whether miR-489 forced expression of miR-489 results in increased sensitivity of tumor cells to insults that induce autophagy as survival mechanism. Since starvation is a fairly common insult that requires autophagy for survival, we examined if miR-489 over expression can reduce tumor cell survival under starvation. We selected MDA-MB-231 cells for this study as previous study has showed that MDA-MB-231 cells are more resistant to starvation compared to other breast cancer cell lines. Study also showed that this aggressive cell line is sensitive to autophagic induction and additionally possesses the ability to proliferate following nutrient deprivation (Y. I. Li et al., 2016). Consistent with this study we also observed that MDA-MB-231 cells were much more resistant to starvation compared to T47D and HCC1954 cells. We transfected MDA-MB-231 cells with scr, mimic or inh under complete media or starvation and performed cell survival assay at indicated time points. We found that miR-489 over expression significantly reduced survival under starvation (p-value = 0.0001) (Fig. 2.10A and 2.10B). miR-489 over expression caused more than 20% growth inhibition after 72hrs of transfection under starvation compared to nutrient rich condition (Fig. 2.10C). Interestingly, this cytotoxic and cytostatic effect began as early as 24hrs under starvation. While this was not observed until

48hrs in nutrient rich medium. Consistent with previous observations, starvation indeed induce autophagy and miR-489 restoration showed stronger autophagy inhibition under starvation as indicated by increased accumulation of LC3B-II and p62 in western blot analysis (Fig. 2.10D). Western blot results also showed significant increase in cleaved caspase 3 upon miR-489 over expression under starvation. We also performed similar experiment on T47D and HCC1954 cells (Fig. 2.10A-F). Both cell lines were significantly affected under starvation (2.10B, 2.10E). We tested whether miR-489 inhibition can protect these cells under stress induced by starvation. miR-489 inhibition marginally increased survival under starvation in HCC1954 (Fig. 2.11E, 2.11F). Interestingly, this protective effect was more prominent in T47D cells (Fig. 2.11B, 2.11C, p-value=0.0017) that possesses higher endogenous miR-489.

2.2.4 AUTOPHAGOSOME ACCUMULATION BY MIR-489 IS PARTIALLY RESPONSIBLE FOR ITS TUMOR SUPPRESSIVE EFFECT.

To examine whether cytotoxic effect of miR-489 is mediated through autophagy inhibition, we blocked autophagy at different stages using pharmacological and RNA interference approach under nutrient rich condition and under starvation and assessed effect of miR-489 on autophagic flux and cell viability. We observed that blocking early stages of autophagy by 3-MA or siATG5 resulted in significant attenuation of cytotoxic effect of miR-489 (Fig. 2.12A-2.12D). This rescue effect was more pronounced under starvation. In fact, 3-MA and siATG5 treatment almost completely prevented miR-489 induced apoptosis as evidenced by western blot analysis of cleaved caspase 3 (Fig. 2.12C, 2.12D).

However, autophagy blockage at later stage by Bafilomycin A1 did not rescue cells from miR-489 induced death. Rather, it mildly synergized the growth inhibition (Fig. 2.12A, 2.13B). These results suggest that increased autophagosome accumulation by miR-489 may account for its cytotoxic effect on these cells. Previous reports have shown that autophagosome accumulation confers cytotoxicity in cancer cells and blocking autophagosome synthesis by chemical inhibitor or by genetic ablation alleviates this cytotoxicity (Button, Roberts, Willis, Hanemann, & Luo, 2017; Choi, Jo, Lee, & Choi, 2011). Starvation is known to induce autophagosome formation. Hence, restoring miR-489 under starvation resulted in pronounced increase in autophagosome accumulation. This might explain why miR-489 further sensitized cells under starvation. We also observed greater rescue from miR-489 induced death under starvation upon blocking autophagosome synthesis by 3-MA or siATG5. Further confirming the idea that miR-489 induced autophagosome accumulation is crucial for its cytotoxic effect. Previous studies have also reported similar observations where perturbation of earlier stages of autophagy attenuated effect of autophagy inhibitors that block later stages (Geng, Kohli, Klocke, & Roth, 2010).

In summary, these data suggest that miR-489 mediated autophagosome accumulation is at least partially responsible for its cytotoxic effect and it further sensitizes cancer cell death under metabolic stress induced by starvation due to further increase in autophagosome accumulation.

2.2.5 miR-489 INHIBITS DOXORUBICIN INDUCED CYTOPROTECTIVE AUTOPHAGY AND SENSITIZES BREAST CANCER CELLS TO DOXORUBICIN

Doxorubicin has been previously shown to induce cytoprotective autophagy (Chittaranjan et al., 2014; Kim et al., 2014). We examined autophagic flux upon miR-489 restoration in doxorubicin treated MDA-MB-231 and HCC1954 cells. Consistent with previous results, we found that doxorubicin indeed increased autophagic flux (Fig. 2.14A, 2.14B). This cytoprotective autophagy was blocked by miR-489 as indicated by increased LC3B-II levels. Previous studies have demonstrated that autophagy inhibition sensitizes breast cancer cells to doxorubicin (Chittaranjan et al., 2014; Kim et al., 2014; Zhou et al., 2015).

We next tested whether miR-489 could sensitize breast cancer cells to certain front-line chemotherapeutic agents that have been shown to induce cytoprotective autophagy. Few studies have demonstrated that miR-489 is severely down regulated in cisplatin and doxorubicin resistant breast cancer cell lines and tumors (X. Chen et al., 2016; Wu et al., 2014). We hypothesized that restoring miR-489 can sensitize breast cancer cells to these chemotherapeutic agents. Using MTT based cell viability assay, we found miR-489 restoration sensitized MDA-MB-231, MDA-MB-468, HCC1954 and MDA-MB-453 to cisplatin and doxorubicin (Fig. 2.14C-2.14F). We observed substantial sensitization of doxorubicin upon miR-489 restoration, while only a mild sensitization effect was observed with cisplatin. Remarkably, double treatment of miR-489 and doxorubicin resulted in almost complete death of MDA-MB-231 and MDA-MB-453 cells (Fig. 2.14C, 2.14D).

2.2.6 AUTOPHAGOSOME ACCUMULATION IS NECESSARY FOR MIR-489 MEDIATED DOXORUBICIN SENSITIZATION

Previous studies have demonstrated that autophagy inhibition sensitizes breast cancer cells to doxorubicin (Chittaranjan et al., 2014; Kim et al., 2014; Zhou et al., 2015). Consistent with these results, we observed sensitization with autophagy inhibitor Bafilomycin A1 and siATG5 (Fig. 2.15A, 2.15B). Several studies have demonstrated that autophagy inhibition at later stage is more effective in sensitizing tumor cells against chemotherapy (Kanematsu et al., 2010; C. Li et al., 2015; Shingu et al., 2009). Consistent with these results, we observed only mild sensitization with siATG5 while miR-489 and Bafilomycin A1 resulted in higher sensitization compared to siATG5. Interestingly, we observed greater sensitization with miR-489 compared to Bafilomycin A1. We then seek to examine role of autophagy in miR-489 mediated doxorubicin sensitization. Blocking autophagy at early step by siATG5 attenuated miR-489 induced drug sensitization (Fig. 2.15A) while blocking late stage autophagy by Bafilomycin A1 further showed mild sensitization at higher doxorubicin concentration (Fig. 2.15B). Furthermore, although ATG5 knockdown attenuated sensitization by miR-489, it failed to completely prevent this sensitization (see Fig. 5C, 0.5μM Dox. treatment). These data suggest that miR-489 may also inhibit additional pathway besides autophagy that render cells resistant to doxorubicin. Apart from inducing autophagic flux, LAPTM4B has been shown to promote chemoresistance (de Ronde et al., 2013; L. Li et al., 2010; Y. Li et al., 2011; Y. Li et al., 2010). Therefore, we seek to examine role of LAPTM4B in miR-489 mediated doxorubicin sensitization.

2.2.7 RESTORATION OF LAPTM4B ATTENUATES MIR-489 INDUCED AUTOPHAGY INHIBITION, APOPTOSIS AND DOXORUBICIN SENSITIZATION.

To directly access role of LAPTM4B, we stably overexpressed LAPTM4B in MDA-MB-231 cell lines (Fig. 2.16A). As suggested by previous studies, LAPTM4B restoration increased autophagic flux and attenuated miR-489 induced autophagy inhibition (Fig. 2.16C). Surprisingly, LAPTM4B restoration increased survival by 23% (p-value = 0.0005) upon miR-489 overexpression (Fig 2.16B). LAPTM4B overexpression not only rescued cells from miR-489 induced apoptosis but also increased survival by 17% (p-value = 0.0175) upon doxorubicin treatment and 33% (p-value = 0.001) upon combination treatment (Fig. 2.16D). To validate this result, we performed western blot analysis to monitor apoptotic marker cleaved caspase 3 and detected significant reduction in cleaved caspase 3 in LAPTM4B overexpressing cell line (Fig. 2.16E).

2.2.8 MIR-489 CAUSES DOXORUBICIN REDISTRIBUTION TO NUCLEUS

LAPTM4B has been shown to sequester doxorubicin in lysosomes preventing their entry into nucleus thereby rendering it less effective (Y. Li, Iglehart, Richardson, & Wang, 2012; Y. Li et al., 2011; Y. Li et al., 2010; Meng et al., 2016). We tested whether miR-489 can induce redistribution of doxorubicin in MDA-MB-231 cells and found that miR-489 indeed increased doxorubicin localization in nucleus (Fig. 2.17A, 2.17B and 2.17C). We then assessed effect of miR-489 on lysosomal integrity. We utilized Acridine orange dye which specifically stains lysosomal-endosomal organelles red. Our flow cytometry and confocal microscopy

results showed reduction in red fluorescence upon miR-489 restoration (Fig. 2.17D and 2.17E). These results indicate that miR-489 affects lysosomal integrity and that this may be one of the mechanism through which miR-489 sensitizes cell to doxorubicin. Collectively, these results indicate that miR-489 sensitizes MDA-MB-231 cells to doxorubicin via inhibiting doxorubicin induced cytoprotective autophagy and through doxorubicin redistribution induced by LAPTM4B downregulation.

2.2.9 RESTORATION OF ULK1 RESCUES CELLS FROM CYTOTOXIC EFFECT OF MIR-489 BUT NOT OF DOXORUBICIN

We also examined role of ULK1 in miR-489 induced doxorubicin sensitization. ULK1 overexpression provided mild but significant rescue from the cytotoxic and cytostatic effect of miR-489 (Fig. 2.18A and 2.18B), but it could not rescue cells from doxorubicin (Fig. 2.18C). A modest rescue was observed in double treatment which may be due to rescue from the effect of miR-489.

2.2.10 MIR-489 SENSITIZES BREAST CANCER CELLS TO CHEMOTHERAPY *IN-VIVO*

Given the in-vitro findings and clinical significance, we tested whether miR-489 could sensitize tumors to doxorubicin in-vivo. To explore the possibility of using miR-489 for therapy, we developed a nanoparticle delivery system to deliver miR-489 into tumor cells (Patel et al., 2016). In-vitro treatment with miR-489 packaged nanoparticle inhibited target genes (Fig. 2.19A), indicating that nanoparticles can effectively deliver miR-489 into tumor cells. Consistent with our in-vitro data, miR-489 indeed sensitized cells to doxorubicin in-vivo (Fig. 2.19B).

Tumor growth in mice treated with doxorubicin alone was moderately reduced compared to control, while mice treated with miR-489 exhibited a significant reduction in tumor growth compared to control (p-value = 0.0441) and doxorubicin (p-value = 0.0284). Tumor growth in mice treated with the combination of doxorubicin and miR-489 was significantly reduced compared to control (by more than 75%; p-value = 0.0066), monotherapy with doxorubicin (by more than 40%; p-value<0.0001), or miR-489 alone (by more than 20%; p-value = 0.0326) (Fig. 2.18B). Our qRT-PCR analysis on tumor samples confirmed down regulation of ULK1 and LAPTM4B mRNA (Fig. 2.19C). Our immunohistochemistry data revealed reduced cytoplasmic staining of LAPTM4B and significant reduction in number of Ki-67-positive cells in combination treatment when compared to the control tumors (Fig. 2.20A and 2.20B, p-value<0.0001). Western blot of tumor samples indicated autophagy inhibition and down-regulation of ULK1 and LAPTM4B (Fig. 2.20C). Together, these data demonstrated that miR-489 delivered through nanoparticles inhibits tumor growth and sensitizes tumor cells to doxorubicin in xenografts.

2.2.11 miR-489 EXPRESSION IS INVERSELY CORRELATED WITH LAPTM4B IN PATIENT SAMPLES AND PREDICTS BETTER SURVIVAL IN 8Q22 AMPLIFIED BREAST CANCERS.

To further define the clinical relevance of our findings, we examined miR-489 and LAPTM4B expression in breast tissues from breast cancer patients (n=14). We found significant inverse correlation between expression of miR-489 and LAPTM4B (Fig.2.21A). Similarly, in-silico analysis on primary tumors revealed

a strong inverse correlation between miR-489 and LAPTM4B expression with a p-value of 0.0000413 (Fig. 2.21B).

Considerable clinical evidences suggest that LAPTM4B over-expression promotes autophagy and chemoresistance (Y. Li et al., 2011; Y. Li et al., 2010). One study show that this over-expression is through amplification of the gene. The gene resides on 8q22 region, which is amplified in 20% of breast cancer patients (Y. Li et al., 2010). Therefore, we evaluated the clinical effect of the gene expression profiles of miR-489 in the patients with 8q22 gain/amplified tumor using a published data set containing 1302 breast cancer patients (Dvinge et al., 2013; Gray & Druker, 2012). Intriguingly, we found that 8q22 amplified patients with high miR-489 have a significantly better survival as compared to low miR-489 (p-value = 0.0005) (Fig. 2.21C). These results indicate potential application of miR-489 as prognostic biomarker in 8q22 amplified breast cancers.

2.3 Summary and Discussion

In this study, we show that miR-489 inhibits autophagy in multiple subtypes of breast cancer cell line. Restoration of miR-489 reduces viability of MDA-MB-231 under stress induced by starvation. Lastly, we show miR-489 can sensitize breast cancer cell lines to doxorubicin *in-vitro* and *in-vivo*. miR-489 imparts these phenotypic effects partly by directly targeting LAPTM4B and ULK1.

Our gene expression analysis reveals downregulation of many autophagy related genes upon miR-489 reconstitution. Although, we observe that miR-489 affects multiple genes involved at different stages of autophagy, we conclude that

miR-489 restoration is mainly associated with defective maturation that leads to AP accumulation. The defect at this fusion step caused by miR-489 is supported by three independent experiment. First, miR-489 restoration leads to concomitant accumulation of LC3B-II and cargo protein p62. Upon completion of the autophagic process, p62 and LC3B-II are degraded via fusion with lysosome. However, blockage at maturation step prevents this degradation and results in simultaneous accumulation of both proteins. Second, no further significant accumulation of LC3B-II was observed in combination treatment of miR-489 and Bafilomycin A1. Last, miR-489 increases AP as shown by more yellow punta demonstrated by microscopic analysis of fluorescent mCherry-EGFP-LC3B reporter. Reduced ULK1 expression levels are commonly associated with decreased autophagic flux due to reduced autophagosome formation. In contrast to this notion, we observed accumulation of AP. However, it is worth to note that while ULK1 is involved in the initiation stage of the autophagy, it is not essential for activation of the LC3 conjugation machinery. Studies show that ULK1 and ULK2 (homolog of ULK1) possess redundant roles in autophagy (Chan, Longatti, McKnight, & Tooze, 2009; Hara et al., 2008). and indeed, it takes a double knockout of *Ulk1* and *Ulk2* to completely block amino acid starvation-induced autophagy in mouse embryonic fibroblasts (E. J. Lee & Tournier, 2011). This could be one of the reason why, despite ULK1 downregulation by miR-489, collective effect is observed at maturation stage. LAPTM4B is a lysosomal transmembrane protein that has been shown to affect maturation of autophagosome. Studies show that knockdown of LAPTM4B results lysosomal membrane permeabilization (Blom et al., 2015) and

increases lysosomal pH which inhibits lysosome and autophagosome fusion (Y. Li et al., 2012). This results in accumulation of autophagosome with simultaneous deposition of LC3B-II and p62. Together, these results indicate that miR-489 inhibits autophagy mainly through inhibiting autophagosome maturation.

Autophagy has a contentious role in tumorigenesis. Loss of autophagy promotes oxidative stress, activation of the DNA damage response and genome instability which are known cause of cancer initiation and progression. (White, Mehnert, & Chan, 2015). However, autophagy has also been seen to promote tumor cell survival. Being a pro-survival mechanism, it allows cell survival under stressful conditions such as starvation and hypoxia. Due to excessive proliferation rate, these conditions are fairly common among tumors (Hu, Jahangiri, Delay, & Aghi, 2012). Autophagy, in such established tumors, promotes survival of cancer cells and inhibition of autophagy leads to tumor growth inhibition. Furthermore, genotoxic stress induced by various chemotherapeutic agents also induces cytoprotective autophagy. Several studies have reported that inhibiting autophagy in such cases leads to tumor growth inhibition and chemo-sensitization. However, impact of autophagy inhibition on tumor cell survival and chemo-sensitization depends on at which stage autophagy in blocked. Studies show that blocking autophagy at later stage have pronounced cytotoxic effect and sensitization. In fact, few studies suggested that blocking early stage autophagy might promote survival and attenuate effect of chemo-therapeutic agent. One such report explained that this contrasting response of autophagy inhibition at different stages is because this toxic effect is attributed to autophagosome accumulation (Button

et al., 2017). Since, inhibition of early stage of autophagy inhibits autophagosome synthesis, it alleviates cytotoxicity induced by autophagosome accumulation. Consistent with this result, blocking early stage of autophagy by 3-MA and siATG5 blunted miR-489 induced cell death. These results suggest application of miR-489 in tumors with increased autophagic flux or autophagy dependency. Few studies demonstrate higher basal autophagic flux and increased dependency of TNBC cells on autophagy for their survival (Maycotte et al., 2014). Intriguingly, we observed significant cytotoxic effect of miR-489 in TNBC cells compared to cell lines of other breast cancer subtypes. TNBC cell line MDA-MB-231 is sensitive to autophagic induction and additionally possesses the ability to proliferate following nutrient deprivation (Y. I. Li et al., 2016). In the current study, we also observed MDA-MB-231 cells are more resistant to starvation compared to estrogen positive T47D cell line and HER2 positive HCC1954 cell line. miR-489 under these conditions can provide useful therapeutic approach to target such resistant and aggressive tumor cells. Interestingly, several groups including us, have shown that miR-489 is significantly down regulated in TNBC patients and cell lines, which might contribute to increased autophagic flux observed in this subtype (X. Chen et al., 2016; Patel et al., 2016). All these evidences suggest a notion that loss of miR-489 in this subtype might play an important role for their survival. It will be interesting to explore if miR-489 mediated severe cytotoxic effect on these cells is specifically due to their increased sensitivity to autophagy inhibition or if miR-489 shuts down other pro-tumorigenic pathways aberrantly overexpressed in this subtype.

miR-489 has long been reported in drug resistance. (X. Chen et al., 2016; Jiang et al., 2014; Miller et al., 2008; Wu et al., 2014). Various drug resistant cell lines, such doxorubicin resistant cell line, tamoxifen resistant cell line and cisplatin resistant cell line, display significantly reduced miR-489 expression. A study showed that MCF7/ADR cells have significantly higher basal autophagy level and inhibition of autophagy leads to sensitization of these resistant cells to doxorubicin(Guo, Tam, Santi, & Parissenti, 2016). Interestingly, restoration of miR-489 leads to significant sensitization towards doxorubicin. A study reported that miR-489 sensitizes MCF7/ADR cells by inhibiting epithelial to mesenchymal transition (Borst et al.) through SMAD3 downregulation (Jiang et al., 2014). Several studies showed cells that underwent EMT require autophagy activation to survive during the metastatic spreading(Gugnoni, Sancisi, Manzotti, Gandolfi, & Ciarrocchi, 2016). Furthermore TGF-β, a master regulator of SMAD3 and EMT, has also been shown to induce autophagy and knockdown of SMAD3 attenuates TGF- β induced autophagy (Kiyono et al., 2009). However, on the other side autophagy has also been shown to contrast the activation of the EMT mainly by selectively destabilizing crucial mediators of this process (Gugnoni et al., 2016). It will be very interesting to explore cross talk between miR-489, autophagy and EMT to gain better understanding of miR-489's role as therapeutic sensitizer.

Restoration of miR-489 in some of these cell lines showed sensitization to specific chemotherapeutic agent (X. Chen et al., 2016; Jiang et al., 2014; Miller et al., 2008; Wu et al., 2014). Many mechanisms exist for drug resistance. The fact that miR-489 sensitizes cells to multiple chemotherapeutic agents indicates that

miR-489 regulates several pathways involved in drug resistance. One study showed miR-489 can sensitize doxorubicin resistant cell line via targeting SPIN1-PI3K-Akt pathway (X. Chen et al., 2016). In the current study, we establish miR-489-LAPTM4B-Autophagy pathway as an additional mechanism involved in doxorubicin resistance (Fig. 2.22). Our findings are consistent with previous studies that show role of LAPTM4B in increased autophagy and anthracycline resistance. Our clinical analysis found patient with 8q22 amplification, who have higher miR-489 expression, have better survival (p-value =0.0005) than patient with lower miR-489 expression. These data indicate potential clinical significance of miR-489 in 8q22 amplified patients, where it can mitigate effects of amplified LAPTM4B and sensitizes patients to doxorubicin. Together, these data suggest a possible application of using miR-489 as a potential biomarker or therapeutic sensitizer in a defined subgroup of resistant breast cancer patients.

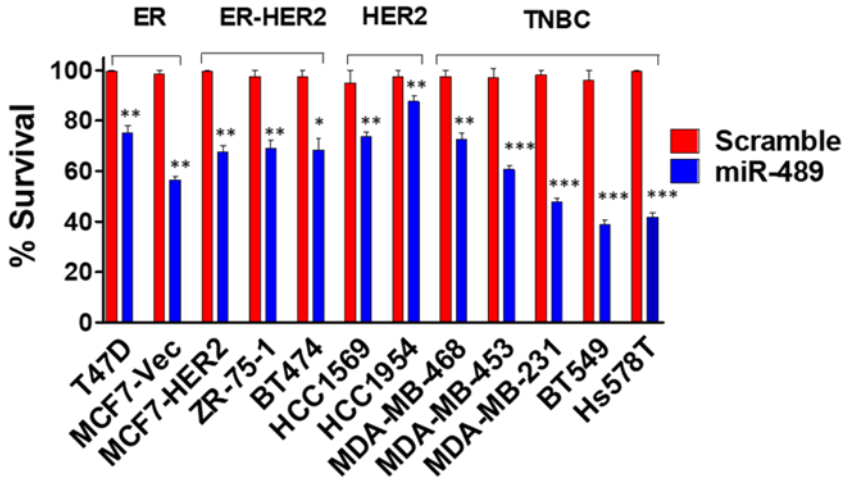

Figure 2.1: Effect of miR-489 on cell viability of 12 different breast cancer cell lines representing all three major subtypes of breast cancer. MTT based cell viability assay showing relative survival of breast cancer cell lines after 72 hours post-transfection with scramble or mimic miR-489 ***, $p<0.001$; **, $p<0.01$; *, $p<0.05$.

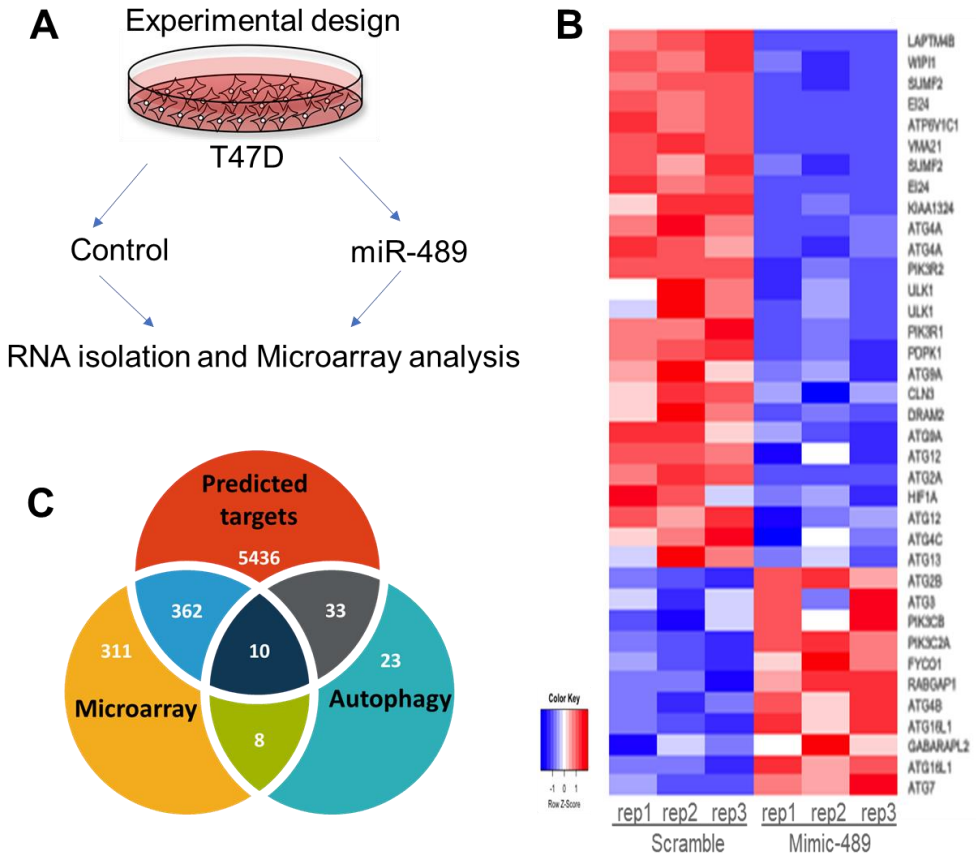

Figure 2.2: Effect of miR-489 on expression of genes regulating autophagy. A. Experimental design. B Heatmap analysis of microarray data for the genes associated with autophagy. Genes were selected based on their differential expression between the scr-transfected cells and mimic-transfected cells. Red and blue indicate high and low gene expression, respectively. C. Hypergeometric analysis was performed using microarray data and putative targets identified using miRNA target–predicting software.

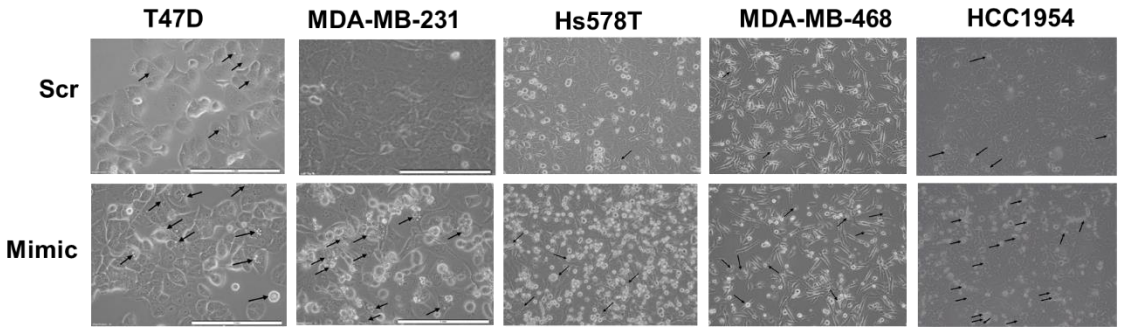

Figure 2.3: Demonstration of morphological changes in breast cancer cells after forced expression of miR-489. Bright-field microscopy images of Scr- or Mimic-transfected cells. Arrow indicates intracellular endosomal, possibly vacuolar structures. Data are representative of three independent experiments. 72 hours post-transfection with scramble or mimic miR-489 ***, p<0.001; **, p<0.01; *,

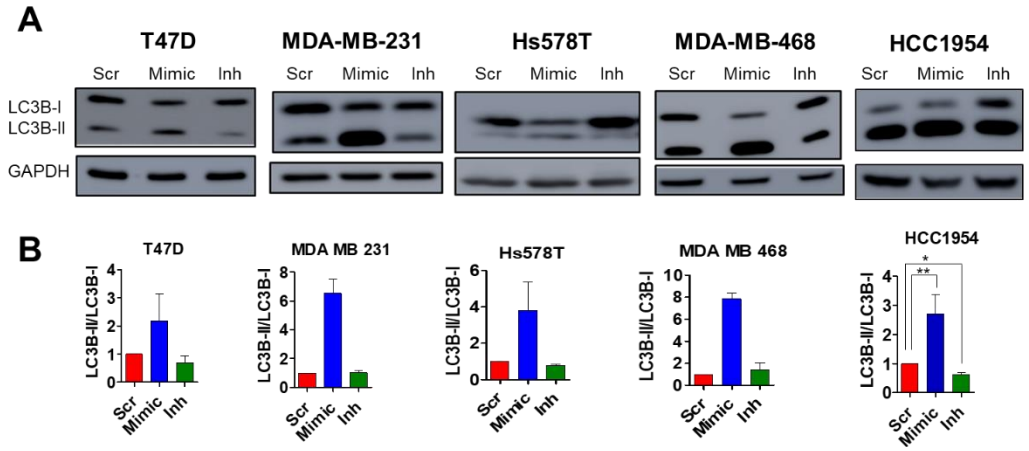

Figure 2.4: Effect of miR-489 on autophagic flux. A. Indicated breast cancer cell lines were transfected with scr, mimic, or Inh. Protein was collected 72 hours post transfection and subject to western blot analysis of autophagy markers. GAPDH was used as a loading control. B. Quantification of LC3B-I and LC3B-II ratio. Data are representative of three independent experiments. 72 hours post-transfection with scramble or mimic miR-489 ***, p<0.001; **, p<0.01; *, p<0.05.

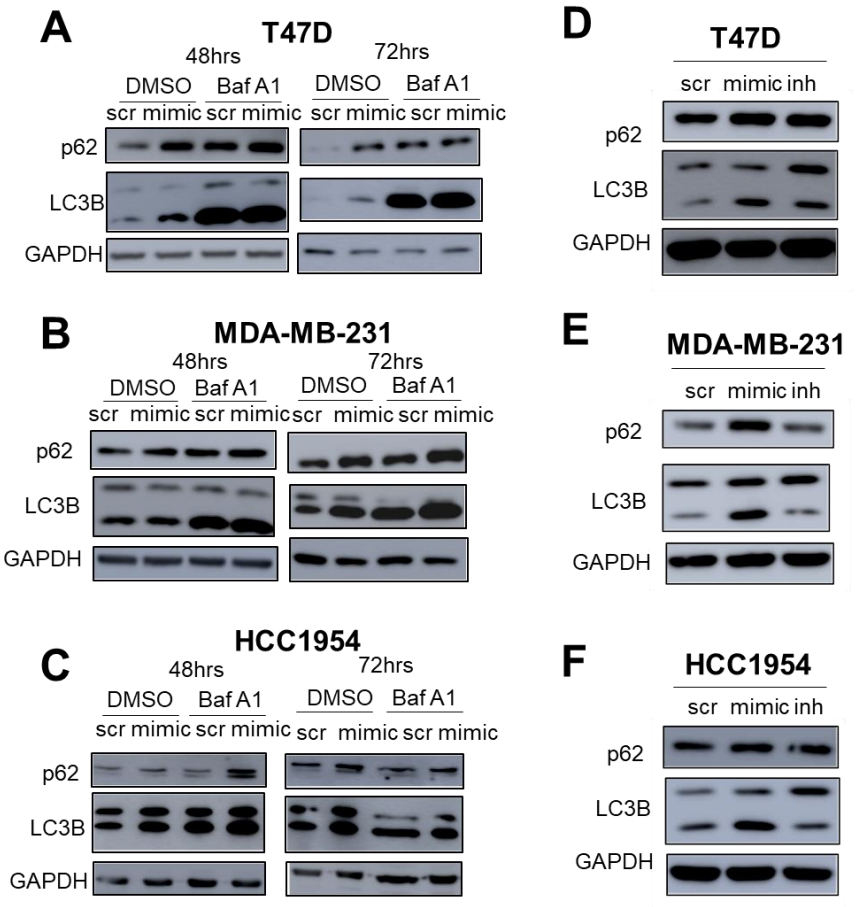

Figure 2.5: miR-489 inhibits autophagy by blocking autophagosome maturation. A-C Bafilomycin A1 blots after reconstituting cells with miR-489. T47D (A), MDA-MB-231 (B) and HCC1954 (C) cell lines were transfected with 28nM scr or mimic, for 48 or 72hrs and p62 and LC3B-II protein expression was assayed by western blot in presence or absence of Bafilomycin A1 (BafA1) (400nM). GAPDH was used as a loading control. D-F. Effect of miR-489 on clearance of p62 and LC3B-II deposition. T47D (D), MDA-MB-231 (E) and HCC1954 (F) cell lines were transfected with 28nM scr, mimic or inhibitor for 72hrs and p62 and LC3B-II protein expression was assayed by western blot.

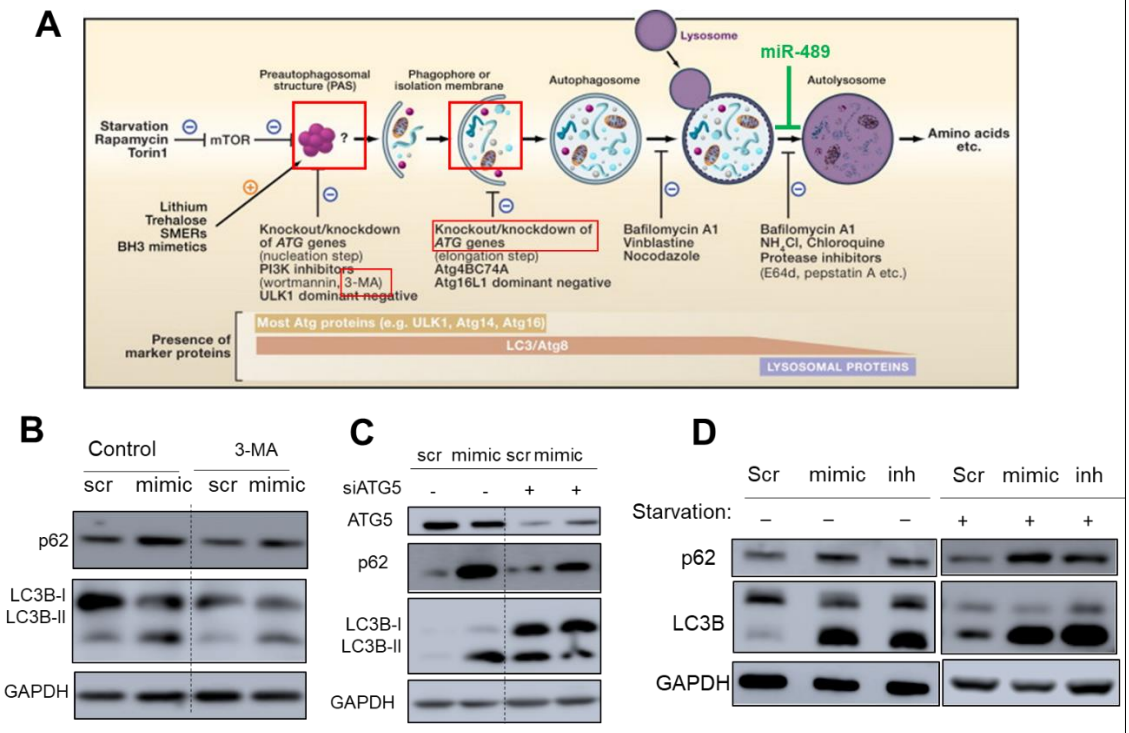

Figure 2.6: Effect of autophagy inducers or inhibitors on miR-489 induced autophagy inhibition. A Schematic diagram showing mechanism of action and effect of each autophagy modulator. B Western blot analysis of autophagic flux after forced expression of miR-489 in presence or absence of 3-MA and siATG5 (C). Cells were transfected with 28nM scr or mimic, for 24hrs, and then treated with 3-MA for 48hrs. Autophagic flux was then analyzed using western blot. GAPDH was used as a loading control. D Starvation increases LC3B-II and p62 deposition by miR-489. Autophagic flux was assessed after forced expression of miR-489 with or without serum by western blot.

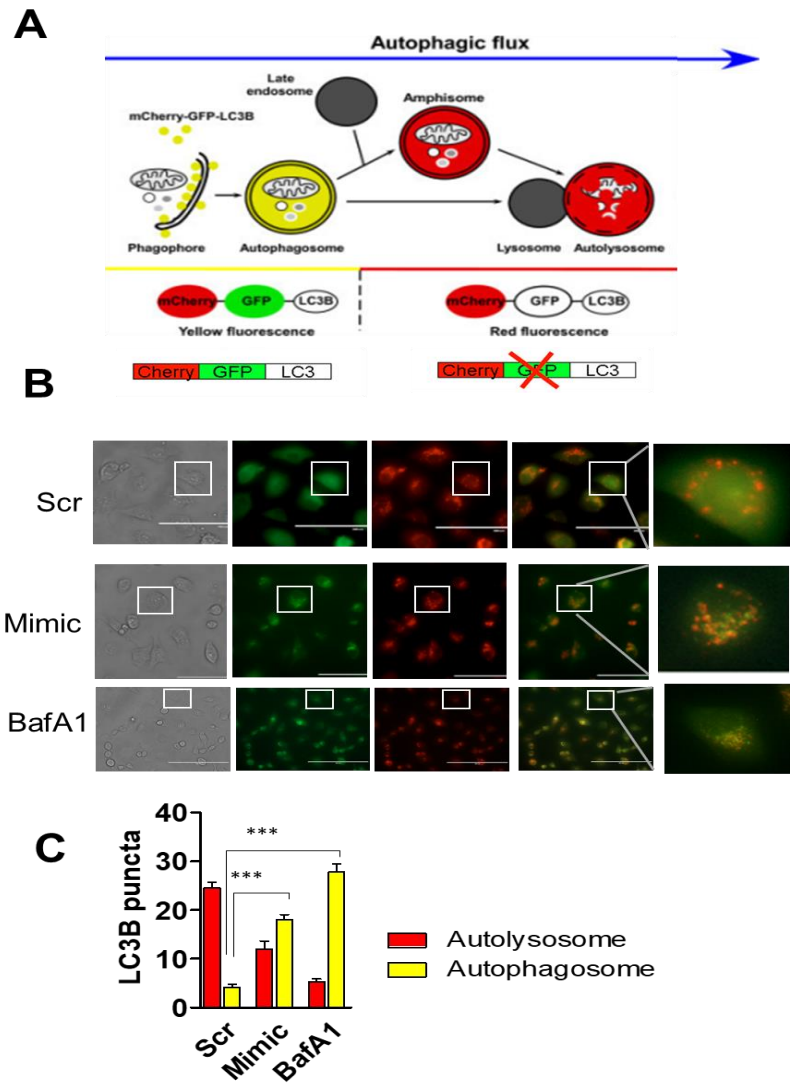

Figure 2.7: miR-489 inhibits autophagy by blocking autophagosome and lysosome fusion. A. Schematic diagram of mCherry-EGFP-LC3B reporter. B. Confocal microscopy of autophagy maturation. MDA-MB-231 cells stably expressing mCherry-EGFP-LC3B fusion protein were transfected with 28nM scr or mimic for 48hrs or Bafilomycin for 4hrs and assayed for co-localization of red and green punta using confocal microscopy. C. Quantitative analysis of red and yellow punta in MDA-MB-231 cells at 48hrs post-transfection of scr or mimic ***, $p<0.001$; **, $p<0.01$; *, $p<0.05$.

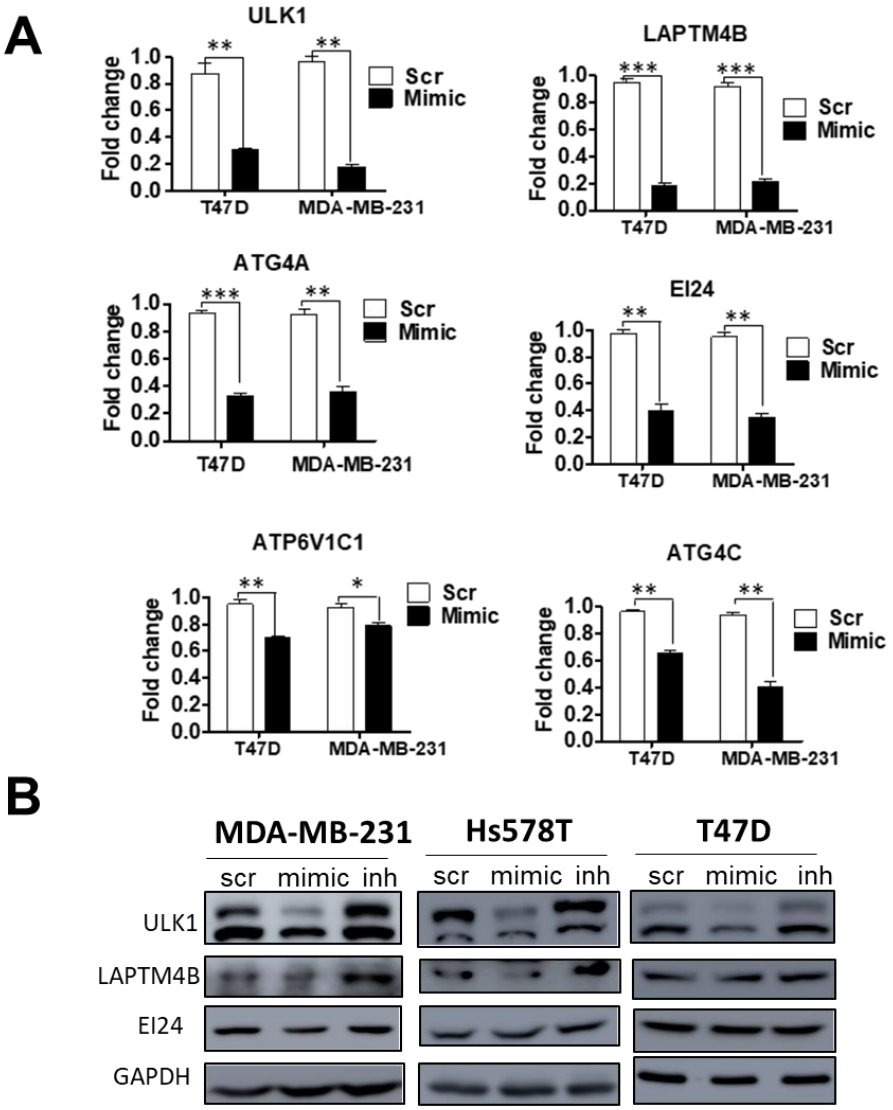

Figure 2.8: miR-489 inhibits autophagy by inhibiting multiple genes involved in the process. A MDA-MB-231 and T47D cell lines were transfected with 28nM scr or mimic. RNA was isolated 72hrs post transfection and qRT-PCR was performed to examine expression level of indicated genes. Data are means of three replicates + SEM. B. Western blot showing expression of potential targets upon transfection of 28nM scr, mimic or inh in indicated cell lines. GAPDH was used as a loading control. ***, p<0.001; **, p<0.01; *, p<0.05.

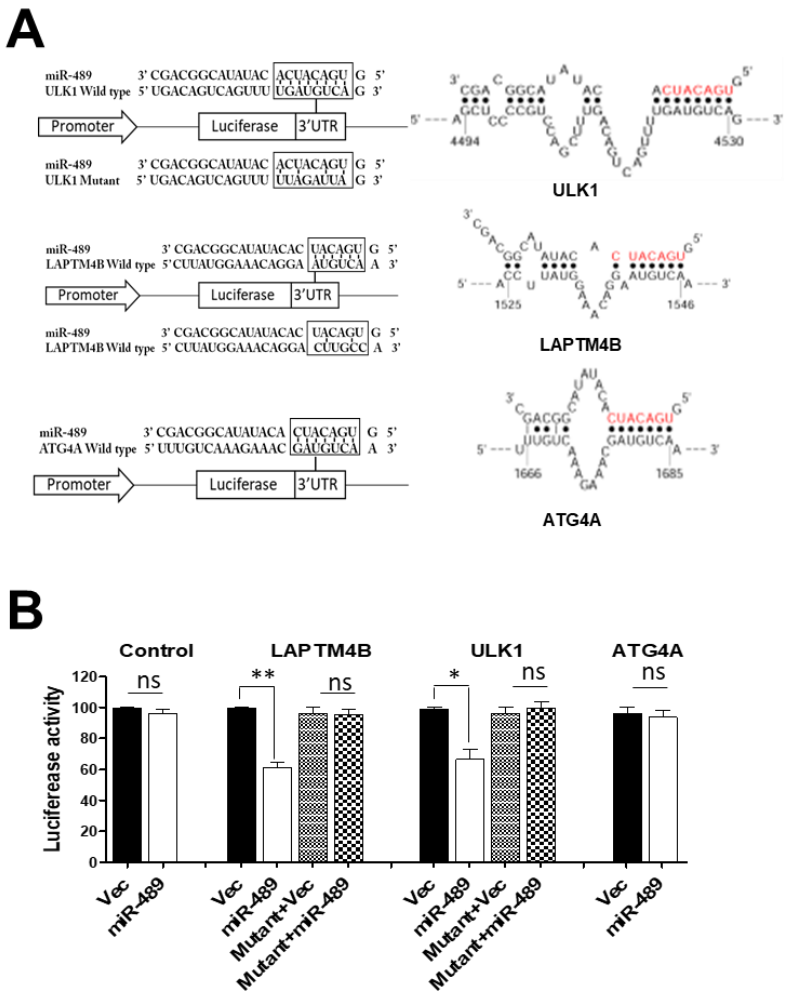

Figure 2.9: LAPTM4B and ULK1 are direct targets of miR-489. A Schematic representation of the target mRNA with putative miR-489 binding site in the 3' UTR by S fold database, where the seed region is highlighted in red. B HEK293T cells were co-transfected with miR-489 expressing vector or empty vector and renilla expressing vector for 72hrs. Firefly luciferase was measured for each condition and normalized with renilla luciferase. Normalized luciferase activity was compared with WT-3'UTR and Mutant 3' UTR of target mRNA. Data are means of three replicates + SEM. ***, $p<0.001$; **, $p<0.01$; *, $p<0.05$.

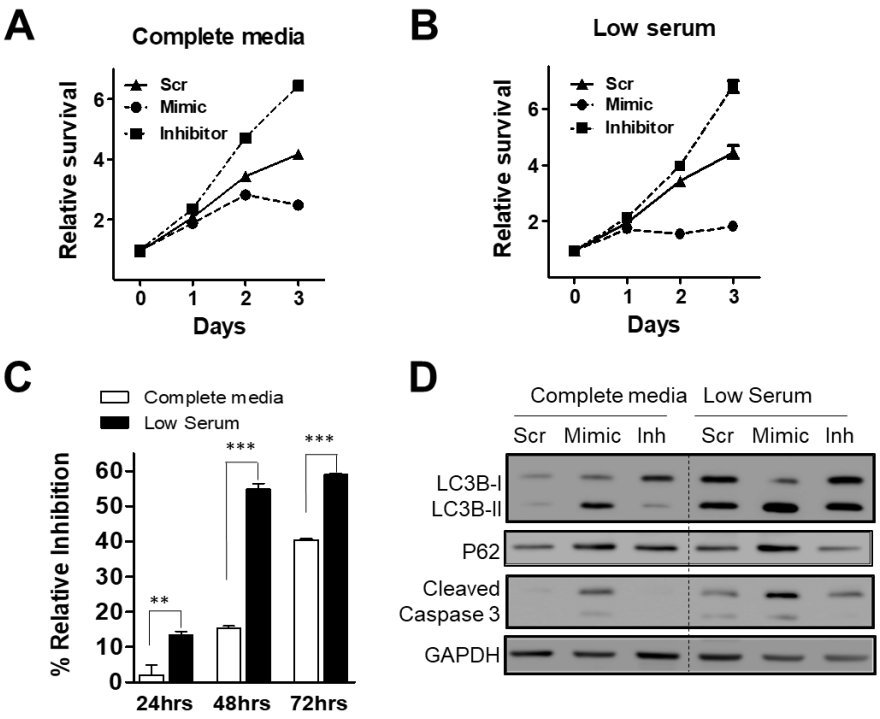

Figure 2.10: miR-489 reduces tumor cell survival and sensitizes tumor cells under metabolic stress induced by starvation via autophagy inhibition. MDA-MB-231 cells were transfected with 28nM scr, mimic or inh in complete media (A) or low serum (B). Cell viability assay was performed at indicated time points (0, 24, 28 and 72hrs) using MTT. *, $p < 0.05$; **, $p < 0.01$; ***, $p < 0.001$. Data are means of three replicates + SEM. C. Relative inhibition by mimic under both conditions at indicated time points. D. MDA-MB-231 cells were transfected with 28nM scr, mimic or inh in complete media or low serum for 72hrs and western blot was performed to investigate expression of cleaved caspase 3 and autophagy markers. GAPDH was used as a loading control. Data are means of three replicates

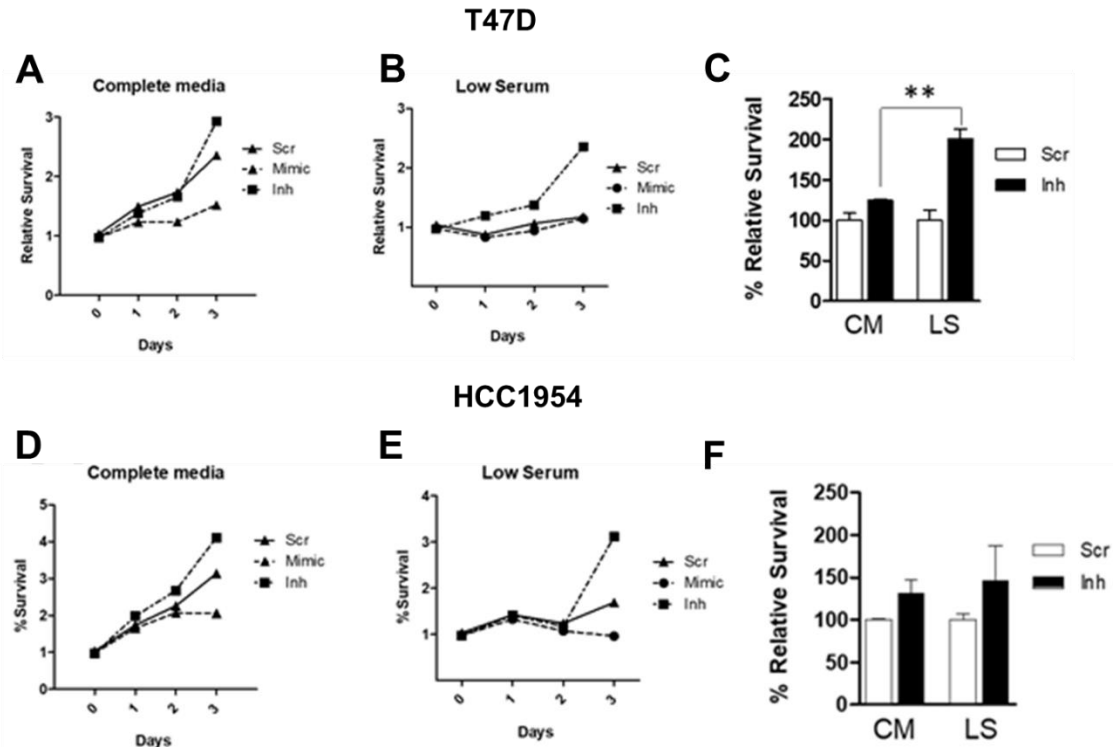

Figure 2.11 Inhibition of endogenous miR-489 imparts resistance to starvation-sensitive cell lines. T47D **(A-C.)** and HCC1954 **(D-F.)** were transfected with 28nM scr or mimic under complete media or low serum condition. Cell viability was measured at indicated time point using MTT assay. *, $p < 0.05$; **, $p < 0.01$; ***, $p < 0.001$. Data are means of three replicates $\pm$ SEM.

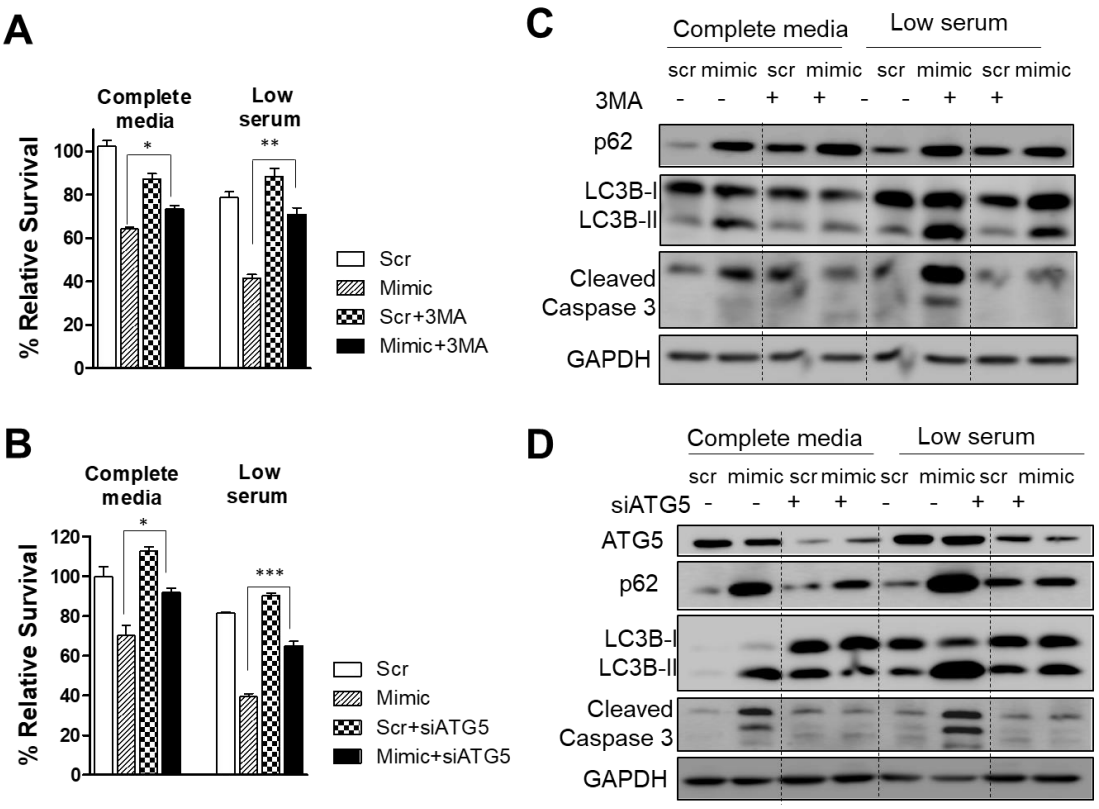

Figure 2.12 Blocking early stage of autophagy attenuates cytotoxic effect of miR-489. MDA-MB-231 cells were transfected with 9.3nM scr or mimic in complete media or low serum in presence or absence of 3-MA (5mM) or siATG5 (50nM) treatment and cell viability assay **(A,B)** and western blot analysis **(C,D)** was performed to examine autophagic flux and apoptosis *, $p < 0.05$; **, $p < 0.01$; ***, $p < 0.001$. Data are means of three replicates $\pm$ SEM.

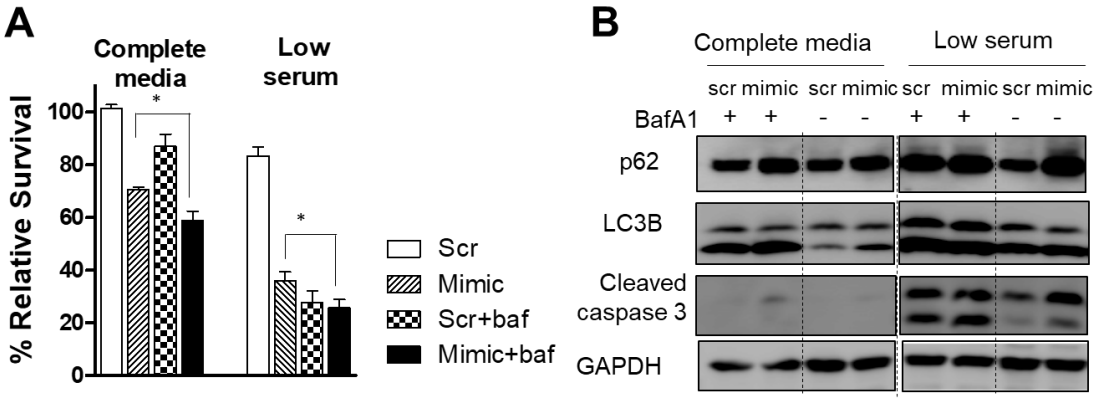

Figure 2.13: Blocking late stage of autophagy fails to protect cells from cytotoxic effect of miR-489. MDA-MB-231 cells were transfected with 9.3nM scr or mimic in complete media or low serum in presence or absence of BafA1 (50nM) and cell viability assay **(A)** and western blot analysis **(B)** was performed to examine autophagic flux and apoptosis *, $p < 0.05$; **, $p < 0.01$; ***, $p < 0.001$. Data are means of three replicates $\pm$ SEM.

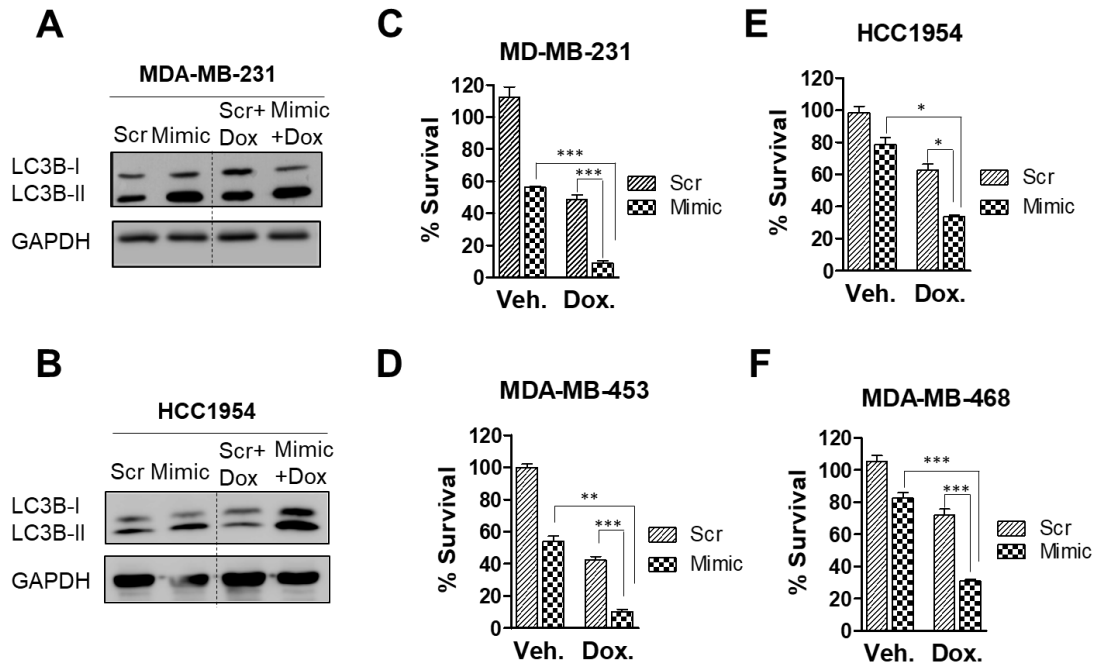

Figure 2.14 Forced expression of miR-489 inhibits doxorubicin induced cytoprotective autophagy and sensitizes cells to doxorubicin. A-B. MDA-MB-231 and HCC1954 cells were transfected with scr or mimic for 72hrs in absence or presence of doxorubicin and autophagy marker LC3B-I and LC3B-II were monitored to examine autophagic flux. C-F. Indicated breast cancer cell lines were transfected with 28nM scr or mimic for 72hrs in presence of doxorubicin (0.75μM) for 48hrs and cell proliferation was measured by MTT assay. Data are representative of three independent experiments. *, $p < 0.05$; **, $p < 0.01$; ***, $p < 0.001$.

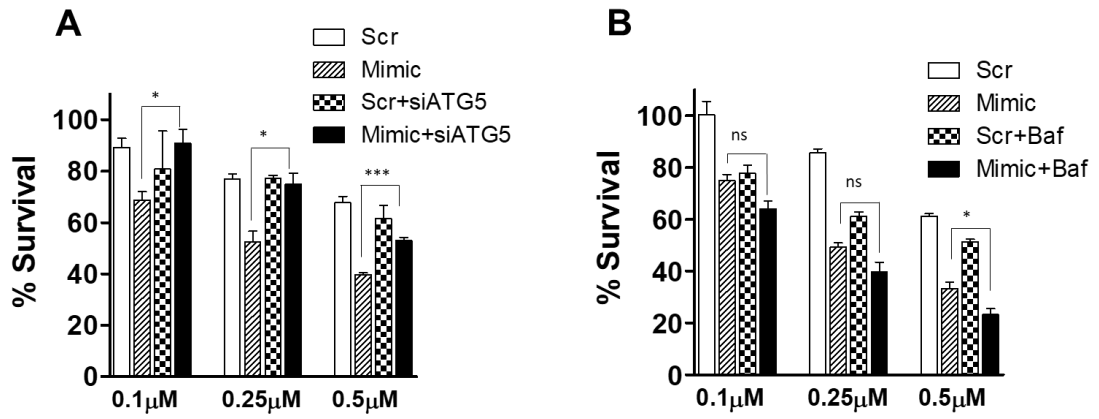

Figure 2.15: Blocking early stage but not late stage autophagy prevents miR-489 mediated doxorubicin sensitization. A. MDA-MB-231 cells were transfected with 9.3nM scr or mimic with or without siATG5 for 24hrs and treated with indicated concentration of doxorubicin for 48hrs and cell proliferation was measured by MTT assay. B. MDA-MB-231 cells were transfected with 9.3nM scr or mimic with for 24hrs and treated with indicated concentration of doxorubicin in presence or absence of Bafilomycin A1 (50nM) for 48hrs and cell proliferation was measured by MTT assay. Data are representative of three independent experiments. *, $p < 0.05$; **, $p < 0.01$; ***, $p < 0.001$.

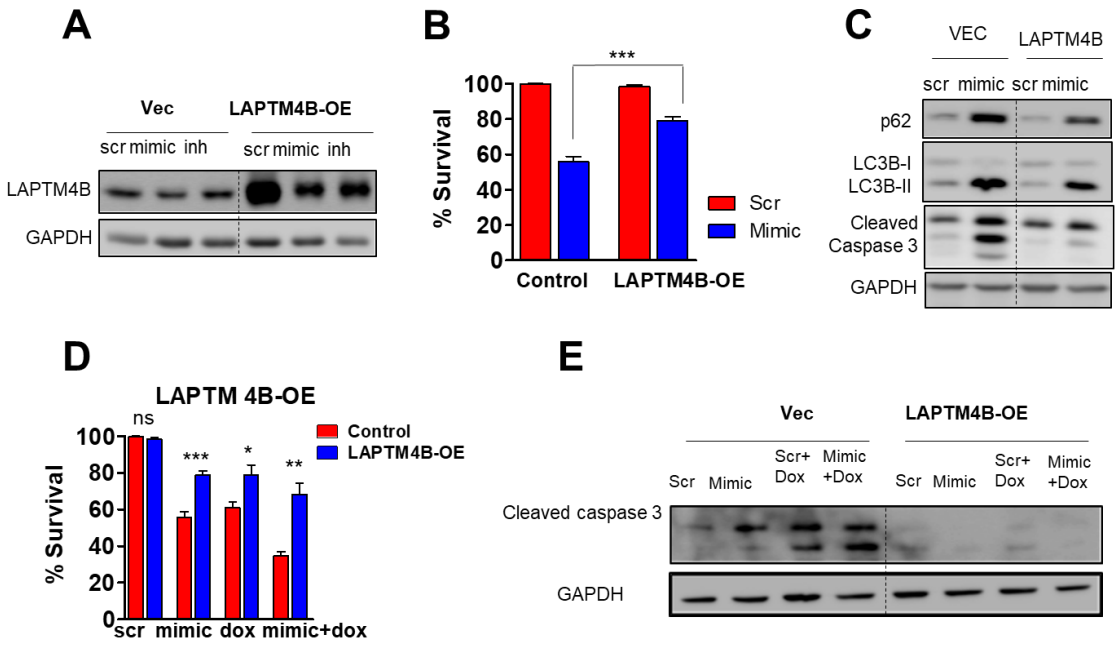

Figure 2.16: LAPTM4B restoration attenuates tumor suppressive effect of miR-489 and prevents miR-489 induced doxorubicin sensitization. A. Western blot indicating stable over expressing LAPTM4B. GAPDH was used as a loading control for western blot analysis. B-C. MDA-MB-231 cells stably expressing LAPTM4B were transfected with 28nM scr or mimic. Cell viability assay (B.) and western blot (C.) was performed 72hrs post transfection to examine autophagic flux and apoptosis. D-E. MDA-MB-231 cells stably expressing LAPTM4B were transfected with 28nM scr or mimic with or without doxorubicin followed by cell viability assay (D.) and western blot analysis (E.)

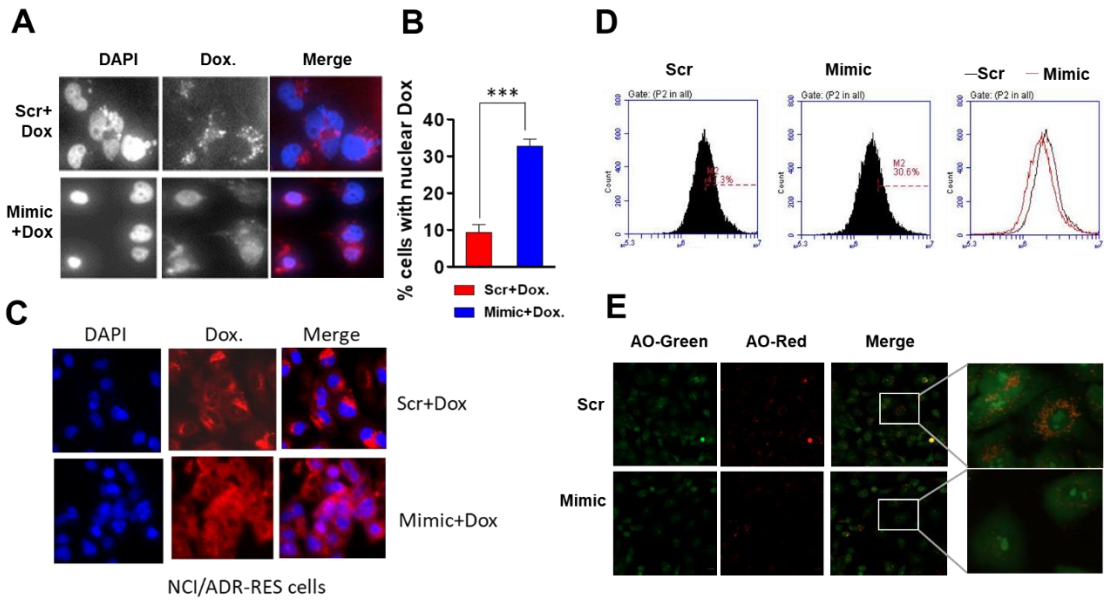

Figure 2.17: Forced expression of miR-489 causes doxorubicin redistribution to nucleus. A. Microscopy analysis of subcellular localization of doxorubicin. Confocal microscopy was performed 72hrs after MDA-MB-231 cells were treated with 28nM scr or mimic with doxorubicin. Data are means of three replicates ± SEM. Data are representative of three independent experiments. B. Quantification of cells with nuclear localization of doxorubicin. C. Microscopy analysis of subcellular localization of doxorubicin. Confocal microscopy was performed 72hrs after NCI/ADR-Res cells were treated with 28nM scr or mimic with doxorubicin. D. MDA-MB-231 cells were transfected with 28nM scr or mimic and stained with Acridine orange (1mg/ml) for 20min and flow cytometry was performed to examine lysosomal integrity. E. Confocal microscopy of MDA-MB-231 cells after transfection with scr or mimic and staining with Acridine orange (1mug/ml) for 20min. Data are representative of three independent experiments.

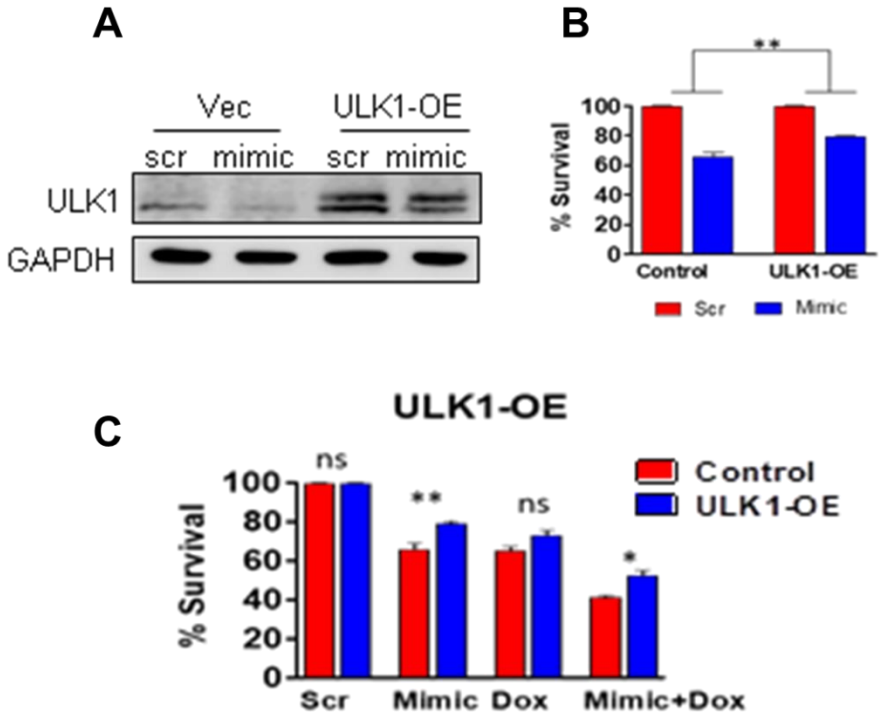

Figure 2.18: ULK1 restoration rescues MDA-MB-231 cells from cytotoxic effect of miR-489 but not from doxorubicin. A-B. MDA-MB-231-ULK1 overexpressing stable cells and vector cells were transfected with scr or mimic for 72hrs followed by (A.) western blot analysis and (B.) MTT assay C. MDA-MB-231 cells stably expressing ULK1 and vector cells were transfected with 28nM scr or mimic with or without doxorubicin and cell viability was measured 72hrs post transfection. Data are representative of three independent experiments. *, $p < 0.05$; **, $p < 0.01$; ***, $p < 0.001$.

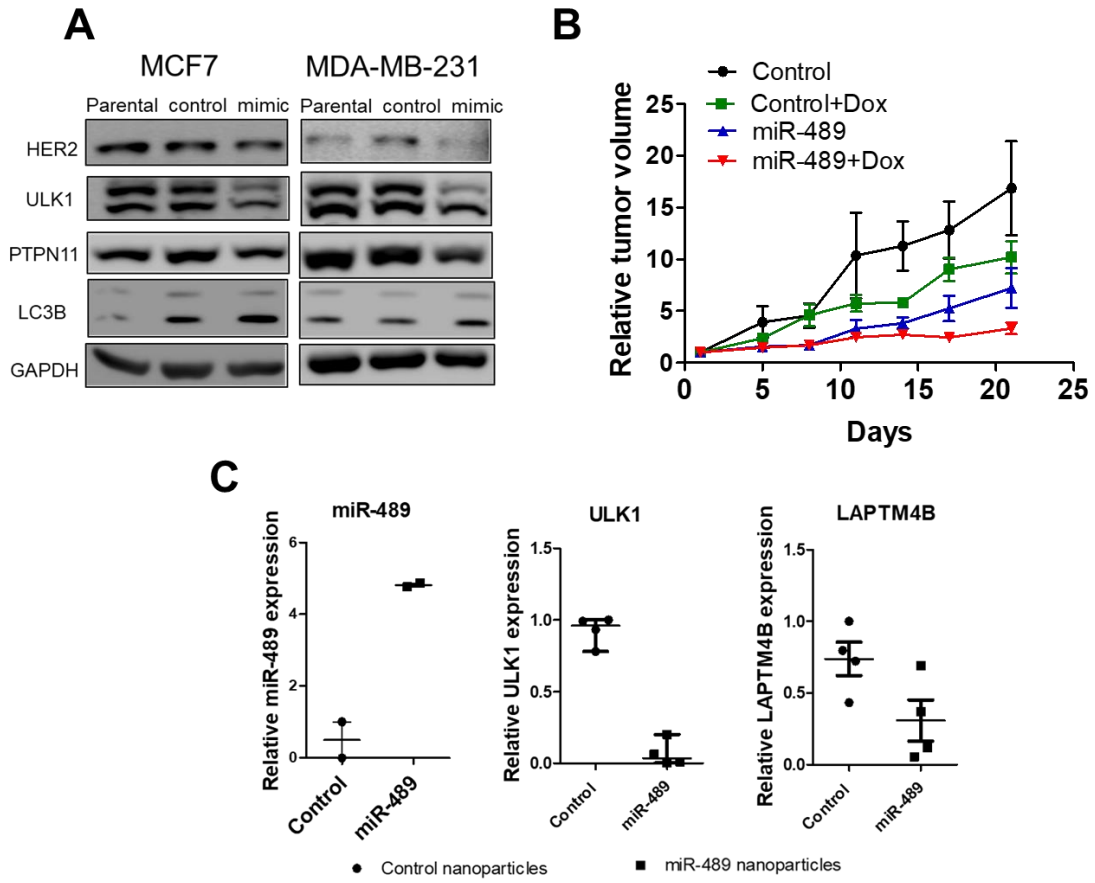

Figure 2.19: Nanoparticle-delivered miR-489 inhibits tumor growth and sensitized cells against doxorubicin *in vivo*. A. *In-vitro* characterization of nanoparticles delivering miR-489. MDA-MB-231 and MCF7 cells were treated with control and miR-489 loaded particles for 72 hours. Western blot indicates successful delivery of microRNA as indicated by downregulation of targets. B. miR-489 inhibits tumor growth and sensitized cells against doxorubicin in xenograft animals. After the tumors were palpable, the animals were randomly assigned into four groups (n=5 per group). All animals were injected with miR-489 or control encapsulated in nanoparticle every third day. The treatment starting day was referred to as 'Day zero' in the figure. Expression of miR-489 and its targets in tumors. RT-PCR was performed on the xenograft tumors samples to measure expression levels of miR-489, ULK1 and LAPTM4B. C. Successful delivery of miR-489 via nanoparticles in tumors. Graph shows relative miR-489 expression (log10 (fold change)) in control or miR-489 loaded nanoparticles and Relative expression of ULK1 and LAPTM4Bin tumors samples.

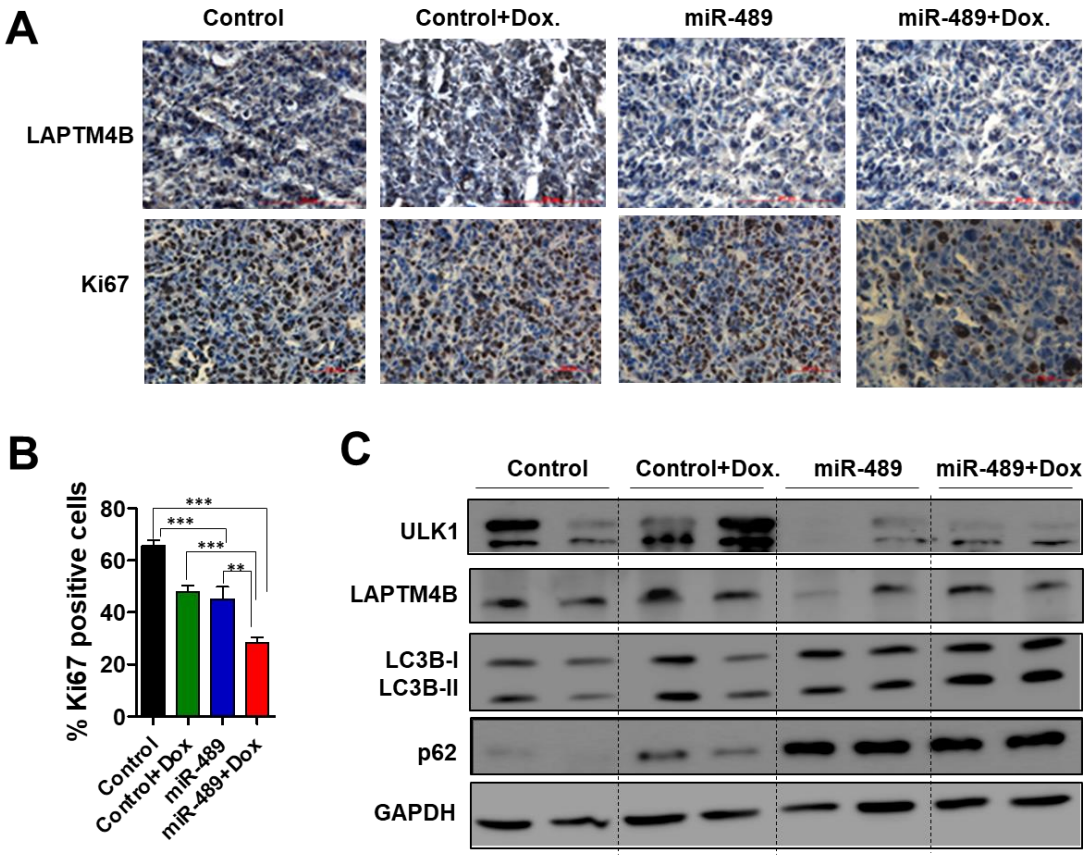

Figure 2.20: Demonstration of tumor growth reduction, doxorubicin sensitization and autophagy inhibition by miR-489 using IHC and western blot analysis. A. IHC analysis revealed reduced expression of LAPTM4B and Ki67 in tumors treated with miR-489 encapsulated nanoparticles. B. Quantification of Ki-67 positive cells in tumors of all four groups. C. Western blot analysis of tumors revealed down regulation of ULK1, LAPTM4B and autophagy inhibition by miR-489. GAPDH was used as a loading control.

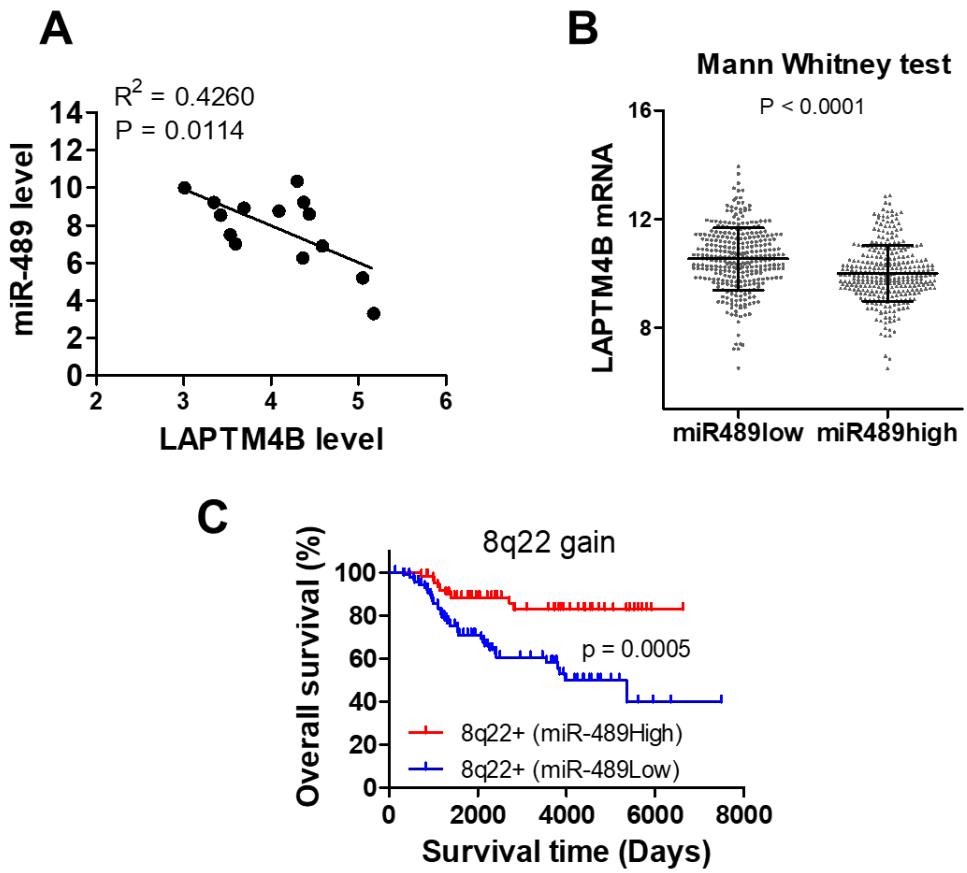

Figure 2.21: Correlation of miR-489 expression with LAPTM4B expression and 8q22 amplification in breast cancer patients. A. miR-489 and LAPTM4B expression was measured in breast tissues form breast cancer patients (n=14) using qPCR. B. Correlation of miR-489 and its potential target gene expression in primary breast cancers. The linear dependence between miR489 and its potential target genes expression was evaluated by Pearson analysis of a published breast cancer data set. C. miR-489 expression predict overall survival of breast cancer patients with 8q22 gain/amplified tumors. Patient survival was estimated using the Kaplan-Meier method and compared with log-rank tests. The Y axis represents the probability of overall survival. *, $p < 0.05$; **, $p < 0.01$; ***, $p < 0.001$.

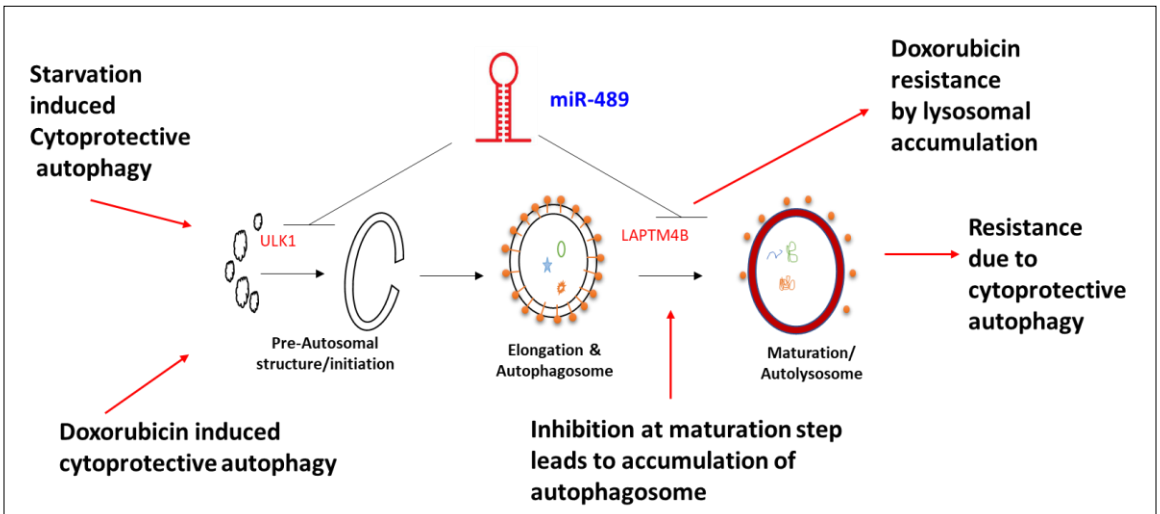

Figure 2.22: Proposed working model depicting role of miR-489 in regulation of autophagy, cell viability and chemo-resistance. Starvation and chemotherapy induced genotoxic stress induces cytoprotective autophagy and increases autophagosome formation and maturation. miR-489, by targeting ULK1 and LAPTM4B, inhibits autophagosome maturation and causes autophagosome accumulation which leads to cell death. miR-489 also causes doxorubicin redistribution to nucleus by inhibiting LAPTM4B and further prevents LAPTM4B

CHAPTER 3

THE ROLE OF MIR-489 IN HORMONE POSITIVE BREAST CANCER AND TAMOXIFEN RESISTANCE

3.1 INTRODUCTION

Oncogenic activation of the estrogen receptor (ER) signaling pathway occurs in over 70% of breast cancers. Although, this subtype of breast cancer has best prognosis due to targeted endocrine therapies, most patients with advanced disease eventually develop resistance to these endocrine therapies, and even for patients treated in the adjuvant setting, there is a consistent risk of relapse that persists indefinitely (Nass & Kalinski, 2015). Furthermore, approximate 50% of patients with locally advanced or metastatic ER+ breast cancer do not respond to first-line endocrine treatment (Clarke, Tyson, & Dixon, 2015). Besides, most patients who initially respond to the therapy eventually develop secondary acquired resistance. Despite significant research efforts and discoveries made in recent years, the precise reasons for endocrine therapy failure in patients with ER+ breast cancer remain largely unknown. Published studies have implicated mutations in the ESR1 gene; epigenetic silencing of ESR1, activated growth factor receptor signaling, including EGFR/HER2 pathway, PI3K-AKT pathway and MAPK pathway and over expression of co-activators such as NCOA3, FOXA1, as important mechanisms of

de novo or acquired resistance (Fan, Maximov, Curpan, Abderrahman, & Jordan, 2015; Jeselsohn, Buchwalter, De Angelis, Brown, & Schiff, 2015; Osborne & Schiff, 2011). This has led to various targeted combination strategies aiming to combat endocrine resistance.

Downregulation of miR-489 has been observed in tamoxifen-resistant breast cancer (Rugo et al., 2016) but its functional involvement remains unexplored. In this study, we systematically investigated the functional roles of estrogen-regulated miR-489 in ER^+ breast cancer. We demonstrated that downregulated miR-489 expression promotes aggressiveness, estrogen-independent growth and acquired tamoxifen resistance of ER^+ breast cancer cells. Thus, patients with ERα breast cancer with low miR-489 expression may represent a subpopulation that is intrinsically resistant to endocrine therapies.

3.2 RESULTS

3.2.1 MIR-489 EXPRESSION IS POSITIVELY CORRELATED WITH ESTROGEN RECEPTOR IN CELL LINES AND PATIENT SAMPLES.

Previously, we and several other labs have demonstrated that miR-489 is a tumor suppressor miRNA and is lost in mammary tumorigenesis (Patel et al., 2016; Soni et al., 2018). However, not much is known about the regulation of miR-489 in breast cancer. Our analysis of miR-489 expression in 13 different breast cancer cell lines suggest that it is highly expressed in hormone positive luminal breast cancer cell lines (Fig 3.1A). Interestingly, miR-489 along with its host gene CALCR is positively correlated with estrogen receptor and its responsive genes such as

PGR and TFF1 expression in clinical samples (Fig. 3.1B). Furthermore, we have observed that miR-489 is highly expressed in luminal cells compared to basal cells (Figure 3.1C). All these evidences suggest that miR-489 may be an estrogen and/or progesterone regulated miRNA.

3.2.2 E2-ERA AXIS REGULATES EXPRESSION OF MIR-489.

To investigate potential role of estrogen in regulation of miR-489 expression, we examined expression level of miR-489 and its host gene CALCR upon estrogen and progesterone stimulation and compared with unstimulated (vehicle treated) cells at different time points in T47D cell lines. We choose T47D cell line as it also expresses functional progesterone receptor and does not require pre-treatment of estrogen to induce progesterone receptor (Cittelly et al., 2013). We observed upregulation of known estrogen responsive genes such as PGR, CXCL12, GREB1 and NRIP1 upon estrogen stimulation and induction of known progesterone responsive gene, EZF upon progesterone stimulation. (Figure 3.2A, 3.2B). Interestingly, we also observed significant upregulation of miR-489 and CALCR in upon estrogen treatment but did not see significant upregulation upon progesterone treatment (Figure 3.2C, 3.2D). We performed similar experiment in two other ER+ breast cancer cell lines MCF7 and BT474. Stimulation with estrogen resulted in significant increase in miR-489 and CALCR expression (Figure 3.2E, 3.2F). Interestingly co-treatment of estrogen and progesterone showed smaller increase, suggesting progesterone reduced induction miR-489 and CALCR expression by estrogen. This result is consistent with previous study that showed progesterone represses some of estrogen regulated genes by affecting estrogen

receptor transcription assembly (Mohammed et al., 2015). To further confirm these results, we examined miR-489 and CALCR expression level upon estrogen depletion. As expected, depletion of estrogen significantly reduced the expression of known estrogen responsive genes along with miR-489 and CALCR in all three cell lines tested (Figure 3.3). These results are consistent with several studies that reported modulation of miR-489 upon estrogen depletion or stimulation (Baran-Gale, Purvis, & Sethupathy, 2016, Bailey, 2015). Interestingly, we observe that CALCR upregulation reached its peak at 24 hours in T47D while it peaked at 72hours for miR-489. We also observed stronger induction of CALCR mRNA compared to miR-489. This suggest that estrogen treatment alters the ratio of miR-489 and CALCR mRNA and that estrogen may affect processing or maturation of miR-489. However, further experiments are needed to test this notion. In summary, these data suggest that miR-489 is an estrogen regulated miRNA in breast cancer.

3.2.3 MIR-489 ACTS AS A NEGATIVE FEEDBACK TO CONFINE ESTROGEN INDUCED PROLIFERATION IN BREAST CANCER

Since, miR-489 expression is ERα regulated, we inspected if miR-489 regulates estrogen responsiveness of ERα breast cancer cells. Previously, we have observed that miR-489 inhibits proliferation of all breast cancer cell lines including ERα+ cell lines (Patel et al., 2016; Soni et al., 2018). We performed cell viability assay using several ER+ cell lines and found that forced expression of miR-489 resulted in a significant decrease, while the inhibition of miR-489 led to a significant increase in total cell viability in all cell line tested (Figure 3.4A). Therefore, we seek to examine role of miR-489 in estrogen induced proliferation.

For functional studies, the effects of forced expression or inhibition of miR-489 were examined in presence of estrogen. The forced expression of miR-489 resulted in a significant decrease, while the inhibition of miR-489 led to a significant increase in total cell viability of MCF-7 and T47D cells over 6 days (Figure 3.4B, 3.4C). Inhibition of miR-489 increased growth by 2-fold in MCF7 cells and 3.5-fold in T47D cells (Figure 3.4D, 3.4E). As expected, estrogen treatment significantly increased colony formation ability of both MCF7 and T47D cells (Figure 3.4F). Forced expression of miR-489 almost completely inhibited estrogen induced colony formation of both cells. Interestingly, inhibition of endogenous miR-489 drastically enhanced estrogen mediated colony formation. These results suggest that miR-489 may also affect cancer stem like cells or progenitor cell population. We then examined effect of miR-489 on cancer stem like cells by flow cytometry using CD24 and CD44 surface markers and by performing mammosphere forming efficiency (Balvers et al, 2015.). Consistent with previous results, we observed that estrogen increased cancer stem like cell population ($CD24^{low}$ $CD44^{high}$) by 3-fold in MCF7 cells (Figure 3.5A, 3.5B) and 10-fold in T47D cells (Figure 3.5C, 3.5D) (Fillmore et al., 2010). As observed in clonogenic assay, inhibition of endogenous miR-489 further increased cancer stem like cell population by more than 3-fold in MCF7 cells and by more than 11-fold in T47D cells. Similarly, we also observed increased mammosphere forming efficiency (MFE) upon estrogen treatment and miR-489 inhibition not only increased MFE but also increased mammosphere size (Figure 3.6A, 3.6B, 3.6C, 3.6D). As observed in colony formation assay, forced expression of miR-489 almost completely prevented mammosphere formation.

Together, these results suggest that estrogen regulated miR-489 acts as a negative feedback to confine estrogen induced tumor cell growth and loss of miR-489 may promote uncontrolled growth of ER+ breast cancers. This may explain why ER+ breast cancers with low mir-489 are more aggressive.

3.2.4 MIR-489 INHIBITS ESTROGEN SIGNALING IN ER POSITIVE BREAST CANCER CELLS

Reconstitution of miR-489 in ER-positive cells reduced their proliferation raised the possibility that miR-489 may inhibit ER signaling. To test this hypothesis, we measured estrogen receptor activity in T47D-ERE-Luc reporter cell line. As expected, we observed inhibition of estrogen receptor activity upon miR-489 over expression and increased activity by inhibiting endogenous miR-489 (Figure 3.7A). We also confirmed this effect in MCF7 cell line by transiently transfecting ERE-Luc reporter plasmid and found similar result (Figure 3.7B). Our gene expression analysis on T47D further supported this results as miR-489 restoration downregulated known estrogen responsive genes (Figure 3.7C). We then validated microarray results by performing qRT-PCR analysis on Estrogen receptor positive and negative cell lines. Interestingly, miR-489 caused down regulation of estrogen responsive genes only in estrogen receptor positive cell lines (Figure 3.8A) but did not affect or in some instances increased the expression of these genes in ER^{-ve} cell lines (Figure 3.8B). These results suggest that miR-489 does not directly target these genes but modulate their expression by inhibiting estrogen signaling. In summary, it seems that miR-489 may act as an endogenous

negative feedback loop to regulate estrogen induced gene expression in estrogen receptor positive breast cancer.

3.2.5 MIR-489 INHIBITS ESTROGEN RECEPTOR NUCLEAR LOCALIZATION BY DIRECTLY TARGETING P38 MAPK

We then sought to elucidate molecular mechanism responsible for miR-489 mediated inhibition of Estrogen-ERα axis. Multiple mechanisms have been identified that regulate Estrogen-ERα mediated gene expression. Direct inhibition of ERα or its co-factors, inhibition of kinases that activates ERα or inhibition of estrogen induced nuclear localization of ERα have been previously reported to regulate estrogen induced gene transcription (Manavathi et al., 2013). We examined if miR-489 exerts its effects by affecting localization of estrogen receptor. Interestingly, forced expression of miR-489 almost completely reversed localization of estrogen receptor from nucleus to cytoplasm in MCF7 and T47D cell lines (Figure 3.9A, 3.9B). Conversely, inhibition of endogenous miR-489 significantly increased nuclear localization. Majority of MCF7 cells showed significant localization of ERα into nucleus while T47D showed some cytoplasmic ER as well. Many factors have been reported to regulate localization of estrogen receptor. Importins and exportins have been shown to regulate nuclear import and export respectively. HSP90 and HSP70 binds to ER alpha and are responsible for its cytoplasmic retention. Various post-translational modifications including phosphorylation have also been shown to regulate estrogen localization. We then looked target prediction tools to find potential miR-489 target responsible for regulation of ERα nuclear transport. We found Importinα 7 and p38 MAPK (H. Lee

& Bai, 2002) as potential miR-489 target which has been previously shown to regulate nuclear localization. However, our western blot results do not show any change in Importinα 7 expression upon miR-489 over-expression or inhibition. Interestingly, forced expression of miR-489 significantly downregulated phosphorylated p38 MAPK and total p38 MAPK (Figure 3.10A). We then performed 3'UTR assay to examine if p38 MAPK is a direct target of miR-489. Forced expression of miR-489 significantly reduced luciferase activity of wild type construct while it did not affect luciferase activity of construct with mutant miR-489 binding site (Figure 3.10B). This result confirms that p38 MAPK is a direct target of miR-489.

Next, we examined effect of p38 MAPK inhibition SB203580 on estrogen receptor localization. We transfected control siRNA or miR-489 mimic for 72hrs or treated with DMSO or 10uM SB203580 for 24hrs in hormone starved cells followed by treatment with estrogen to examine estrogen induced nuclear localization of estrogen receptor. Cell treated with miR-489 showed cytoplasmic localization of ER. Similarly, cells treated with p38 MAPK inhibitor phenocopied effect of miR-489 on ER localization in both cell line tested (Figure 3.11A, 3.11B). Our data suggest that p38 MAPK activation is necessary for nuclear translocation of ERα. Therefore, we tested if estrogen activates p38 MAPK which in turn then mediates nuclear translocation. Since, estrogen induced ERα nuclear translocation occurs within 5-30 minutes, we performed time course of estrogen treatment on MCF7 and T47D cell lines. We observed sharp increase in phospho-p38 MAPK and its downstream target phosphor-ATF2 upon estrogen treatment in both cell lines (Figure 3.12A,

3.12B). These results are consistent with previous studies that showed estrogen mediated activation of p38 MAPK in various tissues (H. Lee & Bai, 2002; Seval, Cakmak, Kayisli, & Arici, 2006). This suggest an evidence of positive feedback loop between E2-ERα axis and p38 MAPK in mammary cells. Binding of E2 leads to activation of p38 MAPK and activation of p38 MAPK leads to nuclear translocation of ERα which is necessary for its function as transcription factor (Figure 3.12C).

3.2.6 MIR-489 INHIBITS ESTROGEN RECEPTOR PHOSPHORYLATION BY INHIBITING MAPK AND PI3K-AKT PATHWAY

Previous studies have shown phosphorylation of ERα at Serine 118 and Serine 167 is necessary for its activity as transcription factor. MAPK and AKT are two major kinases that regulates phosphorylation at Ser 118 and Ser 167 sites respectively (Anbalagan & Rowan, 2015). In our previous study we reported that miR-489 inhibits MAPK and PI3K-AKT pathway. Therefore, we examined effect of miR-489 on estrogen receptor phosphorylation at these sites. As expected, forced expression of miR-489 dramatically reduced phosphorylation of ERα at both phosphorylation sites (Fig 3.13A, 3.13B). We then examined effect of inhibitors of MAPK (U0126), PI3K-AKT (LY294002) and p38 MAPK (SB203580) on estrogen signaling and estrogen induced growth. Consistent with previous studies, we noticed reduction in transcription activity of estrogen in presence of these inhibitors as shown by ERE-Luc reporter assay (Fig. 3.14A). We further confirmed this result by examining expression of known estrogen responsive genes and again found attenuation of estrogen mediated upregulation of these genes (Fig. 3.14B). We

also confirmed effect of inhibitors by measuring their effect on estrogen induced proliferation and noticed significant reduction in proliferation (Fig 3.14C and 3.14D). Additionally, these inhibitors also attenuated enhanced proliferation upon miR-489 inhibition (Fig. 3.14E). These results suggest that miR-489 not only regulates estrogen signaling by inhibiting its nuclear localization but also by inhibiting its phosphorylation.

3.2.7 MIR-489 KNOCK OUT CELLS SHOWS INCREASED SENSITIVITY TO ESTROGEN SIGNALING

Knock-out model is an ideal tool to decipher molecular pathways affected by gene of interest as it enables reverse genetics and allows precise identification of gene functions. We utilized CRIPSR/Cas9 method to generate stable cell line with loss of function mutation in miR-489. Figure 3.15 outlines the strategy and experimental design to generate miR-489 knock out cell line. Our genotyping result showed successful editing at genomic locus of miR-489 (Fig. 3.15).

As expected, our knock out clones demonstrated increased proliferation rate confirmed by MTT based cell viability assay (Figure 3.16A) and CFSE dye based proliferation assay (Figure 3.16B). Figure 3.16C shows morphology of knock cells. Surprisingly, knock clones were smaller in size compared to wild type cells. We validated these clones by examining expression of established targets of miR-489 using western blot analysis. Both clones showed increased protein expression of PTPN11, Cyclin A2, Cyclin D1 and p38 MAPK (Figure 3.17A). Both clones also showed increased phosphorylation of MAPK, AKT and ERα. These

results show hyper activation of ERα, MAPK and PI3K-AKT pathway in knock out cells. Indeed, knock out clones showed higher increase in expression of estrogen responsive genes upon E2 stimulation compared wild type cells (Figure 3.17B). We also observed increased estrogen receptor nuclear localization in knock out cells compared to wild type cells (Figure 3.18) and this nuclear localization was reverse by treatment with p38 inhibitor (Figure 3.19). In addition, knock out clones were hyper sensitive to estrogen stimulated growth. This hyper sensitivity was attenuated by MAPK, PI3K-AKT and p38 MAPK inhibitors (Fig. 3.20). These results suggest increased sensitivity of knock out cells is attributed to higher pERK, pAKT and p-p38MAPK expression. Knock out cells also showed significantly higher (more than 3-fold) cancer stem cells compared to wild type cells upon estrogen stimulation (Figure 3.21A and 3.21B). The increase in CSC population was only observed upon estrogen treatment further suggesting increased estrogen responsiveness upon loss of miR-489.

3.2.8 MIR-489 SENSITIZES BREAST CANCER CELLS TO TAMOXIFEN

Loss of miR-489 increases activity of MAPK and PI3K-AKT signaling pathway. In addition, we have previously established that loss of miR-489 also increases activity of HER2 signaling pathway. All these pathways are known to promote estrogen independent growth and promote tamoxifen resistance. Therefore, we examined role of miR-489 in tamoxifen resistance. We first examined effect of miR-489 on estrogen independent growth. MCF7 and T47D cell lines require estrogen for their proliferation and depletion of estrogen dramatically reduce their survival. Remarkably, inhibition of endogenous miR-489 significantly

increased survival under estrogen depletion (Fig. 3.22A and 3.22B). Mechanistically, inhibition of miR-489 increased estrogen independent phosphorylation of ERα through increased activation of MAPK and/or AKT (Fig. 3.22C and 3.22D). We then examined expression of miR-489 and its host gene CALCR in two different tamoxifen resistant cell lines MCF7-TAMR and MCF7-HER2. Both cell lines are derived differently but reported as tamoxifen resistant cell line. Remarkably, both cell lines showed significant down regulation of miR-489 and CALCR (Figure 3.23A, 3.23B). Analysis of patient datasets obtained from kmplot showed high miR-489 expression predicts better survival in ER+ breast cancer patients who received endocrine therapy (Figure 3.23C). (Lanczky et al., 2016). Similarly, higher CLACR expression also predicts better survival of ER+ breast cancer patient who received tamoxifen treatment (Figure 3.23D) (Mihaly et al., 2013). These analyses strongly suggest therapeutic potential role of miR-489 in tamoxifen resistance. Consistent with clinical analysis, our MTT assay (Figure 3.24A) and Clonogenic assay (Figure 3.24B) showed that miR-489 knock out cells are much more resistant to tamoxifen compared to WT cells. At higher concentration (7.5uM), we noticed 50% growth inhibition in WT cells while knock cells seemed almost unaffected. We the examined whether miR-489 restoration can sensitize tamoxifen resistant cell lines. We first modulated miR-489 expression in MCF7-HER2 cells. This cell line possesses *de novo* tamoxifen resistance due to hyper activation of HER2-PI3K-AKT signaling pathway. Intriguingly, although this cell line showed significant resistance to tamoxifen, they responded similarly as their sensitive counterpart (MCF7Vec) to miR-489 (Figure 3.25A). Forced

expression of miR-489 with tamoxifen sensitized resistant cell lines to Tamoxifen treatment (Figure 3.25B). Our clonogenic assay also showed significant sensitization upon co-treatment (Figure 3.25C). Conversely, inhibition of endogenous miR-489 in sensitive counterpart MCF7-Vec significantly protected cells from tamoxifen induced growth arrest and death (Figure 3.25D, 3.25E). Consistent with previous studies, our western blot analysis showed significant increase in ERα phosphorylation upregulation of HER2, AKT and ERK pathway (Shou et al., 2004). Restoration of miR-489 completely abolished activity of AKT and MAPK and attenuated ERα phosphorylation (Figure 3.25F). We also examined whether miR-489 can over acquired tamoxifen resistance. Like MCF7-HER2, although this cell line showed significant resistance to tamoxifen, they responded similarly as their sensitive counterpart (MCF7-WT) to miR-489 (Figure 3.26A). Forced expression of miR-489 with tamoxifen sensitized resistant cell lines to Tamoxifen treatment (Figure 3.26B). Conversely, inhibition of endogenous miR-489 in sensitive counterpart MCF7-Vec significantly protected cells from tamoxifen induced growth arrest and death (Figure 3.26C). Our clonogenic assay also showed significant sensitization upon co-treatment (Figure 3.26D, 3.26E). Notably, 72 hours treatment with 5uM Tamoxifen had only marginal effect in both resistant cell lines while co-treatment of tamoxifen with miR-489 resulted in around 50% growth inhibition in MCF7-TAM cell line and around 60% in MCF7-HER2 cell line. In summary, data shown here shows miR-489 targets multiple pathways associated with tamoxifen resistant and may provide a useful therapy sensitizer in tamoxifen resistant tumors.

3.3 Summary and Discussion

We report here that the miR-489 is positively regulated by the E2-ERα axis. However, since miR-489 inhibits activity of estrogen signaling, an interesting autoregulatory feedback loop can be proposed between ERα and the mir-489. We suggest that the role of the miR-489 is to balance the positive autoregulatory loop of E2-ERα axis by a negative feedback loop to control activity of ERα. Many autoregulatory feedback loops have been shown to regulate biological activity of a pathway. Similar autoregulatory loops involving miRNAs have been previously shown. For example, while miR-20a directly inhibits transcriptional activity of E2F1-3 by directly binding to their 3' UTR (Sylvestre et al., 2007). Interestingly, in our study we also observed a positive feedback loop between E2-ERα signaling and p38 MAPK. Estrogen activates p38 MAPK within few minutes upon binding to its receptor ERα.This activated p38 MAPK leads to nuclear translocation of ERα which is essential for its transcriptional activity. Similar observation has also been reported for ERK and AKT in regard to estrogen signaling. Like p38 MAPK, estrogen also activates AKT and ERK. Activated ERK and AKT then activates ERα by phosphorylating ERα at Ser1018 and Ser167. miR-489 regulates this positive feedback loop by inhibiting p38 MAPK, AKT and ERK activity (Figure 3.27). One interesting function of the negative feedback loop between ERα and the miR-489 would be to create a fail-safe mechanism to avoid high ERα activity since, high ERα activity is potentially dangerous for the cell and is a major risk factor for breast cancer. In addition, miR-489 could serve as a potential prognostic marker in ER+ breast cancer where ER+ patients with low miRNA may possess hyper activation

of E2-ERα signaling and may potentially represent aggressive cancers. Indeed, clinical analysis of ER+ breast cancer patients suggest that patients with low miR-489 expression have worse survival and have aggressive tumors. Although, endocrine therapy is the most effective way to treat ER+ breast cancer patients, 20-30% of patients acquire resistance to this therapy. Besides, ER+ cancer patients with over expression of growth factors such as EGFR or HER2 possess *de novo* resistance against tamoxifen treatment (Chang, 2012). Our observations here indicate that miR-489 could potentially serve as a useful therapy sensitizer to treat tamoxifen resistance tumors. First, our study along with other reports showed miR-489 is significantly downregulated in tamoxifen resistant cell lines. Intriguingly, it is lost is both acquired and de novo resistant. Second, miR-489 directly inhibits AKT and MAPK pathways which are well established mechanism that promote estrogen independent growth and tamoxifen resistance. Third, miR-489 directly targets HER2 and its downstream molecules including SHP2 and AKT. Furthermore, autophagy and EMT has been reported to promote tamoxifen resistance. MCF7-TAM cells have been reported to undergone EMT and possesses higher basal autophagy (M. H. Lee et al., 2018; Nagelkerke et al., 2014; Ward et al., 2013). Inhibition of both processes have been previously shown to reverse the tamoxifen resistance. Interestingly, miR-489 has previously been reported reverse EMT through inhibition of Smad3 expression which leads to sensitization of doxorubicin. Previously, we have reported its role in autophagy and chemo-resistance(Soni et al., 2018). These data further support role of miR-489 in modulation of tamoxifen resistance.

In summary, these results suggest that miR-489 based therapy may be useful adjuvant therapy not only in resistant patients but also in treatment naïve patients since apart from inhibiting estrogen signaling, it also blocks HER2-PI3K-AKT and MAPK pathways and may potentially reduce emergence of resistance to tamoxifen. These results contribute to the understanding of the complex regulatory pathways regulating ERα activity and are therefore may provide insights to develop novel ER+ breast cancer therapy.

A

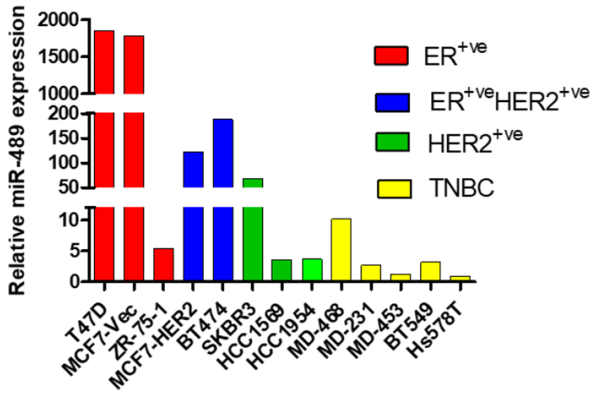

C

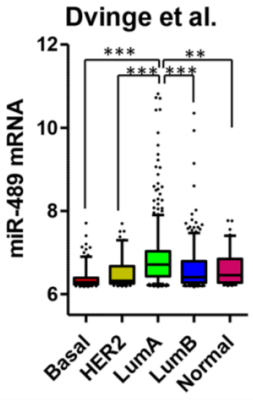

B

Gene Identifier	Correlation coefficient	Parametric p-value
CALCR	0.558	0
ESR1	0.208	0
PGR	0.268	0

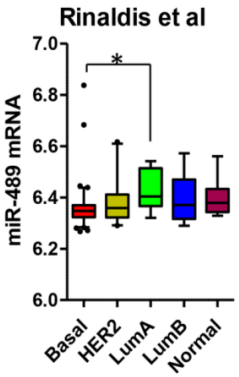

Figure 3.1: miR-489 expression is positively correlated with expression of estrogen receptor. A. Expression of miR-489 in 13 different breast cancer cell lines representing 4 subtypes. Data are means of three replicates + SEM. B. Correlation of miR-489 with its host gene CALCR, estrogen receptor and progesterone receptor in clinical samples. C. Relative expression levels of miR-489in breast cancer subtypes were compared using the one-way ANOVA analysis. The microarray data was extracted from previous publication [51, 52]. *, p value < 0.05; **, p value < 0.01; ***, p value < 0.001. ***, p<0.001; **, p<0.01; *, p<0.05.

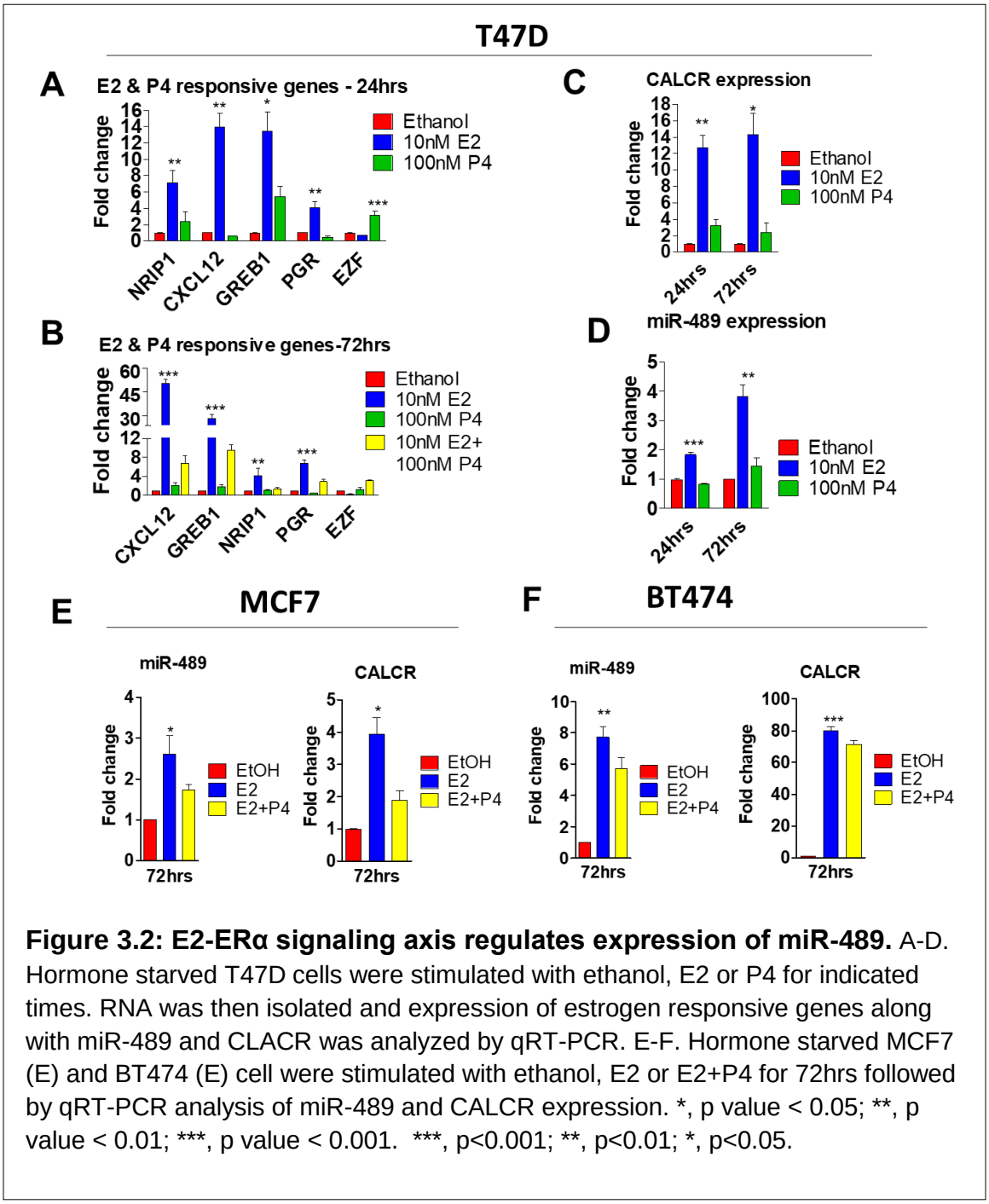

Figure 3.2: E2-ERα signaling axis regulates expression of miR-489. A-D. Hormone starved T47D cells were stimulated with ethanol, E2 or P4 for indicated times. RNA was then isolated and expression of estrogen responsive genes along with miR-489 and CLACR was analyzed by qRT-PCR. E-F. Hormone starved MCF7 (E) and BT474 (E) cell were stimulated with ethanol, E2 or E2+P4 for 72hrs followed by qRT-PCR analysis of miR-489 and CALCR expression. *, p value < 0.05; **, p value < 0.01; ***, p value < 0.001. ***, p<0.001; **, p<0.01; *, p<0.05.

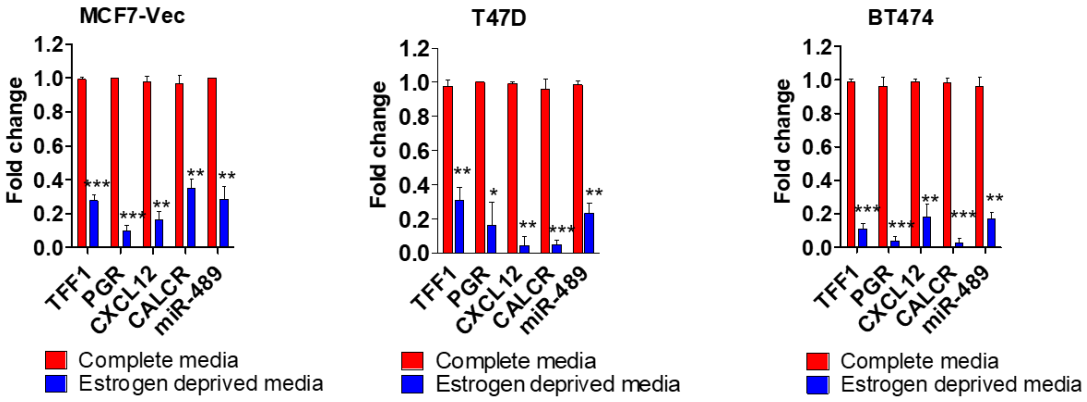

Figure 3.3: Estrogen deprivation down-regulates expression of miR-489. qRT-PCR analysis of miR-489 expression in complete media and in estrogen deprived medium. *, p value < 0.05; **, p value < 0.01; ***, p value < 0.001. ***, p<0.001; **, p<0.01; *, p<0.05.

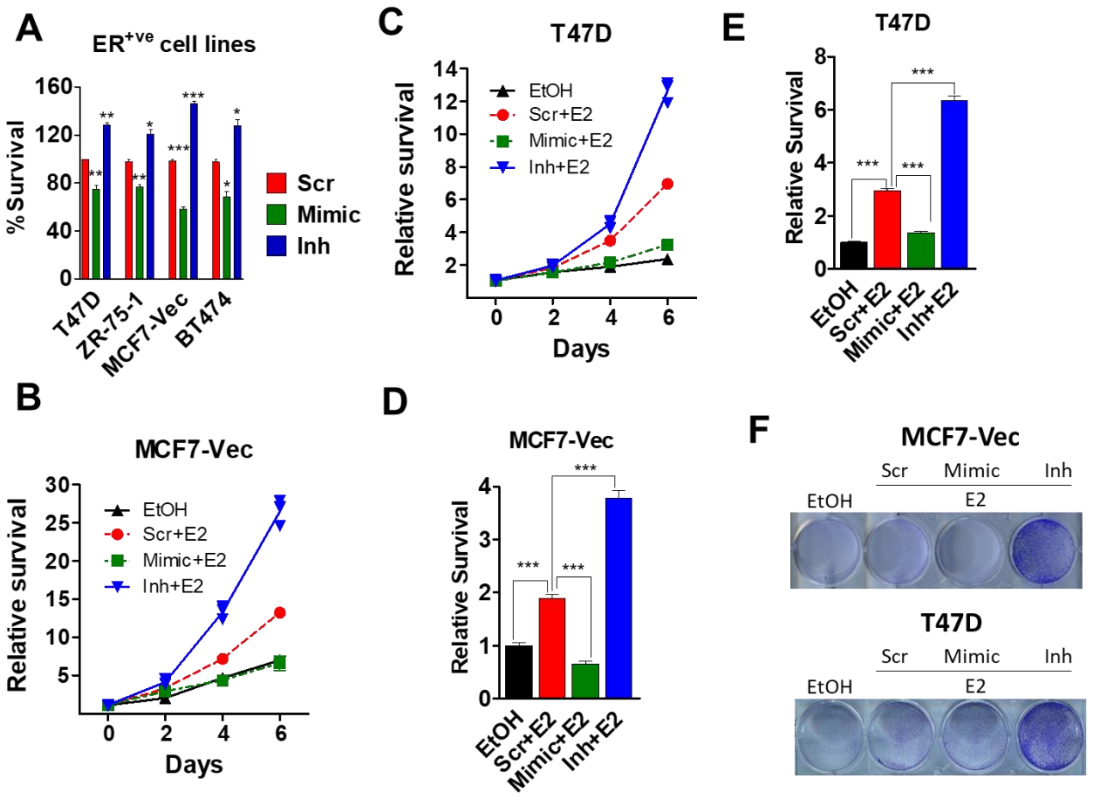

Figure 3.4: miR-489 inhibits estrogen induced proliferation. A. ER+ breast cancer cell lines were transfected with scr, mimic or inh for 72 hours and cell viability was measured using MTT assay. B-C. Hormone starved MCF7 (B) and T47D (C) cell were stimulated with ethanol, E2 in presence of scr, mimic or inh for 6days followed and cell viability was measured using MTT assay. D-E. Relative survival at the end of 6day treatment in MCF7-Vec (D) and T47D (E). F. Hormone starved MCF7-Vec and T47D cells were treated with estrogen in presence of scr, mimic or inh for 8days and clonogenic assay was performed using crystal violet. *, p value < 0.05; **, p value < 0.01; ***, p value < 0.001. ***, p<0.001; **, p<0.01; *, p<0.05.

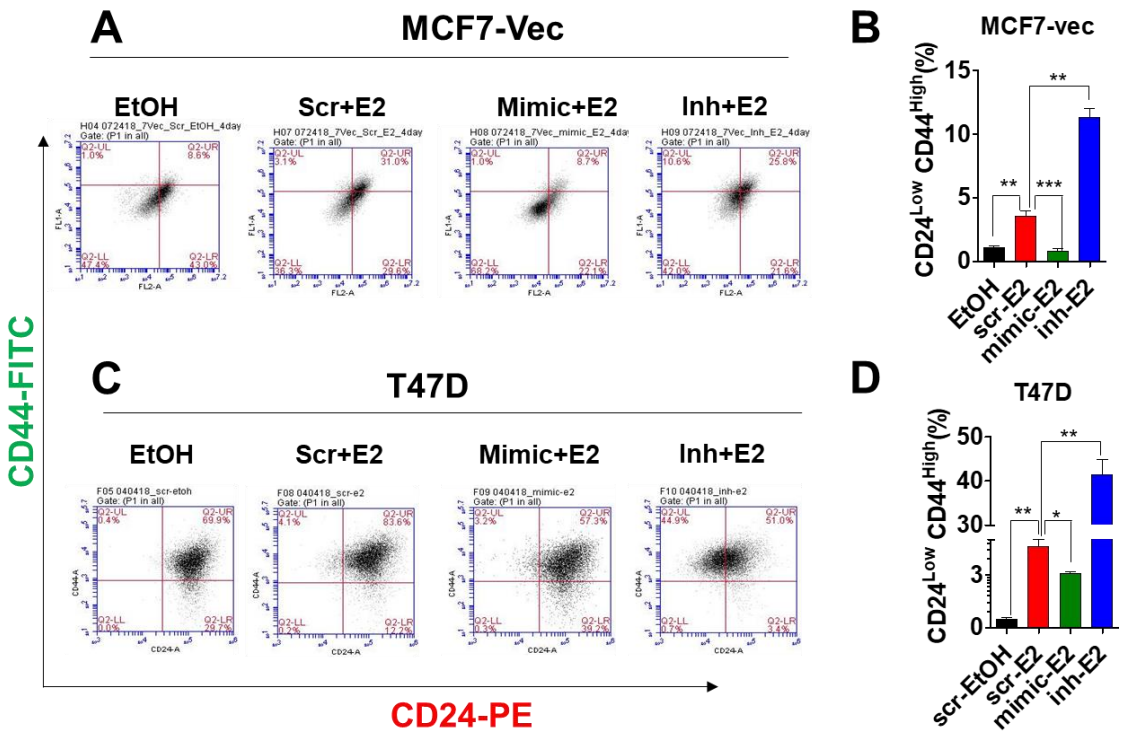

Figure 3.5: Depletion of miR-489 promotes estrogen induced cancer stem cell population. A-D. ER+ breast cancer cell lines MCF7-Vec (A) and T47D (C) were transfected with scr, mimic or inh for 6 days in presence of estrogen and cancer stem cell population was measured by flow cytometry using CD24 CD44 surface markers. B & D. Quantification of CD24low CD44high cells. *, p value < 0.05; **, p value < 0.01; ***, p value < 0.001. ***, p<0.001; **, p<0.01; *, p<0.05.

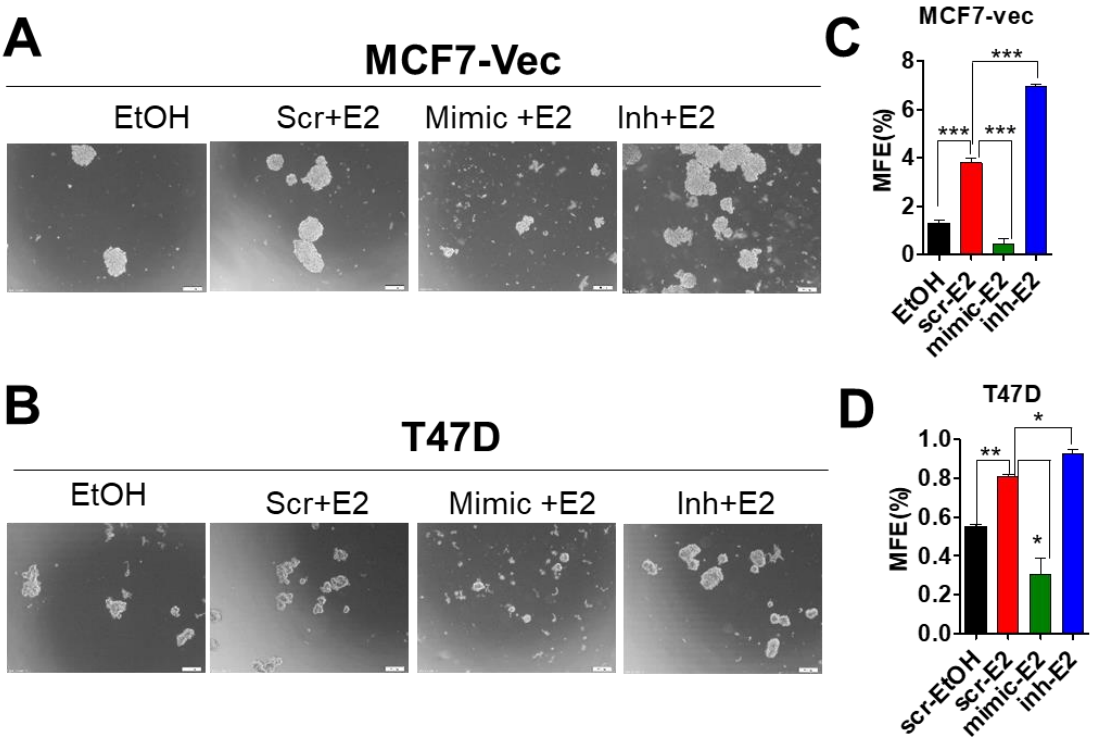

Figure 3.6: Depletion of miR-489 promotes estrogen induced mammosphere formation. A-D. ER+ breast cancer cell lines MCF7-Vec (A) and T47D (B) were transfected with scr, mimic or inh for 6 days in presence of estrogen and cancer stem cell population was measured by mammosphere assay. C-D. Quantification of mammosphere forming efficiency in MCF7-Vec (C) and T47D (D) cells upon indicated treatment. *, p value < 0.05; **, p value < 0.01; ***, p value < 0.001. ***, p<0.001; **, p<0.01; *, p<0.05.

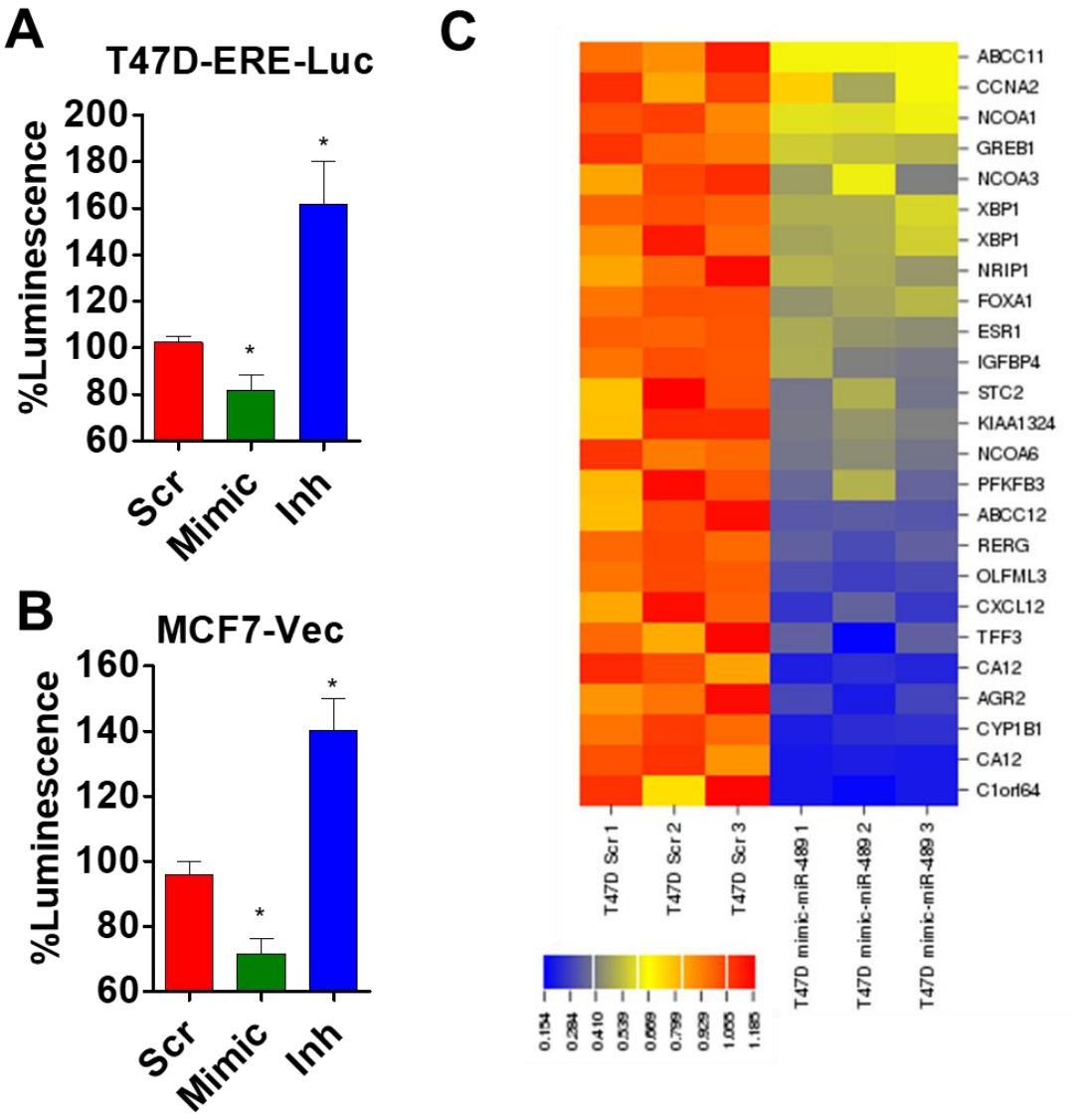

Figure 3.7: miR-489 inhibits estrogen induced gene transcription. A. ERE-reporter cell line T47D was transfected with scr, mimic or inh for 72 hours and luciferase activity was measured to report transcriptional activity of ERα. B. MCF7-Vec cells were transiently transfected with scr, mimic or inh. After 24 hours cells were transfected with ERE-Luc reporter plasmid. 48 hours later luciferase activity was measured. C. Gene expression analysis of T47D cells showing down regulation of known estrogen responsive genes upon miR-489 over expression. *, p value < 0.05; **, p value < 0.01; ***, p value < 0.001. ***, p<0.001; **, p<0.01; *, p<0.05.

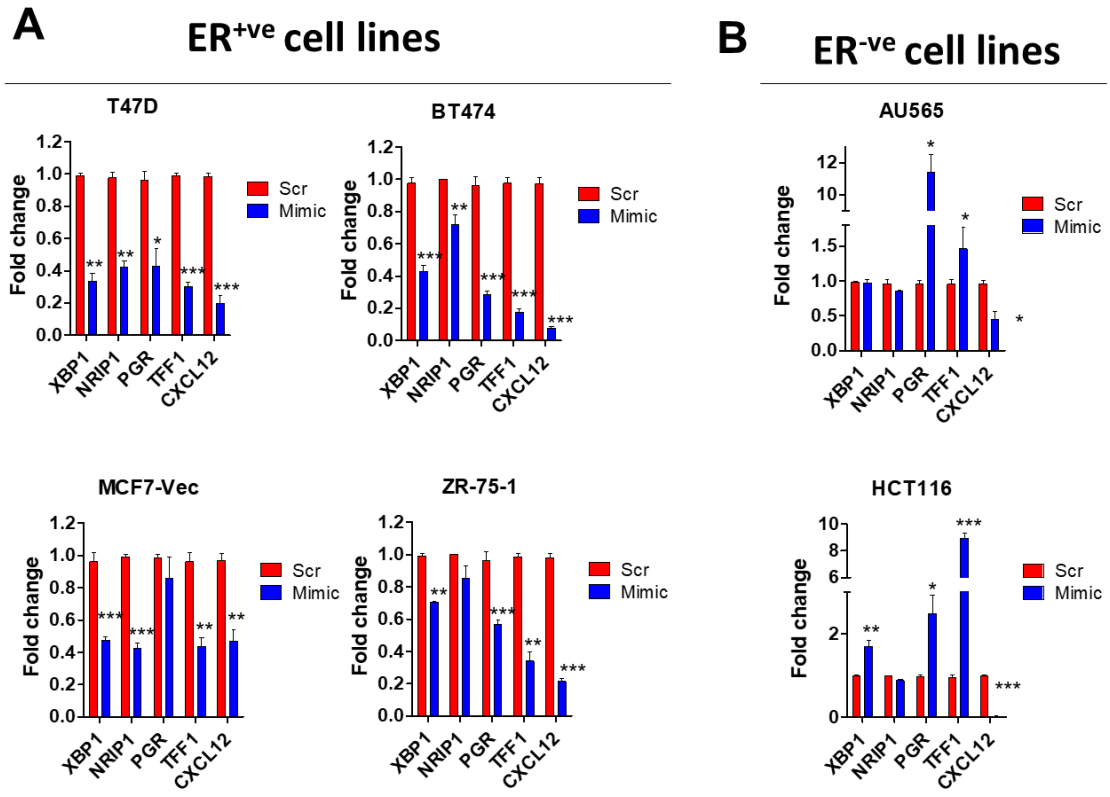

Figure 3.8: miR-489 inhibits expression of estrogen responsive genes. A-B. ER+ cell lines (A) and ER- cell lines (B) were transfected with scr or mimic for 72 hours and qRT-PCR was performed to validate microarray results. *, p value < 0.05; **, p value < 0.01; ***, p value < 0.001. ***, p<0.001; **, p<0.01; *, p<0.05.

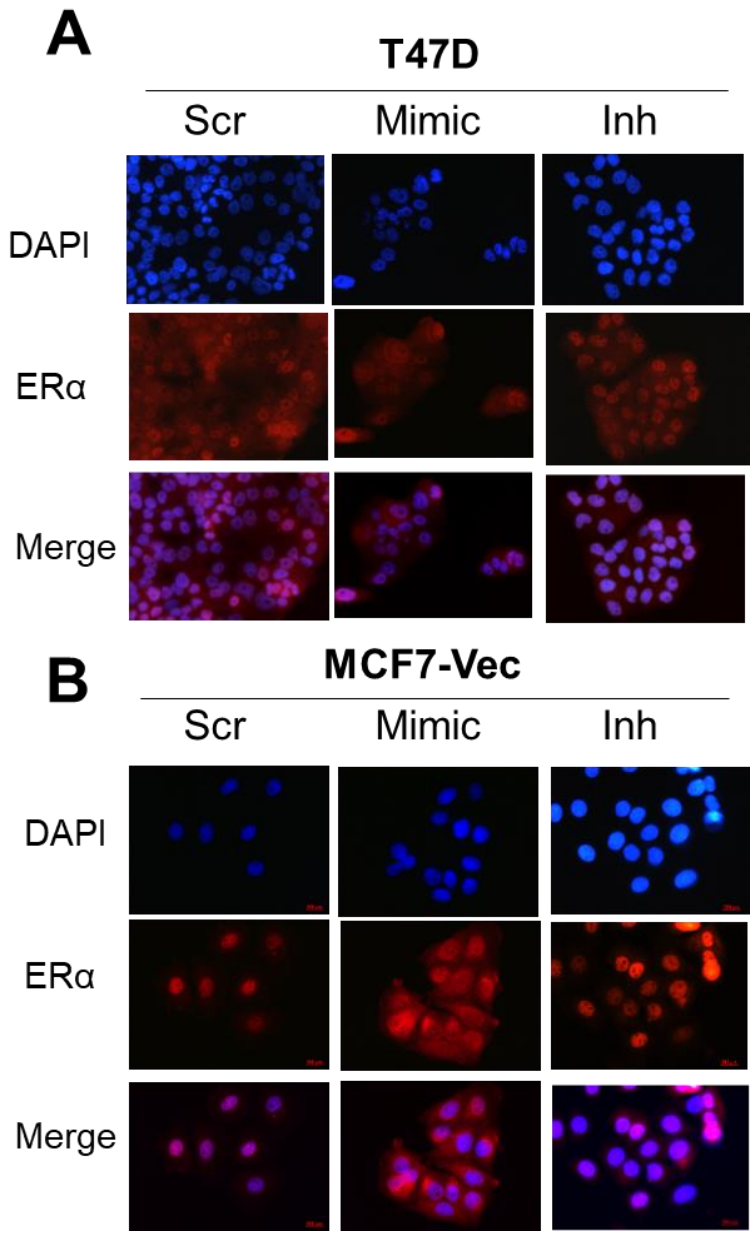

Figure 3.9: miR-489 inhibits estrogen dependent nuclear localization of ERα. A. ER+ cell line T47D (A) and MCF7-Vec (B) were transfected with scr, mimic or inh for 72 hours followed by immunofluorescence. DAPI was used as counter stain to stain nucleus. Images shown here are representative of three biological replicates.

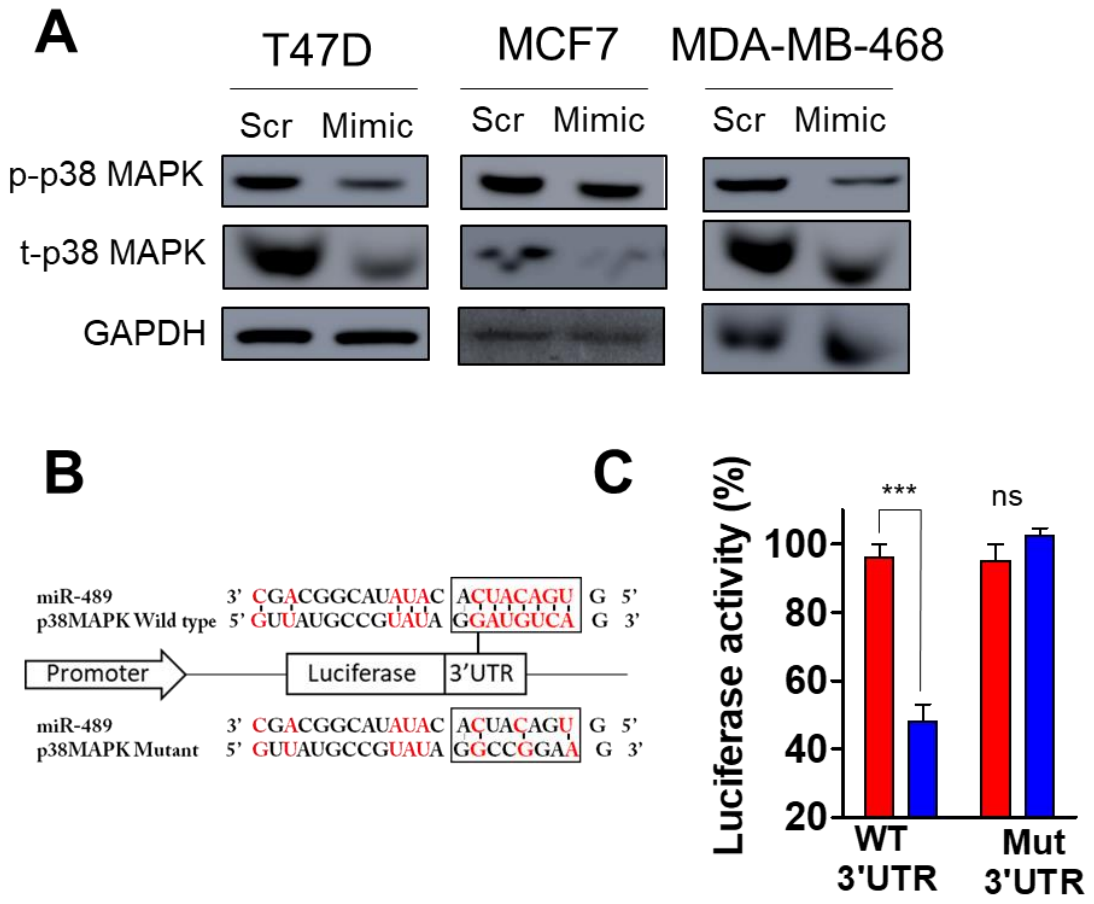

Figure 3.10: p38 MAPK is a direct target of miR-489. A. ER+ cell lines MCF7, T47D and ER- cell line MDA-MB-468 were transfected with scr or mimic for 72 hours. Phospho-p38 MAPK and total p38 MAPK expression was examined by western blot. GAPDH was used as a loading control. B. Schematic diagram of miR-489 binding site in p38 MAPK UTR. C. Luciferase reporter plasmids containing wild type or mutant 3'UTR were co-transfected with vector or miR-489 overexpressing plasmids in HEK293 cells. Renilla luciferase reporter was used for normalization. *, p value < 0.05; **, p value < 0.01; ***, p value < 0.001. ***, p<0.001; **, p<0.01; *, p<0.05.

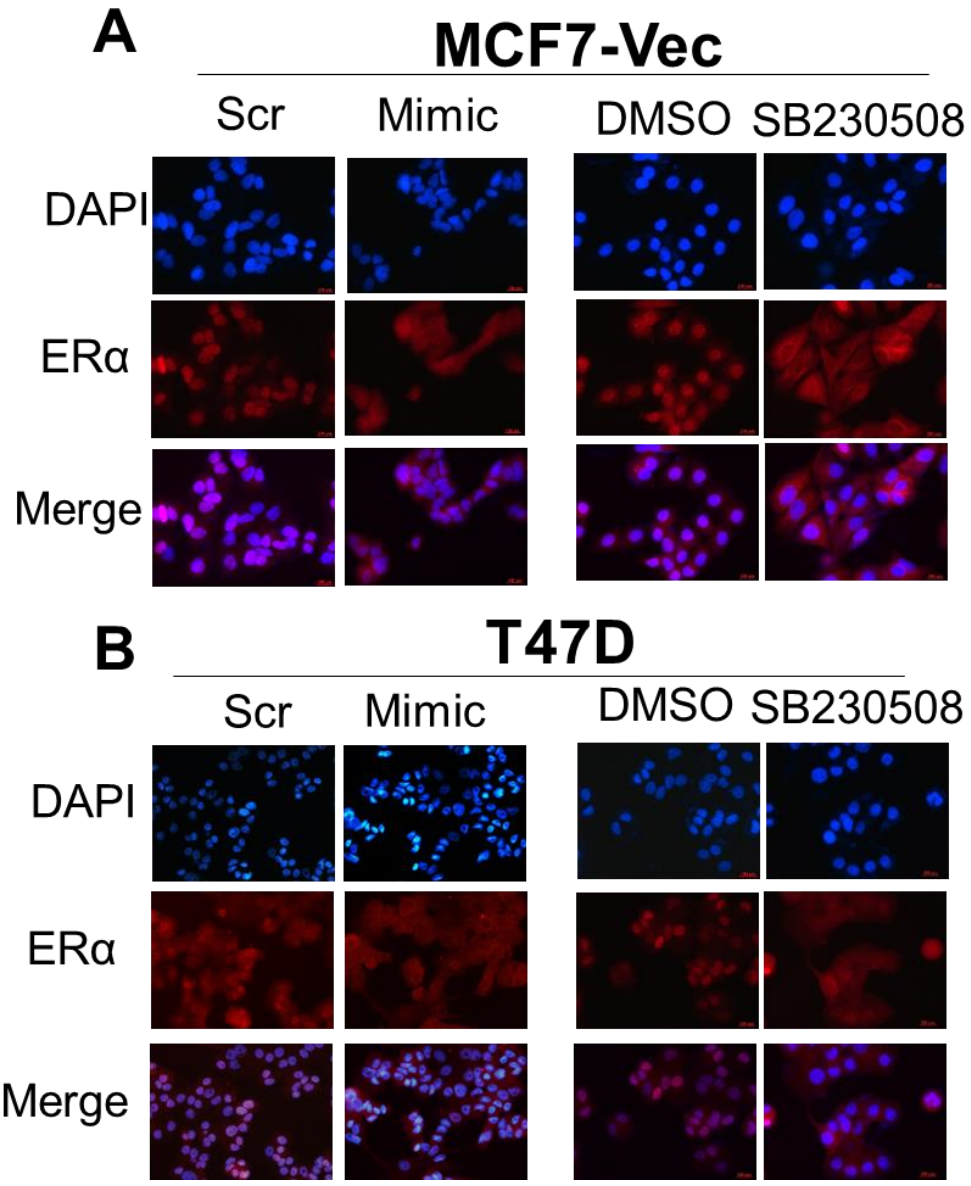

Figure 3.11: p38 MAPK inhibition phenocopies effect of miR-489 on ER localization. A. Estrogen starved ER+ cell lines MCF7-Vec (A) and T47D (B) were transfected with scr or mimic for 72hrs or treated with DMSO or 10uM SB203580 for 24hrs and treated for 15 min with E2. ERα localization was then examined by immunofluorescence. DAPI was used as counter stain to stain nucleus. Images shown here are representative of three biological replicates.

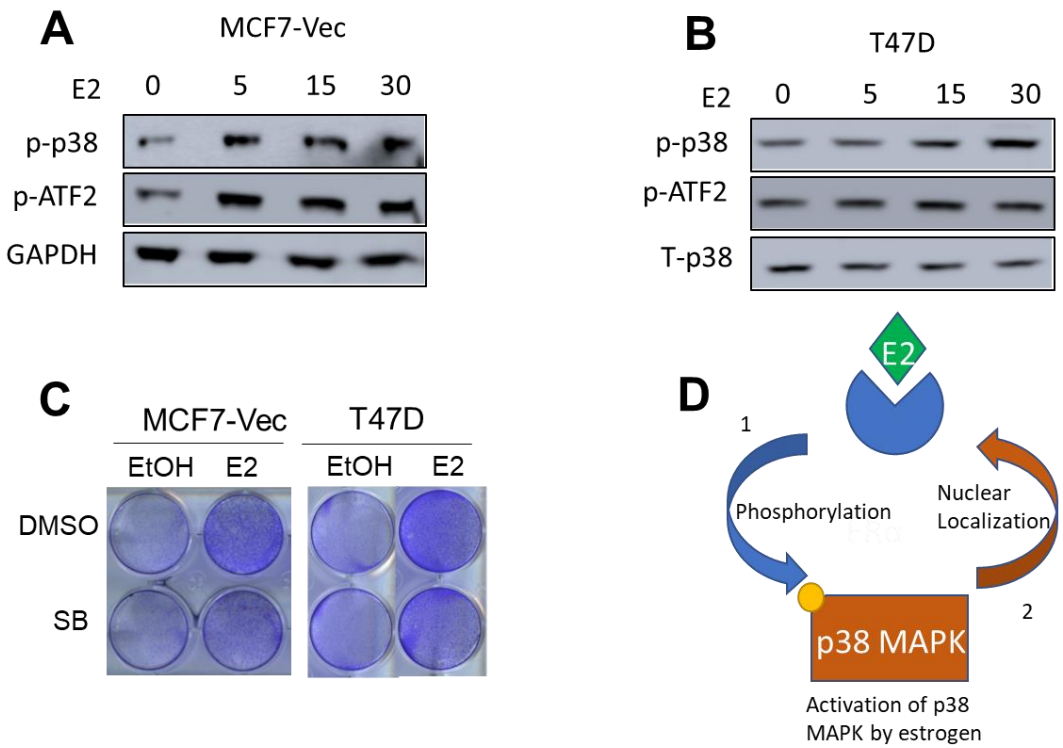

Figure 3.12: Positive feedback loop exists between E2-ERα axis and p38 MAPK. A-B. ER+ cell lines MCF7-Vec (A) and T47D (B) were hormone starved for 3days and then treated with E2 for indicated time points. Western blot analysis was then performed to examine p38 MAPK activation. GAPDH and total p38 MAPK were used as control. C. Hormone starved MCF7-Vec and T47D cells were treated with Ethanol or E2 in presence and absence of p38 MAPK inhibitor for 3 days. Viable cells were then fixed with methanol and stained with crystal violet. D. Proposed positive feedback loop between E2-ERα axis and p38 MAPK.

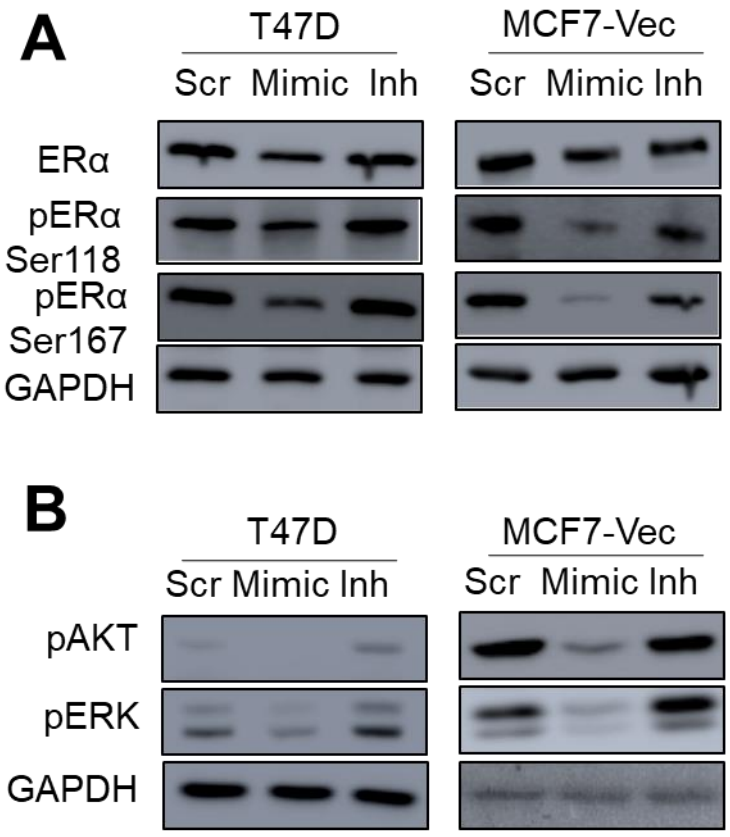

Figure 3.13: miR-489 reduces ERα phosphorylation by inhibiting MAPK and PI3K-AKT pathway. A. ER+ cell lines MCF7-Vec and T47D were transiently transfected with scr, mimic or inh for 3days. Total ERα and its phosphorylation level was inspected by western blot. GAPDH was used as loading control. B. ER+ cell lines MCF7-Vec and T47D were transiently transfected with scr, mimic or inh for 3days. Phosphorylated forms of AKT and ERK kinases were checked by western blot. GAPDH was used as loading control.

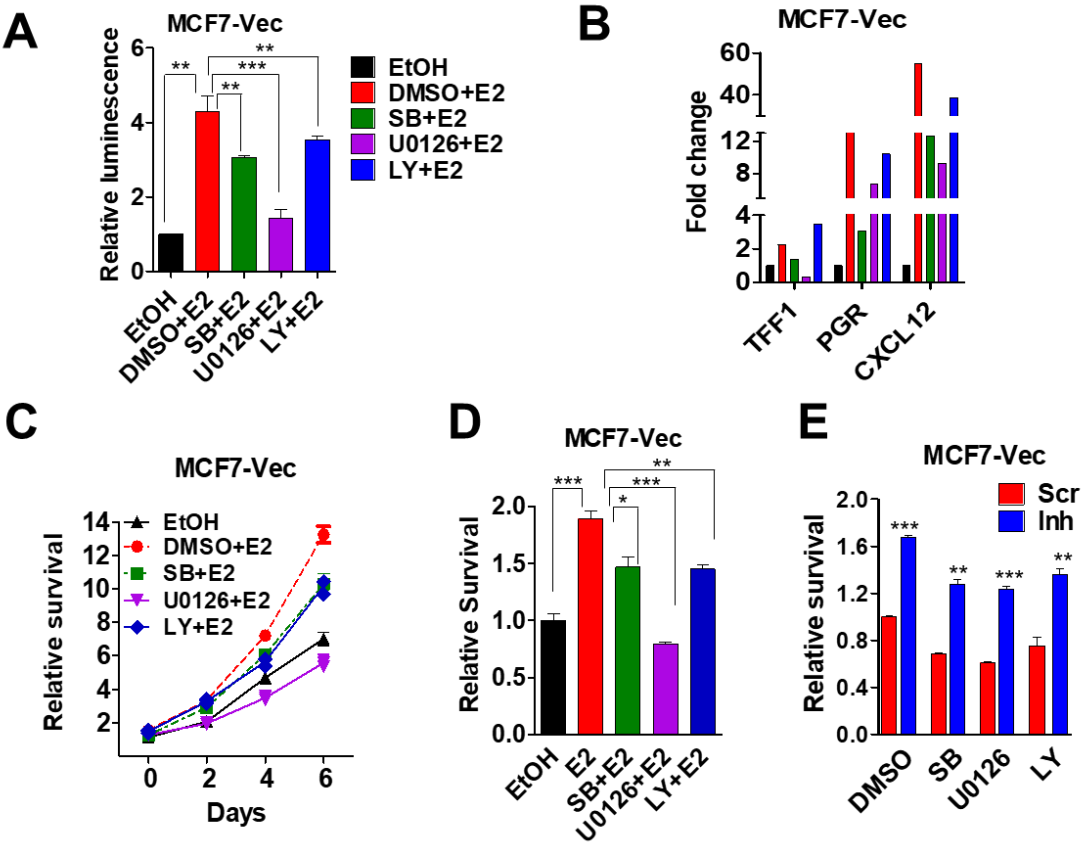

Figure 3.14: miR-489 attenuates estrogen induced transcription and proliferation by Inhibiting p38 MAPK, ERK and PI3K-AKT pathways. A. ER+ cell lines MCF7-Vec and T47D were transiently transfected with scr, mimic or inh for 3days. Total ERα and its phosphorylation level was inspected by western blot. GAPDH was used as loading control. B. ER+ cell lines MCF7-Vec and T47D were transiently transfected with scr, mimic or inh for 3days. Phosphorylated forms of AKT and ERK kinases were checked by western blot. GAPDH was used as loading control. *, p value < 0.05; **, p value < 0.01; ***, p value < 0.001. ***, p<0.001; **, p<0.01; *, p<0.05.

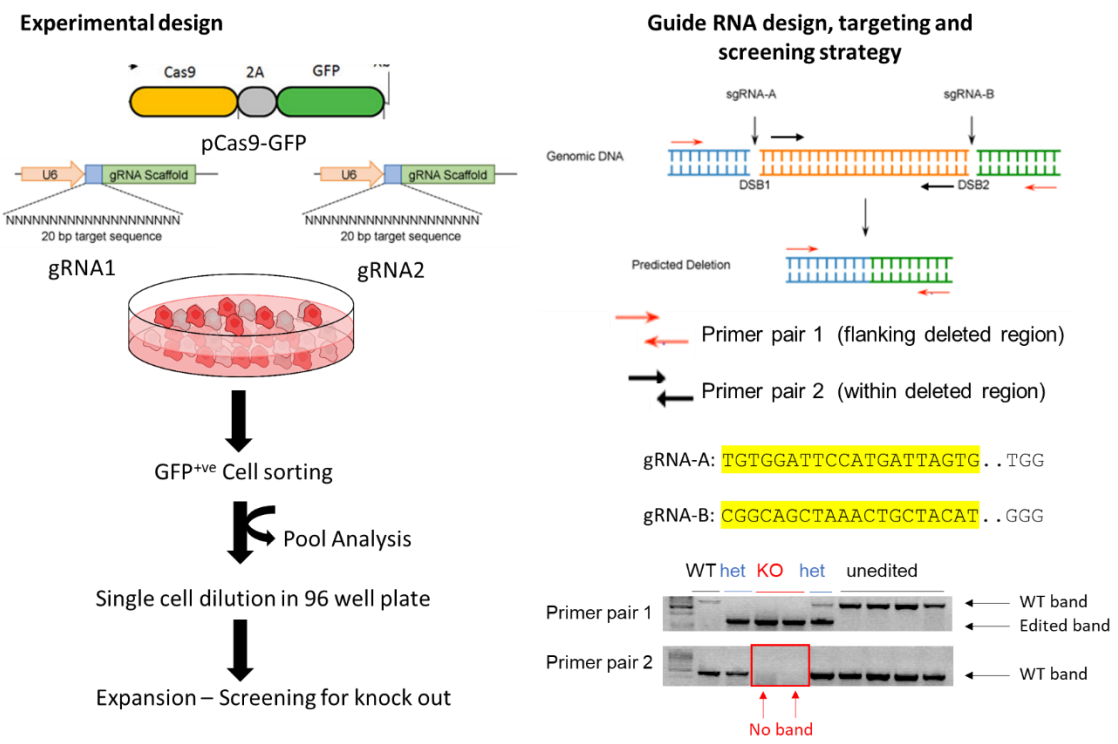

Figure 3.15: Schematic diagram demonstrating strategy and outline to generate miR-489 knock out cell line. Experimental design and strategy to generate miR-489 knock out cells. Figure shows guide RNA design strategy, guide RNA sequences and genotyping of edited clones. Red box indicates knock out clones.

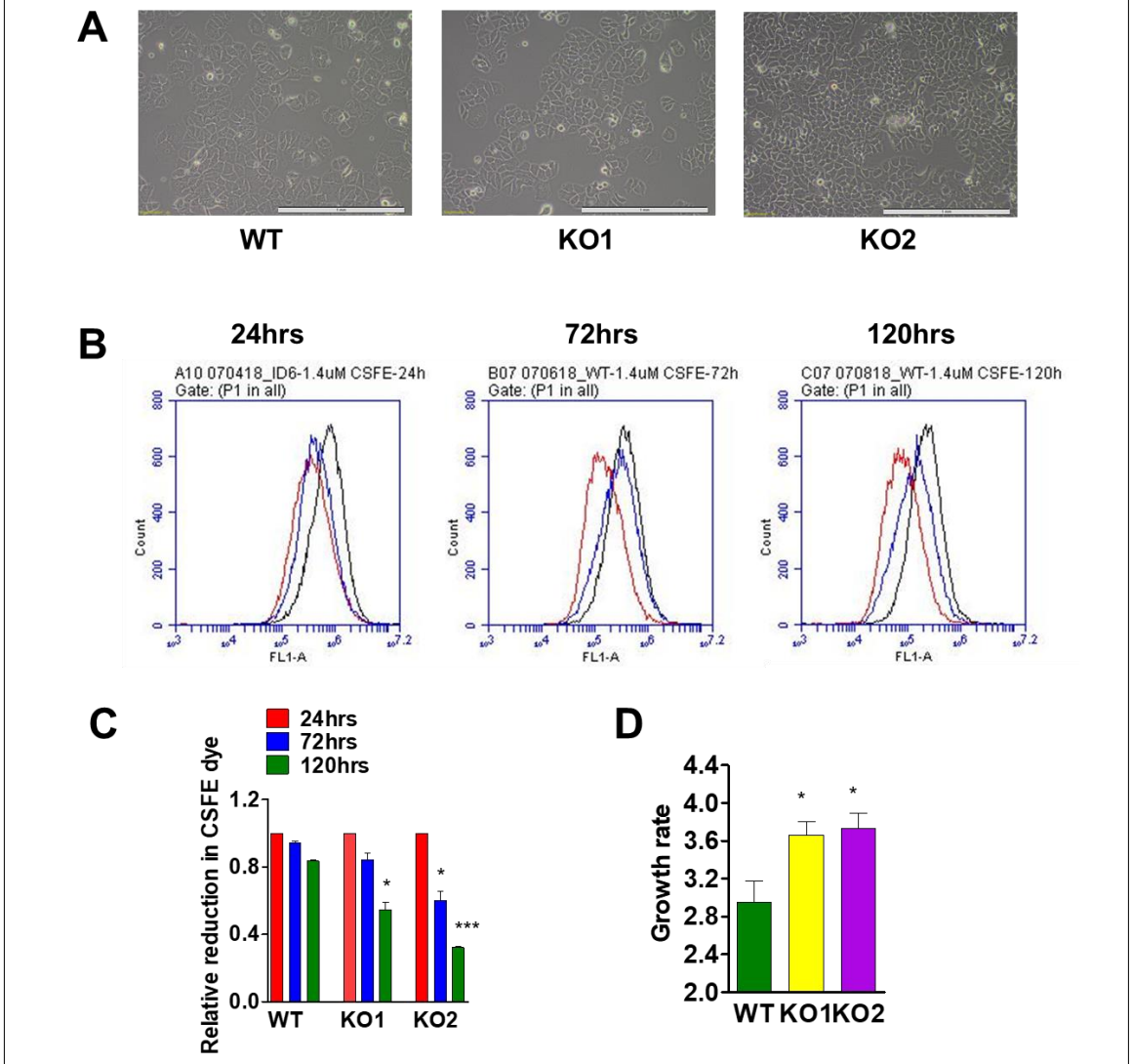

Figure 3.16: miR-489 knock out cells display significant increase in proliferation rate compared to wild type cells. A. Bright field microscopy showing morphology of wild type and knock out (KO) cells. B. WT and KO cells were seeded in six well and cultured for indicated time points, stained for 15min using 1.4uM CFSE dye at 37C and analyzed by flow cytometry. C. Quantitative analysis showing relative decrease in CSFE dye. D. WT and KO cells were seeded in 96 well plate for 24hrs, 48hrs and 96hrs. MTT based viability assay was performed to determine growth rate. *, p value < 0.05; **, p value < 0.01; ***, p value < 0.001. ***, p<0.001; **, p<0.01; *, p<0.05.

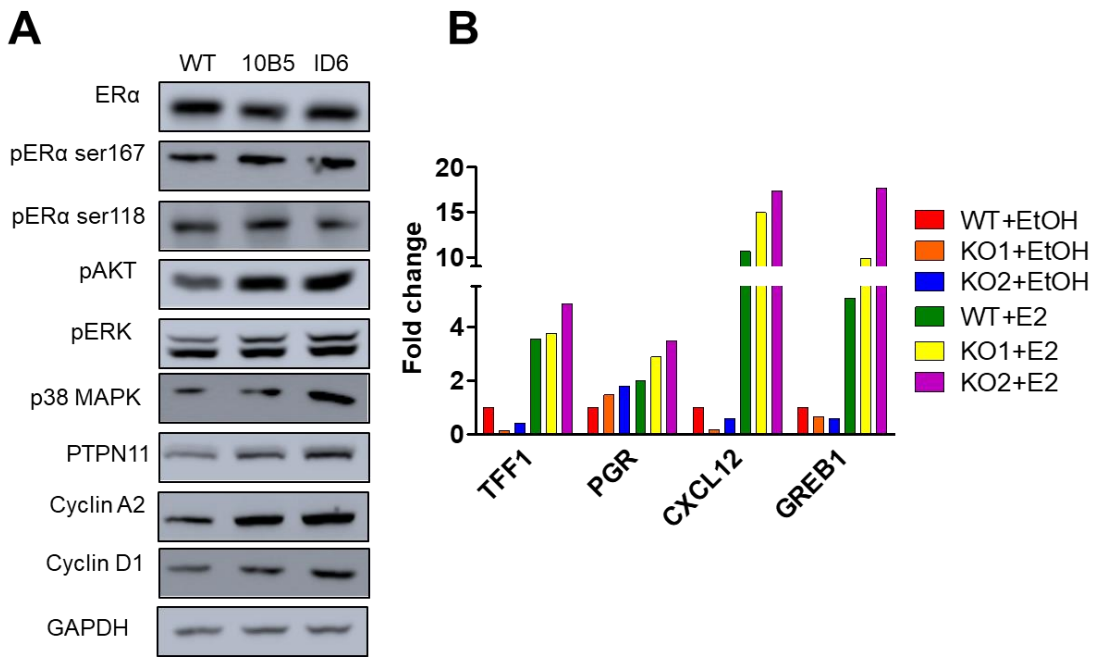

Figure 3.17: Characterization of knock out cells using western blot and qRT-PCR analysis. A Western blot analysis of miR-489 target proteins in WT and KO cells. GAPDH was used as s loading control. B. WT and knock out cells were hormone starved for 3days and stimulated with ethanol for 24 hrs. RNA was isolated and qRT-PCR was performed to examine expression of estrogen responsive genes.

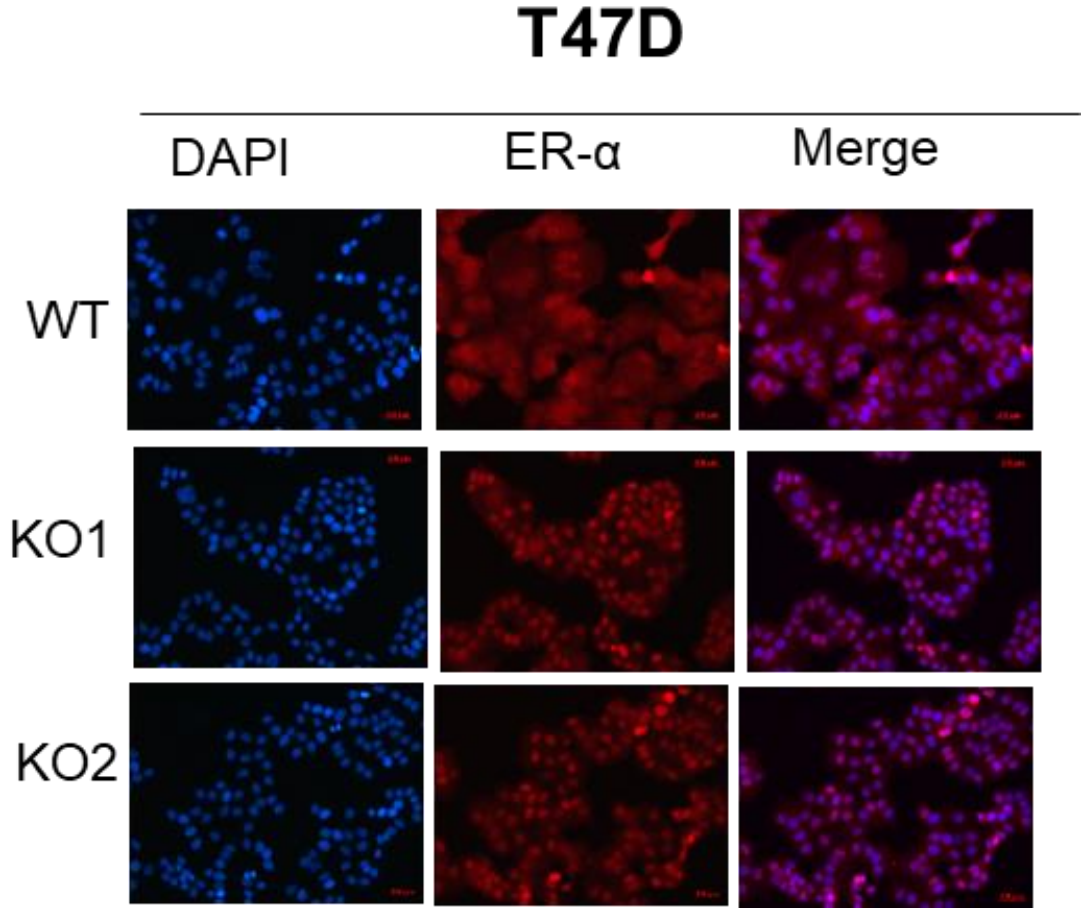

Figure 3.18: miR-489 knock out cells displays increased nuclear localization of ERα. WT and KO cells were seeded on cover slip in 6-well plate. Immunofluorescence microscopy was carried out 48-72 hrs post seeding to examine localization of ERα

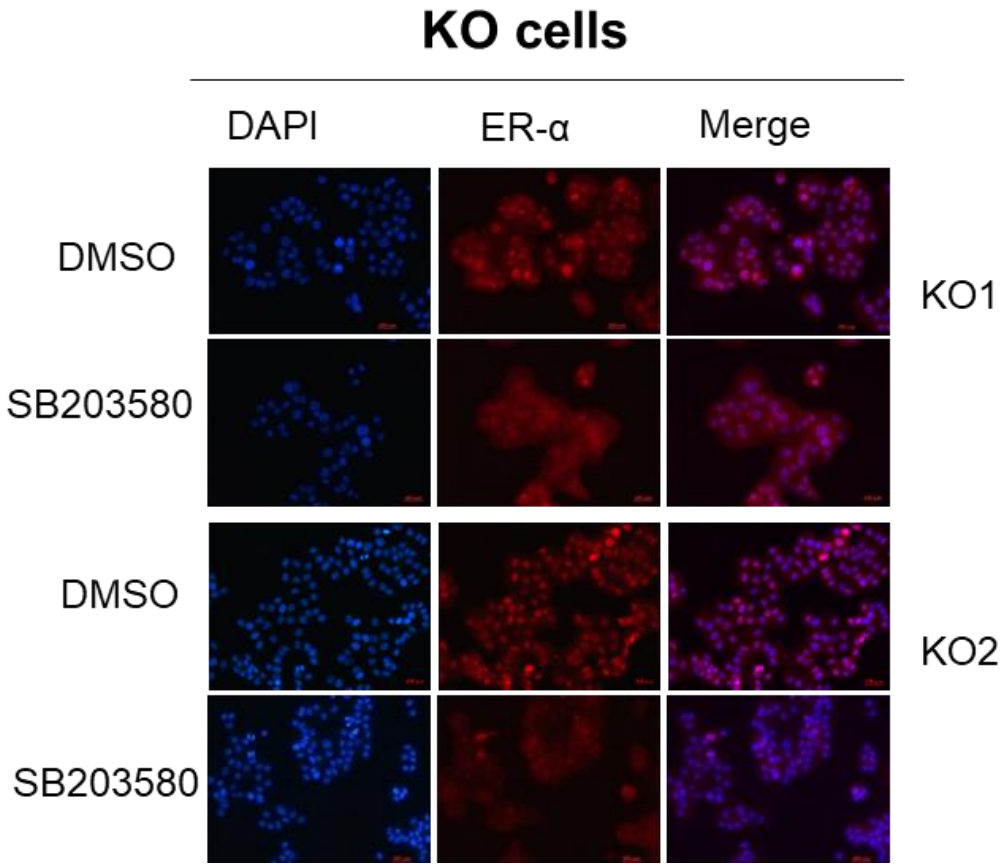

Figure 3.19: Inhibition of p38 MAPK reverses localization of ERα. KO cells were seeded on cover slip in 6-well plate and treated with SB203580 for 24hrs. Immunofluorescence microscopy was then carried out to examine localization of ERα

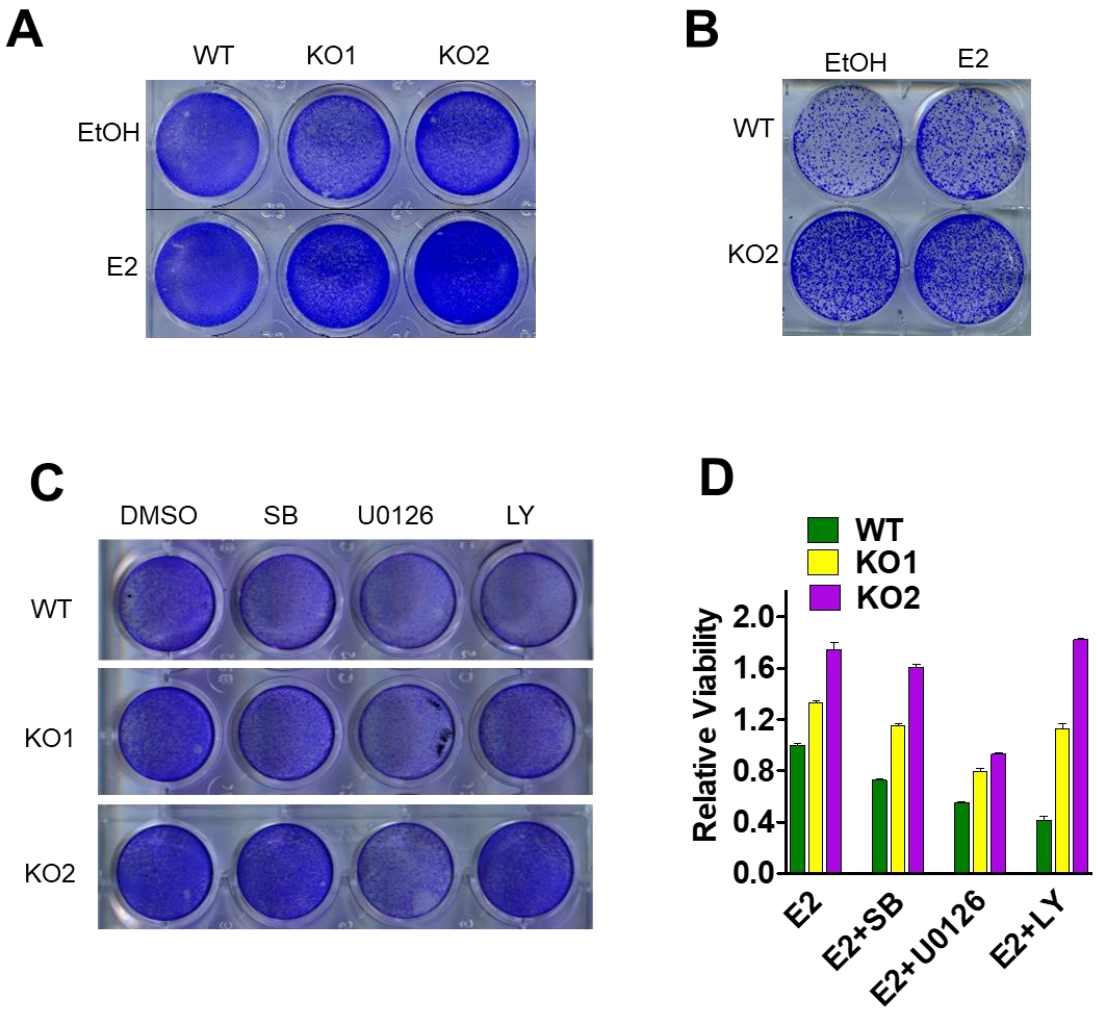

Figure 3.20: miR-489 knock out cells display hyper sensitivity to estrogen induced proliferation via over activation of p38 MAPK, MAPK and AKT pathways. A. Hormone starved WT and KO cells were seeded in 12-well plate and treated with ethanol or E2 for 6-days and clonogenic ability was measured by crystal violet staining. B. Cell treated in A were collected and 10K cells were seeded in 6-well plate in estrogen containing media for colony formation assay. C. Hormone starved cells were seeded in 24-well plate and treated with E2 and indicated inhibitors. Clonogenic assay was performed at the end of 6-day treatment. D. MTT assay of cells treated same as in C.

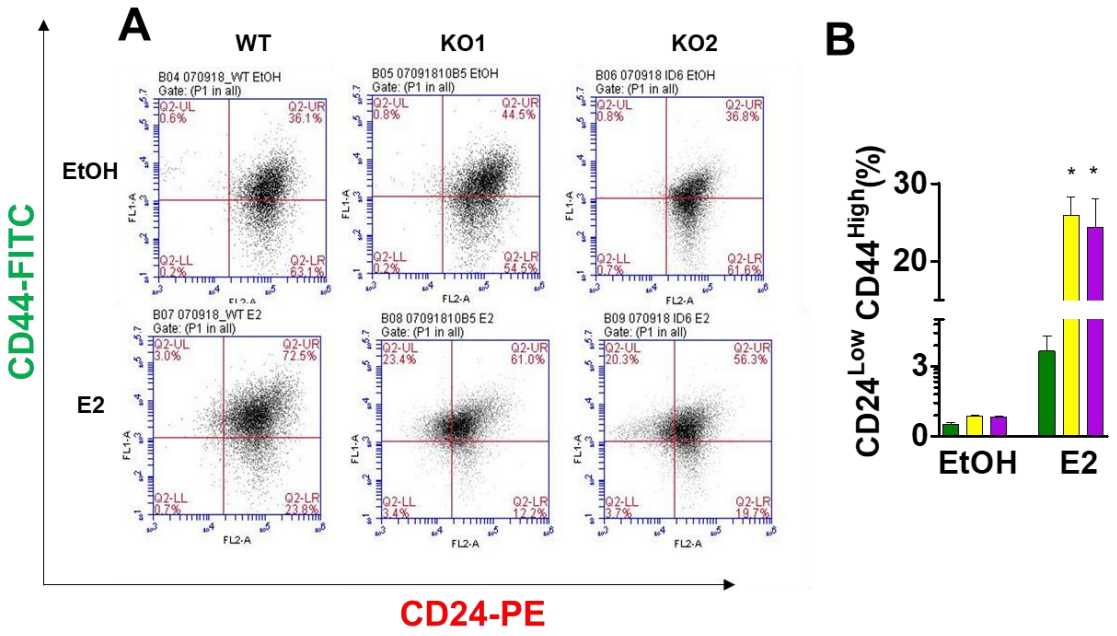

Figure 3.21: Loss of miR-489 increases estrogen induced cancer stem cell expansion. Hormone starved WT and KO cells were treated with ethanol or E2 for 6days and cancer stem cell population were analyzed using flow cytometry. Data are representative of two independent biological replicates. *, p value < 0.05; **, p value < 0.01; ***, p value < 0.001. ***, p<0.001; **, p<0.01; *, p<0.05.

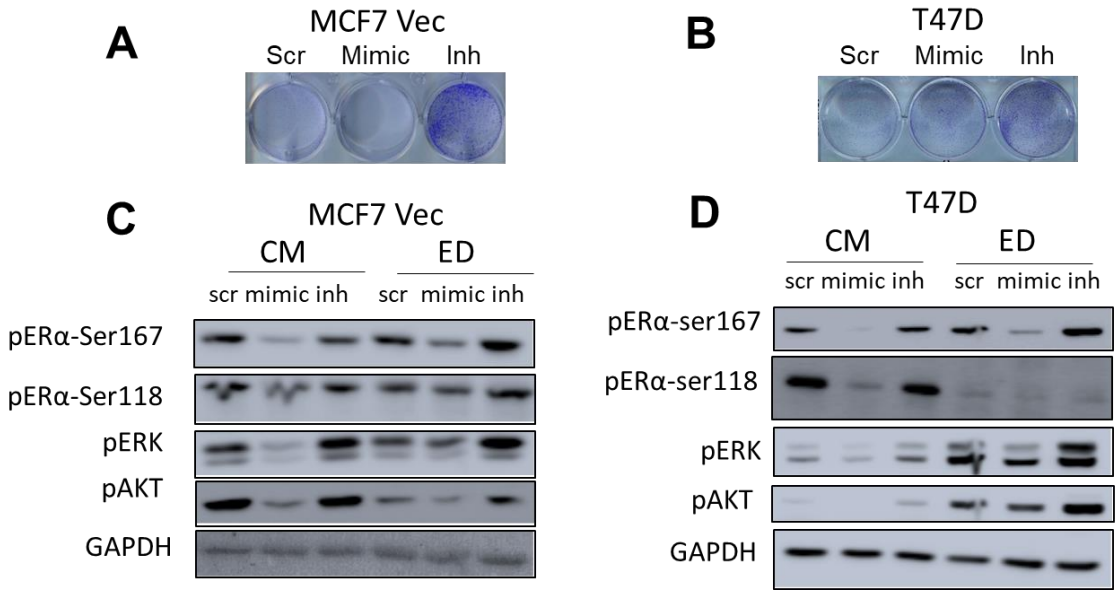

Figure 3.22: Loss of miR-489 increases estrogen independent growth. Hormone starved WT and KO cells were treated with ethanol or E2 for 6days and cancer stem cell population were analyzed using flow cytometry. Data are representative of two independent biological replicates. *, p value < 0.05; **, p value < 0.01; ***, p value < 0.001. ***, p<0.001; **, p<0.01; *, p<0.05.

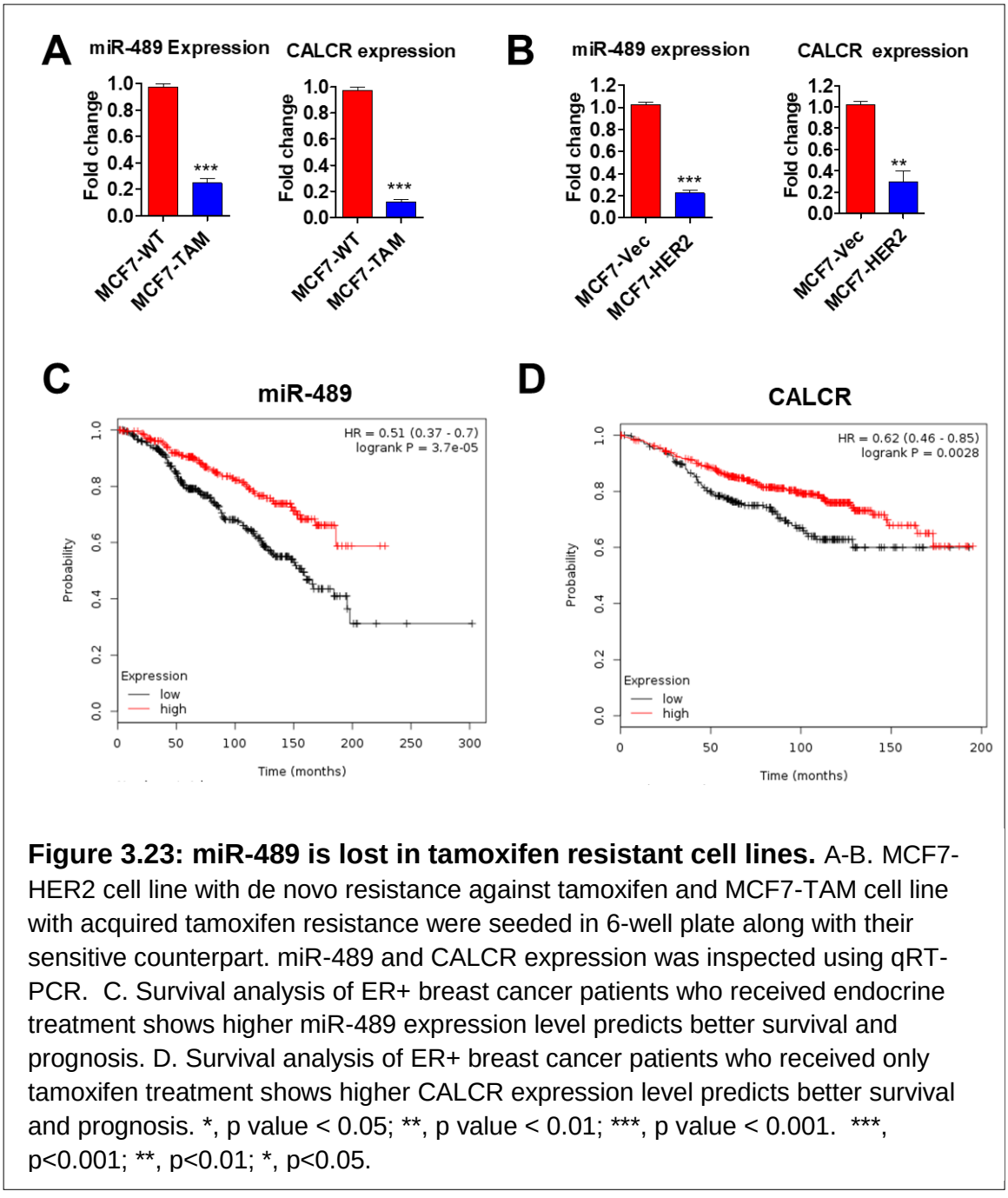

Figure 3.23: miR-489 is lost in tamoxifen resistant cell lines. A-B. MCF7-HER2 cell line with de novo resistance against tamoxifen and MCF7-TAM cell line with acquired tamoxifen resistance were seeded in 6-well plate along with their sensitive counterpart. miR-489 and CALCR expression was inspected using qRT-PCR. C. Survival analysis of ER+ breast cancer patients who received endocrine treatment shows higher miR-489 expression level predicts better survival and prognosis. D. Survival analysis of ER+ breast cancer patients who received only tamoxifen treatment shows higher CALCR expression level predicts better survival and prognosis. *, p value < 0.05; **, p value < 0.01; ***, p value < 0.001. ***, p<0.001; **, p<0.01; *, p<0.05.

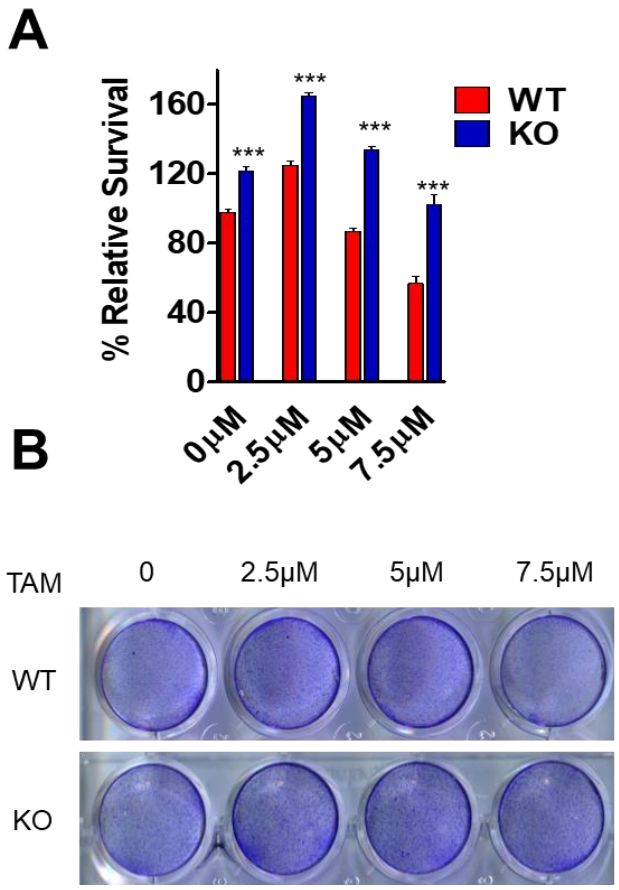

Figure 3.24: Loss of miR-489 promotes tamoxifen resistance. A. Hormone starved WT and KO cells were treated with ethanol or different concentration of tamoxifen for 6days and cell viability was measured using MTT assay (A) and crystal violet (B). Data are representative of two independent biological replicates. *, p value < 0.05; **, p value < 0.01; ***, p value < 0.001. ***, p<0.001; **, p<0.01; *, p<0.05.

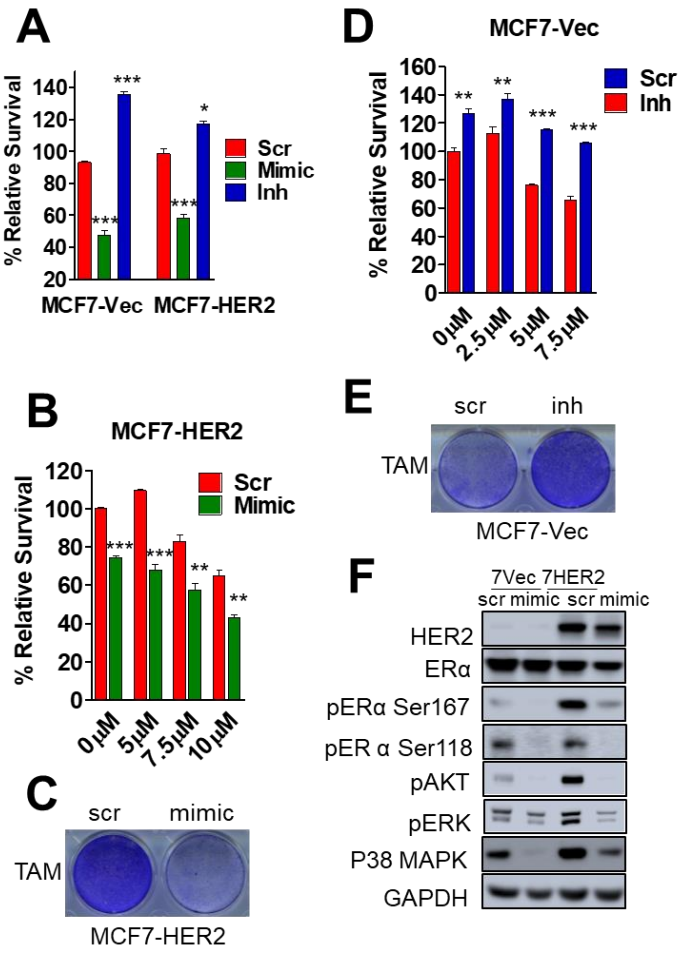

Figure 3.25: miR-489 restoration overcomes *de novo* tamoxifen resistance. A. MCF7-Vec and MCF7-HER2 cells were transfected with scr, mimic or inh for 72 hours and MTT assay was performed to access cell viability. B. MCF7-HER2 cells were treated with ethanol or different concentration of tamoxifen in presence or absence of mimic for 3days and cell viability was measured using MTT assay. C. Clonogenic assay showing survived colonies after MCF7-HER2 cells were treated for 6days with control siRNA or mimic in presence of tamoxifen. D. MCF7-Vec cells were treated with ethanol or different concentration of tamoxifen in presence or absence of miR-489 inhibitor for 3days and cell viability was measured using MTT assay. E. Clonogenic assay showing survived colonies after MCF7-Vec cells were treated for 6days with control siRNA or miR-489 inhibitor in presence of tamoxifen. F. MCF7-Vec and MCF7HER2 cells were transfected with scr or mimic for 72 hours and western blot analysis was done to examine activation of ERα, MAPK and AKT. *, p value < 0.05; **, p value < 0.01; ***, p value < 0.001. ***, p<0.001; **, p<0.01; *, p<0.05.

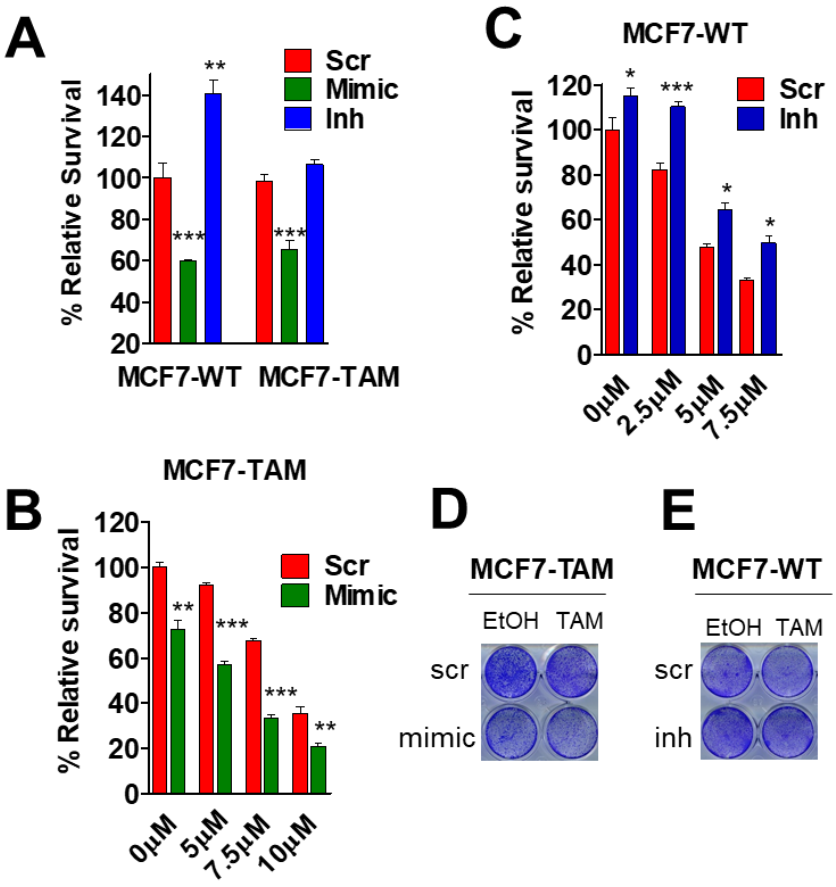

Figure 3.26: miR-489 restoration overcomes acquired tamoxifen resistance. A. MCF7-WT and MCF7-TAM cells were transfected with scr, mimic or inh for 72 hours and MTT assay was performed to access cell viability. B. MCF7-TAM cells were treated with ethanol or different concentration of tamoxifen in presence or absence of mimic for 3days and cell viability was measured using MTT assay. C. MCF7-WT cells were treated with ethanol or different concentration of tamoxifen in presence or absence of miR-489 inhibitor for 3days and cell viability was measured using MTT assay. D. Clonogenic assay showing survived colonies after MCF7-TAM cells were treated for 6days with control siRNA or mimic in presence of tamoxifen. E. Clonogenic assay showing survived colonies after MCF7-WT cells were treated for 6days with control siRNA or miR-489 inhibitor in presence of tamoxifen. *, p value < 0.05; **, p value < 0.01; ***, p value < 0.001. ***, p<0.001; **, p<0.01; *, p<0.05.

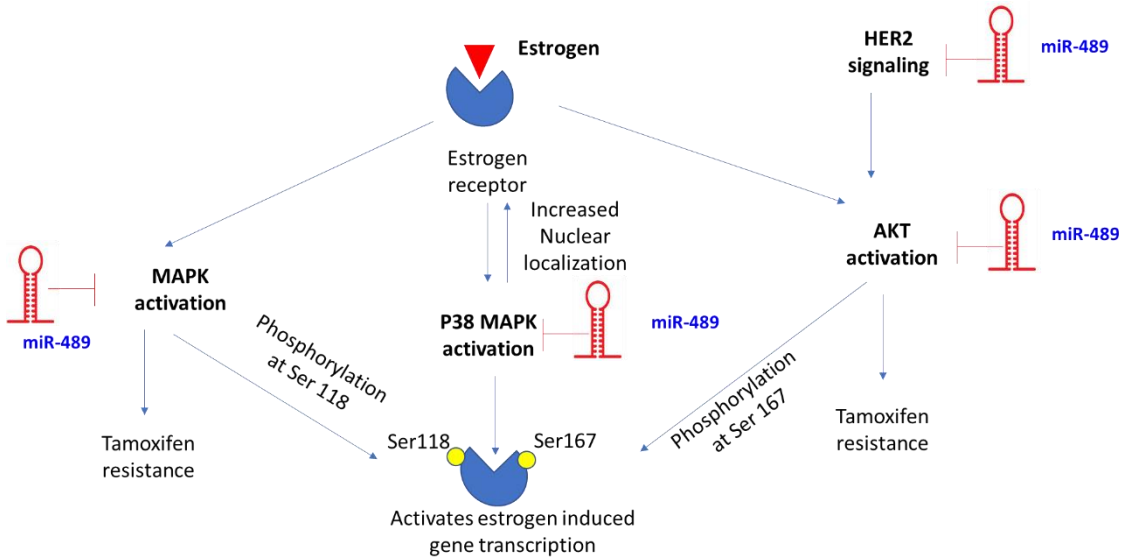

Figure 3.27: Proposed model depicting role of miR-489 in ER signaling and tamoxifen resistance. Estrogen binding to ERα activates p38 MAPK, ERK and AKT. Activation of p38 MAPK leads to nuclear localization of ERα. Activation of ERK and AKT phosphorylates ERα at Ser 118 and Ser 167 which are essential for transcriptional activity of ERα. This E2-ERα axis increases miR-489 expression level which then acts as a negative feedback loop to restrain estrogen mediated gene transcription and proliferation by inhibiting p38 MAPK, pERK and pAKT. Hyper activation of MAPK, HER2, PI3K-AKT pathways promotes estrogen independent growth and tamoxifen resistance. miR-489 may provide promising therapeutic option to sensitize tamoxifen resistant tumors.

CHAPTER 4

SUMMARY AND CONCLUSION

Currently, clinical management of the breast cancer patients is largely based on the use of a standardized set of clinical and pathological criteria for diagnosis and prognosis. Cancer staging system is currently being used to estimate patient prognosis and guide the selection of effective treatments. However, due to complexity and heterogeneity, patients with the same diagnosis and pathological characteristics can show wide variability in clinical outcomes and response to treatment. Therefore, apart from novel therapeutic agents, discovery of molecular markers for more accurate classification of a patient's risk of disease events (prognostic markers) and response to specific treatment options (predictive markers) is also essential for the betterment of treatment. Here, we examined role of miR-489 in breast cancer and report its potential application as a prognostic and predictive marker. Firstly, we report that miR-489 expression analysis may predict aggressiveness of ER+ breast cancer and response to tamoxifen therapy. Furthermore, it can also be useful predictive marker for survival and anthracycline response to breast cancer patient with 8q22 amplification. Patients with 8q22 amplification exhibits increased autophagic flux and are resistant to anthracycline therapy. However, 8q22 amplified patients with high miR-489 displays better survival potentially due to autophagy inhibition and chemo-sensitization by miR-489.

In addition, our results suggest potential therapeutic role of miR-489. Surprisingly, miR-489 functions as tumor suppressor miRNA in all the major subtypes of breast cancer. Intriguingly, miR-489 modulates major proliferation drivers responsible for breast cancer. Our studies show miR-489 inhibits estrogen singling, HER2, PI3K-AKT and MAPK signaling pathway. Along the same line, our clinical analysis suggests that patients with low miR-489 represent aggressive cancers. We also observed similar trend on breast cancer cell lines. Most cell lines with high miR-489 expression levels displays slower proliferation rate compared to cell lines with low miR-489 expression. Therefore, we propose that miR-489 may function as an endogenous proliferation regulator and its loss may potentially be useful for prediction of aggressiveness of breast cancer.

CHAPTER 5

MATERIALS AND METHODS

Cell culture and reagents

MCF7, T47D and HCC1954 were purchased from ATCC in 2013. MDA-MB-231, MDA-MB-468, MDA-MB361, Hs578T, ZR-75-1 and BT474 cells were obtained from Dr. Saraswati Sukuma, Johns Hopkins University, in 2008. MCF7 vector and MCF7 HER2 cell lines were kindly provided by Dr. Rachel Schiff (Baylor College of Medicine). MCF7-WT and tamoxifen resistant cells MCF7-TAMR were obtained from Ozgur Sahin, University of South Carolina in 2018. Cells were grown under standard conditions. Cell lines were tested for Mycoplasma via PCR using the Universal Mycoplasma Detection Kit (ATCC). MDA-MB-231, MDA-MB-468, BT549 and Hs578T were cultured in DMEM containing 10% FBS. MCF7-Vec and MCF7-HER2 cells were cultured in DMEM containing 10% FBS with insulin. T47D, HCC1954, BT474 and ZR-75-were cultured in RPMI containing 10% FBS. MCF7-WT and MCF7-TAMR cells were cultured in phenol red free low glucose DMEM supplemented with 10% FBS, non-essential amino acids and insulin. For estrogen deprivation studies, MCF7 cells were cultured in phenol red free DMEMF12 supplemented with insulin and 10% charcoal stripped FBS. T47D cells were cultured in phenol red free RPMI and 10% charcoal stripped FBS. All cells were cultured at 37°C in a humidified incubator containing 5% CO2.

RNA isolation and RT-PCR

RNA isolation and Quantitative real-time RT-PCR analysis were performed using standard protocol (H. Chen, Chung, & Sukumar, 2004; H. Chen et al., 2008; Liu et al., 2015). The total RNA, including miRNA, was extracted from cells and tissues by using Trizol reagent (Thermo Scientific, Cat#5596026). Reverse-transcription was performed by using M-MLV reverse Transcriptase (Thermo Scientific, Cat#28025013). RT² SYBR Green ROX FAST Mastermix (Qiagen, Cat#330623) was used to detect and quantify genes. Relative expression was normalized to the endogenous control GAPDH or RNU48 using the $2^{-\Delta\Delta Ct}$ method.

cDNA preparation for miRNA analysis

Poly A tail was added to RNA by using Poly A polymerase enzyme. cDNA was prepared by using polydT adaptor. The universal R was used as reverse primer for miRNA detection by qRT-PCR. Here is sequence of poly dT adaptor: GCGAGCACAGAATTAATACGACTCACTATAGGTTTTTTTTTTTTVN and Universal R: GCGAGCACAGAATTAATACGAC.

siRNA, miRNA mimics and inhibitors

miR-489 mimic (Cat#C-300749-07-0010), inhibitor (Cat#IH-303056-01-0002), scramble (Cat#CN-001000-01-50) and ATG5 siRNA (Cat#J-004374-07-0002) were purchased from Dharmacon.

Colony formation assay

We transfected mimic-miR-489 and inhibitor-miR-489 in MCF7 and MD-MBA-231 cells and incubated cells for 24 hr. After incubation, we collected all cells. For MCF-7 10000cells/well and for MD-MBA-231 4000cell/well were plated in 6 well plates in triplicates in DMEM media containing 10% Fetal Bovine Serum (FBS). After one week of incubation in 5% CO_2, cells were washed with 1x phosphate-buffered saline (PBS) and fixed using 100% methanol. Once fixed, cells were washed again with 1x PBS and stained with 0.5% crystal violet. All the visible colonies were photographed and manually counted, and the average with standard error of mean was plotted using graphpad prism software.

MTT Assay

MTT reagent 3-(4, 5-dimethylthiazol-2-yl)-2,5-diphenyltetrazolium bromide (MTT) was used to examine cell viability. Cells were seeded at a density of 4,000 cells/well for MDA-MB-231; 5,000 cells/well for MCF7 & HCC1954 and 10,000 cells/well for T47D in triplicate in 96-well plates. Cells transfected with either 0.32µl/well scrambled, miR-489 mimics, or miR-489 Inhibitor by using 0.32µl/well Lipofectamine RNAi and incubated at 37 °C for 72 hr. Cells were seeded at a density of 13,000 cells/well in triplicate in 24-well plates. Cells transfected with either 1µl/well scrambled, miR-489 mimics, or miR-489 Inhibitor by using 1µl/well Lipofectamine RNAi and incubated at 37 °C for 72 hr. MTT assay was performed according to mention above. At the end of the incubation media was removed and formazan precipitates were dissolved by adding 200 µl of DMSO in each well. OD values were measured at both 570 and 630 nm and final values were calculated

by subtracting OD_{630} from OD_{570}. These values for each time point were used to plot the growth curve for each clone using graphpad prism.

Plasmid constructs

3' UTR of human LAPTM4B, ATG4A, ULK1, PTPN11, p38 MAPK and B-raf was amplified from genomic DNA and cloned into the pGL3-promoter vector at the same XbaI and FseI sites. For the mutation analysis, putative miR-489 target site within 3'UTR of predicted targets was mutated by Q5® High-Fidelity DNA Polymerase (NEB Cat# M0491). All sequences were verified by direct sequencing of the plasmids. LAPTM4B-mCherry was a kind gift from Dr. Thomas Blom and Dr. Elina Ikonen (Blom et al., 2015). pBABE-puro mCherry-EGFP-LC3B was a gift from Jayanta Debnath (Addgene plasmid # 22418) (N'Diaye et al., 2009). pcDNA-ULK1 vector was generated by excising ULK1 from HA-hULK1 (Addgene plasmid # 31963) (Jung et al., 2009) using EcoR1 and Not1 restriction enzymes.

Stable Cell line generation

293T cells were transfected with 3µg of pBABE-puro mCherry-EGFP-LC3B (Addgene #22418, provided through the courtesy of Dr. Jayanta Debnath), 3µg of VSVG plasmid and 2.5µg of ECO plasmid using 17µl of Lipofectamine2000 for 48 hours. After 48 hours, supernatants were collected and spin down at 10,000 RPM at 4 °C to discard any cell debris. MDA-MB -231 cells were infected with virus for 48 hours. Infected cells were treated with puromycin for one week.

Stable cell line expressing ULK1 and LAPTM4B were generated using pcDNA-ULK1 vector, LAPTM4B-mCherry vector and pCDNA-LAPTM4B vectors. MDA-MB-231 cells were transfected with 2.5ug of vector using Lipofetamine 2000.

48-72hrs post transfection, cells were subjected to selection using G418 for 6-8 days. Survived pool was then tested and used for further studies.

miR-489 knock out cells were generated using pCAS9-GFP plasmid kindly provided by Dr. Philips Backhauls and gBlock guide RNA (Integrated DNA Technologies, IDT). T47D cells were co-transfected with pCAS9-GFP and two gBlock guide RNA for 48 hours. Cells were then harvested and subjected to Fluorescence-activated cell sorting (FACS) to collect GFP positive cells. GFP+ve cells were then seeded in 96 well plate at single cell per well dilution and amplified. Each single cell colonies were then screened for miR-489 deletion using genotyping. Potential clones were then validated by examining for miR-489 expression using qRT-PCR and for miR-489 target expression using western blot analysis.

Luciferase assay

Luciferase assay was performed as mentioned earlier (H. Chen et al., 2008; H. Chen et al., 2007; Liu et al., 2015). Briefly, HEK293 cells were seeded at 6.5 x 104 cells/well 24 h prior to the transfection in a 24 well plate. Cells were transfected with 50ng of pGL3 promoter vector containing wild type 3'UTR or mutated 3'UTR of potential target genes, 50ng of pRL-TK (Renilla luciferase vector-Promega) and 100ng of miR-489 pcDNA 3.1 vector or empty pcDNA 3.1 vector. After 72 hrs post transfection, luciferase activity was measured using Dual-luciferase reporter assay system (Promega Cat# E1980) as per manufacturer's instructions and normalized to the levels of Renilla luciferase activity.

Microarray analysis

T47D cells were seeded in 6-well culture dish, treated with 28nM scramble miRNA or miR-489 mimic for 72hrs. RNA was extracted with Trizol reagent, followed by clean-up and DNase I treatment with QIAGEN RNeasy mini kit in accordance with the prescribed protocol provided with the kit. Quality control was performed with Agilent Bioanalyser before performing microarray. The data were normalized using the default quantile normalization with R-bioconductor package lumi version 3.2.2. The microarray data in this manuscript is available on the GEO database (GSE99728). A subset of identified genes was validated by q-PCR.

Autophagy and cell viability assays

Breast cancer cells were transfected with 28nM scr, mimic or inh, for 68hrs, and then treated with Bafilomycin A1 (400nM) or DMSO for 4hrs. The levels of LC3B-I/II and SQSTM1 protein expression were assayed by western blot. MDA-MB-231 cells were transfected with scr, mimic or inhibitor for 24hrs and then treated with 3-MA for 48hrs. Autophagic flux was then assessed by examining LC3B-II and p62 expression using western blot. MDA-MB-231 cells stably expressing mCherry-EGFP-LC3B fusion protein were transfected with scr or mimic for 48hrs and assayed for co-localization of red and green punta using confocal microscopy.

To study effect of miR-489 on cell survival, indicated cell lines were first seeded in 96 well plate in triplicate and transfected with 28nM scr or mimic. Cell viability assay was performed using MTT reagent at 72hrs. To assess effect of miR-489 under metabolic stress, MDA-MB-231, HCC1954 or T47D cells were

seeded in 96-well plate. Cells were transfected with scr, mimic or inh in complete media or in low serum. Cell viability assay was performed using MTT reagent at indicated time points. Expression of cleaved caspase 3, LC3B and p62 was analyzed using western blot. To study role of autophagy in miR-489 induced sensitization under starvation, MDA-MB-231 cells were transfected with 9.3nM scr or mimic in complete media or low serum in presence or absence of 3-MA, siATG5 or Bafilomycin A1 followed by cell viability assay using MTT reagent and western blot analysis to examine effect on autophagy and apoptosis. To examine effect of miR-489 on doxorubicin induced cytoprotective autophagy, MDA-MB-231 and HCC1954 cells were transfected with 28nM scr or mimic with or without doxorubicin. Protein was isolated 72hrs post treatment and western blot was performed.

Chemo-sensitization Assays

To study doxorubicin localization, cells were treated with 28nM scr or mimic for 24hrs then treated with 0.5uM doxorubicin for 48hrs followed by confocal microscopy. MDA-MB-231 cells were transfected with 9.3nM scr or mimic for 24 hours and treated with indicated concentration of doxorubicin in presence or absence of 3-MA (5mM), siATG5 (50nM) or Bafilomycin A1 (50nM) for 48 hours and cell proliferation was measured by MTT assay to examine role of autophagy inhibition in miR-489 mediated doxorubicin sensitization. To assess lysosomal integrity, MDA-MB-231 cells were transfected with 28nM scr or mimic and stained with Acridine orange (1µg/ml) for 20min followed by flow cytometry and confocal microscopy.

Preparation of miR-489-delivering nanoparticle

Liposomes were prepared as described elsewhere with slight modifications (S. D. Li, Chono, & Huang, 2008; S. D. Li & Huang, 2006). Briefly, cationic liposomes consisting of DOTAP and cholesterol (2:1 molar ratio) were prepared using the thin-film hydration method. The film was hydrated with nuclease free water and sonicated using probe sonicator for 15min. The lipid concentration adjusted at 10mg/ml. For miRNA-nanoparticles preparation, 231.4µls of cationic liposomes and 90µls of miRNA were mixed in final volume of 1 ml nuclease free water. The miRNA-liposomes were allowed to stand at room temperature for 10 min. miRNA-nanoparticles were further decorated with sodium hyaluronate by adding 128.56µls of 1mg/ml sodium hyaluronate solution and kept at room temperature for another 10min. The samples were condensed using Millipore centrifugal filter units.

Xenograft experiments

Six weeks old Athymic Female nude mice were purchased from Envigo. All mice were handled and maintained under supervision of veterinarian in accordance with institutional guidelines and under a University of South Carolina Institutional Animal Care and Use Committee (IACUC) approved protocol. All mice were subcutaneously injected with 1×10^6 MDA-MB-231 cells left flank of each mice (n=5/group). Mouse were randomly distributed in four groups when tumor size reached 50-100mm^3. The mice were administered with control nanoparticles or miR-489 loaded nanoparticles every third day. Doxorubicin (4mg/kg) was administered day after injection of miRNA. Tumor volumes were calculated by measuring length and width every third day. After 3 weeks, all mice were sacrificed

and tumors were extracted after euthanizing all animals. Tumor volumes were calculated by modified ellipsoidal formula (1/2(lxw2)).

Clinical samples

Human breast cancer tissue samples were obtained through the South Carolina Tissue Bank with approval from the Institutional Review Board at the University of South Carolina. Tissue samples were randomly collected from patients who were diagnosed with invasive breast ductal carcinoma between 2003 and 2007. RNA was isolated from tumors samples and expression of miR-489, ULK1 and LAPTM4B was analyzed by qRT-PCR. Demographic and histopathology data of the patient samples are listed in Supplementary table 2.

Estrogen and progesterone treatment

To examine effect of estrogen and progesterone on gene expression and proliferation cells were first cultured in estrogen deprivation condition for 3-6 days. For estrogen deprivation, MCF7 cells were cultured in phenol red free DMEMF12 supplemented with insulin and 10% charcoal stripped FBS. T47D cells were cultured in phenol red free RPMI and 10% charcoal stripped FBS. Cells were then trypsinzed and seeded in desired cell culture dish and treated with estrogen and/or progesterone for indicated amount of time.

Flow Cytometry.

CD24 and CD44 antibodies (BD Biosciences) were used to examine cancer stem cell population. After the treatment cells were harvested and washed with PBS. Cells were then resuspended in 1X PBS+2% FBS solution and counted using

Biorad cell counter. 200K cells from each sample were transferred to fresh tube, centrifuged and resuspended in 100uls of 1X PBS+2% FBS. Cells were incubated with CD24-PE and CD44-FITC antibodies for 30min with mixing every 10 minutes. Cells were washed with PBS at the end of incubation, resuspended in 1X PBS+2% FBS and read in BD Accuri C6 flow cytometer. To assess lysosomal integrity, MDA-MB-231 cells were transfected with 28nM scr or mimic and stained with Acridine orange (1µg/ml) for 20min. Cells were then washed and read using BD C6 Accuri flow cytometer.

Mammosphere Assay.

Cells were trypsinized and mechanically separated and passed through 40-µm filters to obtain single cell suspensions. Cells were plated at 10,000 cells per plate density in super–low-attachment plates in mammosphere media and cultured for 6-8 days. Quantification of mammosphere numbers was accomplished by transferring in 96 well plate.

Immunofluorescence.

After indicated treatment, cells were washed with 1X PBS and fixed using 4% paraformaldehyde for 15minutes. Cells were washed thrice with 1X PBS and blocked using 1% Rat Serum, 0.01% triton X-100 and 1X PBS for 1 hour at room temperature. Cells were then incubated overnight with ERα antibody (Santacruz biotechnology) at 4 C. Next day, cells were washed with PBS thrice and incubated with Alexa fluor 594 goat anti-rabbit IgG H&L (Thermo scientific) for 1 hour at room temperature. After 3 washes with PBS, cells were counterstained with DAPI for 12

minutes and mounted on slide. Cells were then imaged using confocal microscope using cy3 and DAPI channel.

Generation of knock out cells

CRISPR/Cas9 gene editing method was used to generate miR-489 knock out cell line. Two guide RNAs flanking pre-miR-489 were designed using guide RNA designing tool (cripsr.mit.edu). G-block guide RNAs were purchased IDT technologies and Cas9-GFP plasmid was obtained from Dr. Philip Buckhaults. G-block guide RNA and Cas9-GFP were co-transfected in T47D cells using T47D avalanche transfection reagent (ez biosystem). 72 hours post transfection, GFP positive cells were sorted using Fluorescent activated cell sorter. Sorted cells were then diluted to single cell and seeded in 6 96-well plate. Rest of the cells were seeded on 10-cm dish. Colonies grown from single clone were then expanded and screened for miR-489 deletion using genotyping.

Western Blotting

Protein extracts were obtained from whole cell lysates from breast cancer cell lines or mammary epithelial cells from mouse mammary gland. Isolation of protein in-vitro was performed using M-PER (mammalian protein extraction reagent, Thermofisher, Grand Island, NY) with a protease inhibitor (Sigma, St. Louis, MO) following manufacturer's instructions. Proteins were separated on 7% precast acrylamide gels, transferred to nitrocellulose blots, and probed with primary with antibodies protein of interest. Blots were incubated with primary antibodies overnight at 4ºC, washed with PBS/0.01% Tween-20, probed with HRP-conjugated secondary antibody (Bio-rad, Hercules, CA) for 1 hour at room

temperature, washed, and visualized with ECL enhanced chemiluminescence kit (ThermoFisher Scientific Cat#). Blots were visualized using either the GE ImageQuant LAS 4000 (GE Healthcare Bio-Sciences, Pittsburgh, PA). As internal controls for equal loading, blots were re-probed with either Hrp-conjugated Anti-β-actin (Santacruz Biotechnology, Santa Cruz, CA) or Anti-GAPDH Rabbit pAb (Santa Cruz Biotechnology, Santa Cruz, CA) after stripping the blot with a mild stripping buffer. Western images were quantified using GE ImageQuant Software. All primary antibodies were obtained from cell signaling. DEK was purchased from protein technology.

Histology

Tumor-bearing mice were sacrificed, and tumor specimens were fixed in freshly prepared 4% paraformaldehyde in PBS, pH 7.2. Tissue blocks were embedded in paraffin, 5 μm sections obtained and then stained with hematoxylin and eosin (H&E) (VWR, West Chester, PA) for visual examination.

Immunohistochemistry

Immunohistochemistry (IHC) was performed using 5 μM sections of xenografted tumor, spontaneous tumor and mammary gland fixed in Formalin overnight. Parraffin-embedded tissue sections on poly-L-lysine-coated slides were dewaxed in xylene (2 x 5 minutes) and rehydrated by washing in decreasing concentration of ethanol: 2 x 3 minutes in 100 percent ethanol, 2 x 3 minutes 95 percent ethanol and 1 x 3 minutes 75 percent ethanol. Antigen reterival was carried out by incubating slides in preheated citrate buffer (95 °C, pH6) for 30 minutes. Sections were blocked with 3 percent peroxide for 10 minutes. Sections were blocked with

0.1 percent BSA/PBS buffer for 1 hr at room temperature. Primary antibodies Ki-67 (cell signaling Cat#9027) and LAPTM4B (Cat#2242). For, mouse tissue, Ki-67 was obtained from BD (Cat#550609). Antibody for SHP2 was obtained from protein tech (Cat#24570-1-AP). All antibody dilutions were used accordingly instruction. All primary antibody was incubated for overnight at 4 C. Unbound antibodies were removed by using 0.1 percent tween/PBC buffer three times. Sections were incubated with anti-rabbit or mouse biotinylated antibody. Signal was amplified by using avidin-biotin complex (ABC kit) from Vector Laboratories. Sections were developed using DAB from Vector Laboratories. For Ki-67 positive cell counting in tumors, total 1000 cells were counted from each individual tumor. For Ki-67 positive cell counting in mammary gland, 3 independent ducts and TEBs were counted from each mammary gland tissue. Total of 5 pairs of sister mice were used.

Statistical Analysis

The statistical analyses were conducted with R and GraphPad software packages. A Student t test or ANOVA test was used for comparison of quantitative data. The clinical effect of the gene expression profiles of miR-489 in the patients with 8q22 gain/amplified tumor was evaluated using a published data set containing 1302 breast cancer patients (Dvinge et al., 2013; Gray & Druker, 2012) The median expression value was used as the cutoff to classify miR-489 expression as high or low. Recurrence-free survival was estimated using the Kaplan-Meier method and compared with log-rank test. The linear correlations between miR-489 and potential target genes expression in primary breast cancer tissues were evaluated

with Pearson correlation coefficient analysis. Values of $P < 0.05$ were considered significant.

Chi-square tests were made with the Schoenfeld residuals to check the proportional hazard assumption of the selected model. Values of $P < 0.05$ were considered significant.

All data are shown as the mean ± standard deviation (SD); comparisons of two groups were analyzed using the two-tailed t-test with Welch's correction using GraphPad Prism version 5.00 for Windows, (GraphPad Software, San Diego California USA, www.graphpad.com). P-values of $p<0.05$, $p<0.01$, and $p<0.001$ are indicated with (*), (**), and (***), respectively, and all considered statistically significant.

REFERENCES

Anbalagan, M., & Rowan, B. G. (2015). Estrogen receptor alpha phosphorylation and its functional impact in human breast cancer. *Mol Cell Endocrinol, 418 Pt 3*, 264-272. doi: 10.1016/j.mce.2015.01.016

Balvers, R. K., Lamfers, M. L., Kloezeman, J. J., Kleijn, A., Berghauser Pont, L. M., Dirven, C. M., & Leenstra, S. (2015). ABT-888 enhances cytotoxic effects of temozolomide independent of MGMT status in serum free cultured glioma cells. *J Transl Med, 13*, 74. doi: 10.1186/s12967-015-0427-y

Banegas, M. P., Tao, L., Altekruse, S., Anderson, W. F., John, E. M., Clarke, C. A., & Gomez, S. L. (2014). Heterogeneity of breast cancer subtypes and survival among Hispanic women with invasive breast cancer in California. *Breast Cancer Res Treat, 144*(3), 625-634. doi: 10.1007/s10549-014-2882-1

Baran-Gale, J., Purvis, J. E., & Sethupathy, P. (2016). An integrative transcriptomics approach identifies miR-503 as a candidate master regulator of the estrogen response in MCF-7 breast cancer cells. *RNA, 22*(10), 1592-1603. doi: 10.1261/rna.056895.116

Bartel, D. P. (2004). MicroRNAs: genomics, biogenesis, mechanism, and function. *Cell, 116*(2), 281-297.

Blom, T., Li, S., Dichlberger, A., Back, N., Kim, Y. A., Loizides-Mangold, U., . . . Ikonen, E. (2015). LAPTM4B facilitates late endosomal ceramide export to control cell death pathways. *Nat Chem Biol, 11*(10), 799-806. doi: 10.1038/nchembio.1889

Borst, P., Schinkel, A. H., Smit, J. J., Wagenaar, E., Van Deemter, L., Smith, A. J., . . . Zaman, G. J. (1993). Classical and novel forms of multidrug resistance and the physiological functions of P-glycoproteins in mammals. *Pharmacol Ther, 60*(2), 289-299.

Button, R. W., Roberts, S. L., Willis, T. L., Hanemann, C. O., & Luo, S. (2017). Accumulation of autophagosomes confers cytotoxicity. *J Biol Chem, 292*(33), 13599-13614. doi: 10.1074/jbc.M117.782276

Chakraborty, C., Sharma, A. R., Sharma, G., Doss, C. G. P., & Lee, S. S. (2017). Therapeutic miRNA and siRNA: Moving from Bench to Clinic as Next Generation Medicine. *Mol Ther Nucleic Acids, 8*, 132-143. doi: 10.1016/j.omtn.2017.06.005

Chan, E. Y., Longatti, A., McKnight, N. C., & Tooze, S. A. (2009). Kinase-inactivated ULK proteins inhibit autophagy via their conserved C-terminal domains using an Atg13-independent mechanism. *Mol Cell Biol, 29*(1), 157-171. doi: 10.1128/MCB.01082-08

Chang, M. (2012). Tamoxifen resistance in breast cancer. *Biomol Ther (Seoul), 20*(3), 256-267. doi: 10.4062/biomolther.2012.20.3.256

Chen, H., Chung, S., & Sukumar, S. (2004). HOXA5-induced apoptosis in breast cancer cells is mediated by caspases 2 and 8. *Mol Cell Biol, 24*(2), 924-935.

Chen, H., Lee, J. S., Liang, X., Zhang, H., Zhu, T., Zhang, Z., . . . Sukumar, S. (2008). Hoxb7 inhibits transgenic HER-2/neu-induced mouse mammary tumor onset but promotes progression and lung metastasis. *Cancer Res, 68*(10), 3637-3644. doi: 10.1158/0008-5472.CAN-07-292

Chen, H., Zhang, H., Lee, J., Liang, X., Wu, X., Zhu, T., . . . Sukumar, S. (2007). HOXA5 acts directly downstream of retinoic acid receptor beta and contributes to retinoic acid-induced apoptosis and growth inhibition. *Cancer Res, 67*(17), 8007-8013. doi: 10.1158/0008-5472.CAN-07-1405

Chen, X., Wang, Y. W., Xing, A. Y., Xiang, S., Shi, D. B., Liu, L., . . . Gao, P. (2016). Suppression of SPIN1-mediated PI3K-Akt pathway by miR-489 increases chemosensitivity in breast cancer. *J Pathol, 239*(4), 459-472. doi: 10.1002/path.4743

Chittaranjan, S., Bortnik, S., Dragowska, W. H., Xu, J., Abeysundara, N., Leung, A., . . . Gorski, S. M. (2014). Autophagy inhibition augments the anticancer effects of epirubicin treatment in anthracycline-sensitive and -resistant triple-negative breast cancer. *Clin Cancer Res, 20*(12), 3159-3173. doi: 10.1158/1078-0432.CCR-13-2060

Choi, J., Jo, M., Lee, E., & Choi, D. (2011). Induction of apoptotic cell death via accumulation of autophagosomes in rat granulosa cells. *Fertil Steril, 95*(4), 1482-1486. doi: 10.1016/j.fertnstert.2010.06.006

Cittelly, D. M., Finlay-Schultz, J., Howe, E. N., Spoelstra, N. S., Axlund, S. D., Hendricks, P., . . . Richer, J. K. (2013). Progestin suppression of miR-29 potentiates dedifferentiation of breast cancer cells via KLF4. *Oncogene, 32*(20), 2555-2564. doi: 10.1038/onc.2012.275

Clarke, R., Tyson, J. J., & Dixon, J. M. (2015). Endocrine resistance in breast cancer--An overview and update. *Mol Cell Endocrinol, 418 Pt 3*, 220-234. doi: 10.1016/j.mce.2015.09.035

de Ronde, J. J., Lips, E. H., Mulder, L., Vincent, A. D., Wesseling, J., Nieuwland, M., . . . Wessels, L. F. (2013). SERPINA6, BEX1, AGTR1, SLC26A3, and LAPTM4B are markers of resistance to neoadjuvant chemotherapy in HER2-negative breast cancer. *Breast Cancer Res Treat, 137*(1), 213-223. doi: 10.1007/s10549-012-2340-x

Debnath, J. (2011). The multifaceted roles of autophagy in tumors-implications for breast cancer. *J Mammary Gland Biol Neoplasia, 16*(3), 173-187. doi: 10.1007/s10911-011-9223-3

Dvinge, H., Git, A., Graf, S., Salmon-Divon, M., Curtis, C., Sottoriva, A., . . . Caldas, C. (2013). The shaping and functional consequences of the microRNA landscape in breast cancer. *Nature, 497*(7449), 378-382. doi: 10.1038/nature12108

Eskelinen, E. L. (2011). The dual role of autophagy in cancer. *Curr Opin Pharmacol, 11*(4), 294-300. doi: 10.1016/j.coph.2011.03.009
Fan, P., Maximov, P. Y., Curpan, R. F., Abderrahman, B., & Jordan, V. C. (2015). The molecular, cellular and clinical consequences of targeting the estrogen receptor following estrogen deprivation therapy. *Mol Cell Endocrinol, 418 Pt 3*, 245-263. doi: 10.1016/j.mce.2015.06.004
Fillmore, C. M., Gupta, P. B., Rudnick, J. A., Caballero, S., Keller, P. J., Lander, E. S., & Kuperwasser, C. (2010). Estrogen expands breast cancer stem-like cells through paracrine FGF/Tbx3 signaling. *Proc Natl Acad Sci U S A, 107*(50), 21737-21742. doi: 10.1073/pnas.1007863107
Fulda, S., & Kogel, D. (2015). Cell death by autophagy: emerging molecular mechanisms and implications for cancer therapy. *Oncogene, 34*(40), 5105-5113. doi: 10.1038/onc.2014.458
Geng, Y., Kohli, L., Klocke, B. J., & Roth, K. A. (2010). Chloroquine-induced autophagic vacuole accumulation and cell death in glioma cells is p53 independent. *Neuro Oncol, 12*(5), 473-481. doi: 10.1093/neuonc/nop048
Gray, J., & Druker, B. (2012). Genomics: the breast cancer landscape. *Nature, 486*(7403), 328-329. doi: 10.1038/486328a
Gugnoni, M., Sancisi, V., Manzotti, G., Gandolfi, G., & Ciarrocchi, A. (2016). Autophagy and epithelial-mesenchymal transition: an intricate interplay in cancer. *Cell Death Dis, 7*(12), e2520. doi: 10.1038/cddis.2016.415
Guo, B., Tam, A., Santi, S. A., & Parissenti, A. M. (2016). Role of autophagy and lysosomal drug sequestration in acquired resistance to doxorubicin in MCF-7 cells. *BMC Cancer, 16*(1), 762. doi: 10.1186/s12885-016-2790-3
Hara, T., Takamura, A., Kishi, C., Iemura, S., Natsume, T., Guan, J. L., & Mizushima, N. (2008). FIP200, a ULK-interacting protein, is required for autophagosome formation in mammalian cells. *J Cell Biol, 181*(3), 497-510. doi: 10.1083/jcb.200712064
Hayes, E. L., & Lewis-Wambi, J. S. (2015). Mechanisms of endocrine resistance in breast cancer: an overview of the proposed roles of noncoding RNA. *Breast Cancer Res, 17*, 40. doi: 10.1186/s13058-015-0542-y
Heiser, L. M., Sadanandam, A., Kuo, W. L., Benz, S. C., Goldstein, T. C., Ng, S., . . . Spellman, P. T. (2012). Subtype and pathway specific responses to anticancer compounds in breast cancer. *Proc Natl Acad Sci U S A, 109*(8), 2724-2729. doi: 10.1073/pnas.1018854108
Higgins, M. J., & Baselga, J. (2011). Targeted therapies for breast cancer. *J Clin Invest, 121*(10), 3797-3803. doi: 10.1172/JCI57152
Hopkins, A. L., & Groom, C. R. (2002). The druggable genome. *Nat Rev Drug Discov, 1*(9), 727-730. doi: 10.1038/nrd892
Hu, Y. L., Jahangiri, A., Delay, M., & Aghi, M. K. (2012). Tumor cell autophagy as an adaptive response mediating resistance to treatments such as antiangiogenic therapy. *Cancer Res, 72*(17), 4294-4299. doi: 10.1158/0008-5472.CAN-12-1076
Iorio, M. V., Ferracin, M., Liu, C. G., Veronese, A., Spizzo, R., Sabbioni, S., . . . Croce, C. M. (2005). MicroRNA gene expression deregulation in human

breast cancer. *Cancer Res, 65*(16), 7065-7070. doi: 10.1158/0008-5472.CAN-05-1783

Jeselsohn, R., Buchwalter, G., De Angelis, C., Brown, M., & Schiff, R. (2015). ESR1 mutations-a mechanism for acquired endocrine resistance in breast cancer. *Nat Rev Clin Oncol, 12*(10), 573-583. doi: 10.1038/nrclinonc.2015.117

Jiang, L., He, D., Yang, D., Chen, Z., Pan, Q., Mao, A., . . . Ma, X. (2014). MiR-489 regulates chemoresistance in breast cancer via epithelial mesenchymal transition pathway. *FEBS Lett, 588*(11), 2009-2015. doi: 10.1016/j.febslet.2014.04.024

Jung, C. H., Jun, C. B., Ro, S. H., Kim, Y. M., Otto, N. M., Cao, J., . . . Kim, D. H. (2009). ULK-Atg13-FIP200 complexes mediate mTOR signaling to the autophagy machinery. *Mol Biol Cell, 20*(7), 1992-2003. doi: 10.1091/mbc.E08-12-1249

Kanematsu, S., Uehara, N., Miki, H., Yoshizawa, K., Kawanaka, A., Yuri, T., & Tsubura, A. (2010). Autophagy inhibition enhances sulforaphane-induced apoptosis in human breast cancer cells. *Anticancer Res, 30*(9), 3381-3390.

Kaur, J., & Debnath, J. (2015). Autophagy at the crossroads of catabolism and anabolism. *Nat Rev Mol Cell Biol, 16*(8), 461-472. doi: 10.1038/nrm4024

Kikkawa, N., Hanazawa, T., Fujimura, L., Nohata, N., Suzuki, H., Chazono, H., . . . Seki, N. (2010). miR-489 is a tumour-suppressive miRNA target PTPN11 in hypopharyngeal squamous cell carcinoma (HSCC). *Br J Cancer, 103*(6), 877-884. doi: 10.1038/sj.bjc.6605811

Kim, D. G., Jung, K. H., Lee, D. G., Yoon, J. H., Choi, K. S., Kwon, S. W., . . . Kim, Y. S. (2014). 20(S)-Ginsenoside Rg3 is a novel inhibitor of autophagy and sensitizes hepatocellular carcinoma to doxorubicin. *Oncotarget, 5*(12), 4438-4451. doi: 10.18632/oncotarget.2034

Kiyono, K., Suzuki, H. I., Matsuyama, H., Morishita, Y., Komuro, A., Kano, M. R., . . . Miyazono, K. (2009). Autophagy is activated by TGF-beta and potentiates TGF-beta-mediated growth inhibition in human hepatocellular carcinoma cells. *Cancer Res, 69*(23), 8844-8852. doi: 10.1158/0008-5472.CAN-08-4401

Klein-Hitpass, L., Schorpp, M., Wagner, U., & Ryffel, G. U. (1986). An estrogen-responsive element derived from the 5' flanking region of the Xenopus vitellogenin A2 gene functions in transfected human cells. *Cell, 46*(7), 1053-1061.

Klionsky, D. J., Abdelmohsen, K., Abe, A., Abedin, M. J., Abeliovich, H., Acevedo Arozena, A., . . . Zughaier, S. M. (2016). Guidelines for the use and interpretation of assays for monitoring autophagy (3rd edition). *Autophagy, 12*(1), 1-222. doi: 10.1080/15548627.2015.1100356

Kubista, E. (2001). [Breast cancer: figures and facts]. *Wien Med Wochenschr, 151*(21-23), 548-551.

Lanczky, A., Nagy, A., Bottai, G., Munkacsy, G., Szabo, A., Santarpia, L., & Gyorffy, B. (2016). miRpower: a web-tool to validate survival-associated

miRNAs utilizing expression data from 2178 breast cancer patients. *Breast Cancer Res Treat, 160*(3), 439-446. doi: 10.1007/s10549-016-4013-7

Le Romancer, M., Poulard, C., Cohen, P., Sentis, S., Renoir, J. M., & Corbo, L. (2011). Cracking the estrogen receptor's posttranslational code in breast tumors. *Endocr Rev, 32*(5), 597-622. doi: 10.1210/er.2010-0016

Lee, E. J., & Tournier, C. (2011). The requirement of uncoordinated 51-like kinase 1 (ULK1) and ULK2 in the regulation of autophagy. *Autophagy, 7*(7), 689-695.

Lee, H., & Bai, W. (2002). Regulation of estrogen receptor nuclear export by ligand-induced and p38-mediated receptor phosphorylation. *Mol Cell Biol, 22*(16), 5835-5845.

Lee, H. Y., & Doudna, J. A. (2012). TRBP alters human precursor microRNA processing in vitro. *RNA, 18*(11), 2012-2019. doi: 10.1261/rna.035501.112

Lee, M. H., Koh, D., Na, H., Ka, N. L., Kim, S., Kim, H. J., . . . Lee, M. O. (2018). MTA1 is a novel regulator of autophagy that induces tamoxifen resistance in breast cancer cells. *Autophagy, 14*(5), 812-824. doi: 10.1080/15548627.2017.1388476

Lee, Y., Ahn, C., Han, J., Choi, H., Kim, J., Yim, J., . . . Kim, V. N. (2003). The nuclear RNase III Drosha initiates microRNA processing. *Nature, 425*(6956), 415-419. doi: 10.1038/nature01957

Li, C., Liu, Y., Liu, H., Zhang, W., Shen, C., Cho, K., . . . Zhao, S. (2015). Impact of autophagy inhibition at different stages on cytotoxic effect of autophagy inducer in glioblastoma cells. *Cell Physiol Biochem, 35*(4), 1303-1316. doi: 10.1159/000373952

Li, J., Qu, W., Jiang, Y., Sun, Y., Cheng, Y., Zou, T., & Du, S. (2016). miR-489 Suppresses Proliferation and Invasion of Human Bladder Cancer Cells. *Oncol Res, 24*(6), 391-398. doi: 10.3727/096504016X14666990347518

Li, L., Wei, X. H., Pan, Y. P., Li, H. C., Yang, H., He, Q. H., . . . Zhou, R. L. (2010). LAPTM4B: a novel cancer-associated gene motivates multidrug resistance through efflux and activating PI3K/AKT signaling. *Oncogene, 29*(43), 5785-5795. doi: 10.1038/onc.2010.303

Li, S. D., Chono, S., & Huang, L. (2008). Efficient gene silencing in metastatic tumor by siRNA formulated in surface-modified nanoparticles. *J Control Release, 126*(1), 77-84. doi: 10.1016/j.jconrel.2007.11.002

Li, S. D., & Huang, L. (2006). Targeted delivery of antisense oligodeoxynucleotide and small interference RNA into lung cancer cells. *Mol Pharm, 3*(5), 579-588. doi: 10.1021/mp060039w

Li, Y., Iglehart, J. D., Richardson, A. L., & Wang, Z. C. (2012). The amplified cancer gene LAPTM4B promotes tumor growth and tolerance to stress through the induction of autophagy. *Autophagy, 8*(2), 273-274. doi: 10.4161/auto.8.2.18941

Li, Y., Zhang, Q., Tian, R., Wang, Q., Zhao, J. J., Iglehart, J. D., . . . Richardson, A. L. (2011). Lysosomal transmembrane protein LAPTM4B promotes autophagy and tolerance to metabolic stress in cancer cells. *Cancer Res, 71*(24), 7481-7489. doi: 10.1158/0008-5472.CAN-11-0940

Li, Y., Zou, L., Li, Q., Haibe-Kains, B., Tian, R., Li, Y., . . . Wang, Z. C. (2010). Amplification of LAPTM4B and YWHAZ contributes to chemotherapy resistance and recurrence of breast cancer. *Nat Med, 16*(2), 214-218. doi: 10.1038/nm.2090

Li, Y. I., Libby, E. F., Lewis, M. J., Liu, J., Shacka, J. J., & Hurst, D. R. (2016). Increased autophagic response in a population of metastatic breast cancer cells. *Oncol Lett, 12*(1), 523-529. doi: 10.3892/ol.2016.4613

Liu, S., Jin, K., Hui, Y., Fu, J., Jie, C., Feng, S., . . . Chen, H. (2015). HOXB7 promotes malignant progression by activating the TGFbeta signaling pathway. *Cancer Res, 75*(4), 709-719. doi: 10.1158/0008-5472.CAN-14-3100

Manavathi, B., Dey, O., Gajulapalli, V. N., Bhatia, R. S., Bugide, S., & Kumar, R. (2013). Derailed estrogen signaling and breast cancer: an authentic couple. *Endocr Rev, 34*(1), 1-32. doi: 10.1210/er.2011-1057

Maycotte, P., Gearheart, C. M., Barnard, R., Aryal, S., Mulcahy Levy, J. M., Fosmire, S. P., . . . Thorburn, A. (2014). STAT3-mediated autophagy dependence identifies subtypes of breast cancer where autophagy inhibition can be efficacious. *Cancer Res, 74*(9), 2579-2590. doi: 10.1158/0008-5472.CAN-13-3470

Meng, Y., Wang, L., Chen, D., Chang, Y., Zhang, M., Xu, J. J., . . . Zhang, Q. Y. (2016). LAPTM4B: an oncogene in various solid tumors and its functions. *Oncogene, 35*(50), 6359-6365. doi: 10.1038/onc.2016.189

Mihaly, Z., Kormos, M., Lanczky, A., Dank, M., Budczies, J., Szasz, M. A., & Gyorffy, B. (2013). A meta-analysis of gene expression-based biomarkers predicting outcome after tamoxifen treatment in breast cancer. *Breast Cancer Res Treat, 140*(2), 219-232. doi: 10.1007/s10549-013-2622-y

Miller, T. E., Ghoshal, K., Ramaswamy, B., Roy, S., Datta, J., Shapiro, C. L., . . . Majumder, S. (2008). MicroRNA-221/222 confers tamoxifen resistance in breast cancer by targeting p27Kip1. *J Biol Chem, 283*(44), 29897-29903. doi: 10.1074/jbc.M804612200

Mizushima, N., Yoshimori, T., & Levine, B. (2010). Methods in mammalian autophagy research. *Cell, 140*(3), 313-326. doi: 10.1016/j.cell.2010.01.028

Mohammed, H., Russell, I. A., Stark, R., Rueda, O. M., Hickey, T. E., Tarulli, G. A., . . . Carroll, J. S. (2015). Progesterone receptor modulates ERalpha action in breast cancer. *Nature, 523*(7560), 313-317. doi: 10.1038/nature14583

Mukherji, S., Ebert, M. S., Zheng, G. X., Tsang, J. S., Sharp, P. A., & van Oudenaarden, A. (2011). MicroRNAs can generate thresholds in target gene expression. *Nat Genet, 43*(9), 854-859. doi: 10.1038/ng.905

N'Diaye, E. N., Kajihara, K. K., Hsieh, I., Morisaki, H., Debnath, J., & Brown, E. J. (2009). PLIC proteins or ubiquilins regulate autophagy-dependent cell survival during nutrient starvation. *EMBO Rep, 10*(2), 173-179. doi: 10.1038/embor.2008.238

Nagelkerke, A., Sieuwerts, A. M., Bussink, J., Sweep, F. C., Look, M. P., Foekens, J. A., . . . Span, P. N. (2014). LAMP3 is involved in tamoxifen

resistance in breast cancer cells through the modulation of autophagy. *Endocr Relat Cancer, 21*(1), 101-112. doi: 10.1530/ERC-13-0183
Nass, N., & Kalinski, T. (2015). Tamoxifen resistance: from cell culture experiments towards novel biomarkers. *Pathol Res Pract, 211*(3), 189-197. doi: 10.1016/j.prp.2015.01.004
O'Lone, R., Frith, M. C., Karlsson, E. K., & Hansen, U. (2004). Genomic targets of nuclear estrogen receptors. *Mol Endocrinol, 18*(8), 1859-1875. doi: 10.1210/me.2003-0044
Olena, A. F., & Patton, J. G. (2010). Genomic organization of microRNAs. *J Cell Physiol, 222*(3), 540-545. doi: 10.1002/jcp.21993
Osborne, C. K., & Schiff, R. (2011). Mechanisms of endocrine resistance in breast cancer. *Annu Rev Med, 62*, 233-247. doi: 10.1146/annurev-med-070909-182917
Pan, B., Feng, B., Chen, Y., Huang, G., Wang, R., Chen, L., & Song, H. (2015). MiR-200b regulates autophagy associated with chemoresistance in human lung adenocarcinoma. *Oncotarget, 6*(32), 32805-32820. doi: 10.18632/oncotarget.5352
Patel, Y., Shah, N., Lee, J. S., Markoutsa, E., Jie, C., Liu, S., . . . Chen, H. (2016). A novel double-negative feedback loop between miR-489 and the HER2-SHP2-MAPK signaling axis regulates breast cancer cell proliferation and tumor growth. *Oncotarget, 7*(14), 18295-18308. doi: 10.18632/oncotarget.7577
Peng, Y., & Croce, C. M. (2016). The role of MicroRNAs in human cancer. *Signal Transduct Target Ther, 1*, 15004. doi: 10.1038/sigtrans.2015.4
Ramalingam, P., Palanichamy, J. K., Singh, A., Das, P., Bhagat, M., Kassab, M. A., . . . Chattopadhyay, P. (2014). Biogenesis of intronic miRNAs located in clusters by independent transcription and alternative splicing. *RNA, 20*(1), 76-87. doi: 10.1261/rna.041814.113
Rugo, H. S., Rumble, R. B., Macrae, E., Barton, D. L., Connolly, H. K., Dickler, M. N., . . . Burstein, H. J. (2016). Endocrine Therapy for Hormone Receptor-Positive Metastatic Breast Cancer: American Society of Clinical Oncology Guideline. *J Clin Oncol, 34*(25), 3069-3103. doi: 10.1200/JCO.2016.67.1487
Schmidt, M. F. (2014). Drug target miRNAs: chances and challenges. *Trends Biotechnol, 32*(11), 578-585. doi: 10.1016/j.tibtech.2014.09.002
Seval, Y., Cakmak, H., Kayisli, U. A., & Arici, A. (2006). Estrogen-mediated regulation of p38 mitogen-activated protein kinase in human endometrium. *J Clin Endocrinol Metab, 91*(6), 2349-2357. doi: 10.1210/jc.2005-2132
Shah, N. R., & Chen, H. (2014). MicroRNAs in pathogenesis of breast cancer: Implications in diagnosis and treatment. *World J Clin Oncol, 5*(2), 48-60. doi: 10.5306/wjco.v5.i2.48
Shingu, T., Fujiwara, K., Bogler, O., Akiyama, Y., Moritake, K., Shinojima, N., . . . Kondo, S. (2009). Inhibition of autophagy at a late stage enhances imatinib-induced cytotoxicity in human malignant glioma cells. *Int J Cancer, 124*(5), 1060-1071. doi: 10.1002/ijc.24030

Shou, J., Massarweh, S., Osborne, C. K., Wakeling, A. E., Ali, S., Weiss, H., & Schiff, R. (2004). Mechanisms of tamoxifen resistance: increased estrogen receptor-HER2/neu cross-talk in ER/HER2-positive breast cancer. *J Natl Cancer Inst, 96*(12), 926-935.

Soni, M., Patel, Y., Markoutsa, E., Jie, C., Liu, S., Xu, P., & Chen, H. (2018). Autophagy, Cell Viability and Chemo-resistance are Regulated by miR-489 in Breast Cancer. *Mol Cancer Res*. doi: 10.1158/1541-7786.MCR-17-0634

Sylvestre, Y., De Guire, V., Querido, E., Mukhopadhyay, U. K., Bourdeau, V., Major, F., . . . Chartrand, P. (2007). An E2F/miR-20a autoregulatory feedback loop. *J Biol Chem, 282*(4), 2135-2143. doi: 10.1074/jbc.M608939200

Ward, A., Balwierz, A., Zhang, J. D., Kublbeck, M., Pawitan, Y., Hielscher, T., . . . Sahin, O. (2013). Re-expression of microRNA-375 reverses both tamoxifen resistance and accompanying EMT-like properties in breast cancer. *Oncogene, 32*(9), 1173-1182. doi: 10.1038/onc.2012.128

Wei, R., Cao, G., Deng, Z., Su, J., & Cai, L. (2016). miR-140-5p attenuates chemotherapeutic drug-induced cell death by regulating autophagy through inositol 1,4,5-trisphosphate kinase 2 (IP3k2) in human osteosarcoma cells. *Biosci Rep, 36*(5). doi: 10.1042/BSR20160238

Welboren, W. J., Sweep, F. C., Span, P. N., & Stunnenberg, H. G. (2009). Genomic actions of estrogen receptor alpha: what are the targets and how are they regulated? *Endocr Relat Cancer, 16*(4), 1073-1089. doi: 10.1677/ERC-09-0086

White, E., Mehnert, J. M., & Chan, C. S. (2015). Autophagy, Metabolism, and Cancer. *Clin Cancer Res, 21*(22), 5037-5046. doi: 10.1158/1078-0432.CCR-15-0490

Winter, J., Jung, S., Keller, S., Gregory, R. I., & Diederichs, S. (2009). Many roads to maturity: microRNA biogenesis pathways and their regulation. *Nat Cell Biol, 11*(3), 228-234. doi: 10.1038/ncb0309-228

Wu, H., Xiao, Z., Zhang, H., Wang, K., Liu, W., & Hao, Q. (2014). MiR-489 modulates cisplatin resistance in human ovarian cancer cells by targeting Akt3. *Anticancer Drugs, 25*(7), 799-809. doi: 10.1097/CAD.0000000000000107

Yuan, P., He, X. H., Rong, Y. F., Cao, J., Li, Y., Hu, Y. P., . . . Liu, M. F. (2017). KRAS/NF-kappaB/YY1/miR-489 Signaling Axis Controls Pancreatic Cancer Metastasis. *Cancer Res, 77*(1), 100-111. doi: 10.1158/0008-5472.CAN-16-1898

Zhai, H., Fesler, A., Ba, Y., Wu, S., & Ju, J. (2015). Inhibition of colorectal cancer stem cell survival and invasive potential by hsa-miR-140-5p mediated suppression of Smad2 and autophagy. *Oncotarget, 6*(23), 19735-19746. doi: 10.18632/oncotarget.3771

Zhang, B., Ji, S., Ma, F., Ma, Q., Lu, X., & Chen, X. (2016). miR-489 acts as a tumor suppressor in human gastric cancer by targeting PROX1. *Am J Cancer Res, 6*(9), 2021-2030.

Zhou, J., Li, G., Zheng, Y., Shen, H. M., Hu, X., Ming, Q. L., . . . Gao, N. (2015). A novel autophagy/mitophagy inhibitor liensinine sensitizes breast cancer cells to chemotherapy through DNM1L-mediat12ed mitochondrial fission. *Autophagy, 11*(8), 1259-1279. doi: 10.1080/15548627.2015.1056970

APPENDIX A

PROOF OF PERMISSION TO REPRODUCE A MANUSCRIPT

http://aacrjournals.org/content/authors/copyright-permissions-and-access

Article Reuse by Authors

Authors of articles published in AACR journals are permitted to use their article or parts of their article in the following ways without requesting permission from the AACR. All such uses must include appropriate attribution to the original AACR publication. Authors may do the following as applicable:

- Reproduce parts of their article, including figures and tables, in books, reviews, or subsequent research articles they write;
- Use parts of their article in presentations, including figures downloaded into PowerPoint, which can be done directly from the journal's website;
- Post the accepted version of their article (after revisions resulting from peer review, but before editing and formatting) on their institutional website, if this is required by their institution. The version on the institutional repository must contain a link to the final, published version of the article on the AACR journal website so that any subsequent corrections to the published record will continue to be available to the broadest readership. The posted version may be released publicly (made open to anyone) 12 months after its publication in the journal;
- Submit a copy of the article to a doctoral candidate's university in support of a doctoral thesis or dissertation.